UNIVERSITY OF CAPE TOWN

Dissertation

A Mathematical Model for Predicting Classification Performance in Wet Fine Screens

MWALE ADOLPH NTAJA

A Mathematical Model for Predicting Classification Performance in Wet Fine Screens

By: Mwale Adolph Ntaja (MWLADO001)

Submitted to The University of Cape Town in fulfilment of the requirements for the degree of MSc.Eng in Chemical Engineering

Faculty of Engineering and Built Environment

UNIVERSITY OF CAPE TOWN

Supervisors :

Prof. Aubrey Mainza[1], Dr Daramy Kallon[2], Aaron Paul Bepswa[1]

1. Department of Chemical Engineering, University of Cape Town
2. Department of Mechanical and Industrial Engineering Technology, University of Johannesburg

November 2015

Declaration

I know the meaning of plagiarism and declare that all of the work in the dissertation, save for that which is properly acknowledged, is my own.

I hereby grant the University of Cape Town free licence to reproduce for the purpose of research either the whole or any portion of the contents in any manner whatsoever of the above dissertation.

Signature: 

Adolph N. Mwale

Abstract

Screening is a well-known classification process in the minerals processing industry. The process involves separation of fine particles from coarse particles based on size and is applicable to both dry and fine screening. Fine screening is normally carried out wet. Until recently, fine wet screening had been limited to relatively low throughput applications. Developments in the recent past have seen the evolution of fine screening to high capacity applications. It has found application in operations such as closed circuits with a mill in place of hydrocyclones. However, even though developments are increasing, there has been a process model developmental lag. A fine wet screen model that can be used for unit simulation purposes to predict screen performance outcomes or integration into other models to simulate and predict process performance is necessary. Most existing screen models are for dry and coarse screening applications.

This thesis is aimed at developing a fine wet screen process model for predicting wet screening performance in the 45 – 150 µm range. Pilot plant testwork was conducted using a UG2-Chrome ore blend as feed. The tests were conducted at feed rates that ranged from 9 – 35 tph and solids concentrations in the range 30 – 60 $wt\%$. Screen aperture sizes of 45, 75, 106 and 150 µm were used in the testwork. A derrick screen pilot plant with recirculation was used for the testwork. A factorial experiment was conducted at two levels of throughput and solids concentration each per screen size tested Test samples were collected from the feed, overflow and underflow streams for each experimental condition investigated and analysed for particle size distribution

The test results showed that the lowest performance was experienced at the 60 $wt\%$ solids and 25 tph feed rate condition where a cut size value of 10 µm was recorded. The highest performance was observed at the $30\ wt\%$ solids and feed rate of 9 tph condition with a recorded cut size value of 36 µm on a 45 µm aperture size. In general, the test results indicated an increase in carryover of undersize material to the oversize stream when the tests were

performed with fine aperture size screen panels, at high feed rates and at high solids concentrations.

A model was commissioned to predict fine wet screening at the aperture size range tested in this work. The proposed model consists of two main components: the first one describes screening as a rate process whose performance depends on the rate of change of mass fraction of a given size class with screen length; and the second part of the model correlates the undersize material that bypasses classification to particle size and feed conditions. The sum of the two parts constitutes a fine wet screen model that completely describes the partition curve that adequately predicts the bypass material on a size by size basis. The model has shown excellent prediction of the studied conditions with R^2 values generally above 0.95. The model is capable of predicting performances outside the studied bounds because its prediction capability is based on feed conditions. The sharpness of separation and cut size models were also developed with acceptable fits.

It is recommended that a water split model be developed in future and that particle size distribution changes in the feed be accounted for in the model. The current model has to be readjusted in response to changes in feed particle size distribution.

Dedication

This work is dedicated to my family, my wife Kasongo and my two sons Raymond and Ryan; I am greatly indebted to you. You took you time off from normal life to allow me to acquire this degree. Your moral support has been priceless and words cannot express how grateful I am to have you in my life.

Acknowledgments

My sincere gratitude goes to my primary supervisor Professor Aubrey Mainza for his remarkable advice on this work. His advice has been invaluable. I would also love to mention my special thanks to Dr Daramy Vandi Von Kallon from the University of Johannesburg for his priceless advice on this work. My gratitude also to Paul Bepswa for the valuable discussions we had concerning this work. Special thanks to the Centre for Minerals research and the comminution unit in the department of chemical engineering for sponsoring my project in partnership with Anglo Platinum. I would also like to acknowledge and give thanks to Derrick Corporation and Mintek for allowing me to use their facility to carry out my experiments. Special thanks to all my friends, old and new, that I interacted with during my study duration, you encouragements and ideas were very valuable.

Lastly, surely not least, would love to give glory and praise with thanks in my heart to God the Almighty for all that I have achieved to this point. I owe it all onto you God.

Contents

List of figures

List of tables

CHAPTER 1: INTRODUCTION

1 Background

The purpose of this thesis is to develop a model for fine wet screening using Derrick screen pilot plant test data for validation. The model is designed to predict the screening performance curve based on operating conditions.

In mineral processing operations, comminution is one of the most important and energy intensive stages during mineral upgrading operations. The comminution process involves crushing and milling of ores to sizes that allow for liberation of the valuable mineral in the ore to take place. The ground ore is usually subjected to classification where particles coarser than the liberation size are recirculated back to the size reduction stage and finer particles are allowed to proceed to downstream processes (Wills & Napier-munn 2006). Different kinds of classification devices are in use for classifying ore particles according to their sizes using different mechanisms. The most commonly used devices are hydrocyclones, because of their robustness, high capacity and low maintenance costs (Gupta & Yan 2006). Vibrating screens, whose principal separation mechanism is by size, are another type of classification device used in mineral processing operations (Albuquerque et al. 2008). Screens classify particles by separating particles that are larger (coarse particles) from those that are smaller (fine particles) by presenting a barrier of a given aperture size to the flow of material. The screening process involves material transport along the screen, stratification of fine particles on the particle bed to the screen surface (Soldinger 1999) and the eventual passage of undersize particles through the apertures of the screen. The process depends upon many variables, which include the particle size distribution of the feed, the nature of vibrations designed to induce the motion of particles, the open area of the screen, and to some extent, the materials of construction of the screening surface (King 2001; Gupta & Yan 2006; Wills & Napier-munn 2006). The screening process can be performed under wet or dry conditions, with fine materials predominantly screened wet. Wet screen designs in the past were characterised by low capacity, high panel wear rate

and required inconveniently large installation space to match up to capacity demands (Valine & Wennen 2002; Albuquerque et al. 2008). However, recent screen developments have improved in design to overcome some of these challenges. One such screen is the multi-deck Derrick screen that employs a series of screens stacked one on top of the other and fed with an equal feed distribution mechanism. This has drastically reduced installation space requirements and tremendously improved the screen capacity (Derrick 1973; Kelley & Mckeon 2005; Pelevin & Lazebnaya 2009). The wear rate has been improved through the introduction of high wear resistant urethane panels (Kelley 2007). Even though few wet screen design has improved to these level, fine wet screen modeling has still lagged behind. Developing a fine wet screen model will enhance fine wet screening studies, operations and performance simulations.

1.1 Context of study

Recent advances in screen design have demonstrated that screens have great potential to be used in grinding circuits in place of hydrocyclones (Kirk 1984; Albuquerque et al. 2008). Studies done by Pelevin & Lazebnaya, (2009) that compared the derrick screen to the hydrocyclone in an iron ore concentrator (KMAruda) in Russia showed that the screen reduced circulating loads from ranges of 110-120% to 30-60% reducing overgrinding of the ore and increasing mill capacity. Such improvements have paved the way for the use of screens in other ore processing operations. To incorporate screens in grinding circuits by either completely replacing the hydrocyclone with the screen or operating the screen in hybrid combination with the cyclone, a large number of trials are required at great cost. In order to avoid the high cost of physical trials, simulations of the process using appropriate models could be used. Unfortunately, in as much as screen designs have advanced, wet screen model developments have lagged behind where most existing screen models are developed for dry screens (Karra 1979; Ferrara et al. 1987). Moreover, wet screen operation, optimisation and design have generally been attempted by approaches based on experience rather than theory due to lack of theoretical guidelines (Rogers & Brame 1985; Valine & Wennen 2002).

This thesis intends to provide model that will predict the wet screening process and the classification performance curve based on feed conditions. There has been an increased use of models in simulations of integrated plant operations in mineral processing for feasibility studies, prediction of performance results, selection of alternative processes and as an aid in designing (Ferrara et al. 1987). As noted above, fine wet screen modelling has been rather stagnant with most models developed since the last wet screen developed by Rogers (1982) being applicable only to course dry screening (Subasinghe et al. 1989; Subasinghe et al. 1990; Soldinger 1999; Trumic & Magdalinovic 2011). This thesis is focused on developing a screen model applicable to fine and wet screening operations. Firstly fine wet screen data had to be generated using four different size aperture panels (150, 106, 75 and 45 um) on a derrick screen pilot plant, followed by the development of the wet screen model in Chapter 6.

1.2 Thesis Overview

This section provides an overview of the contents of each chapter in this thesis.

Chapter 2: Theory and Literature Review

Chapter 2 looks at the principles underlying screen operations by focusing on the screen performance evaluation methods, factors that affect performance of the screen and a review of screen performance prediction models that have been developed by previous authors..

***Chapter 3:* Experimental apparatus**

This chapter discusses the experimental apparatus used to generate test data and the design of the pilot scale equipment used to conduct experiments.

***Chapter 4:* Methodology**

This chapter outlines procedures followed during data collection.

Chapter 5: Results and discussion

In this chapter results are presented and discussed with major focus on the effect of operational variables on screen performance.

Chapter 6: Model development

This chapter describes the methods used to develop the fine wet screening model and demonstrates how well the model fits experimental results obtained from the pilot scale testwork presented in Chapter 5.

Chapter 7: Conclusions and recommendations

In this chapter, key findings are highlighted and recommendations for future work are made.

.

CHAPTER 2: LITERATURE REVIEW

2 Review

2.1 Classification by screening

Screening is a separation process that classifies particles according to size. The screen presents a barrier which allows particles smaller than the aperture to go through and larger ones retained and transported to the oversize shown in Figure 2-1(Gupta & Yan 2006).

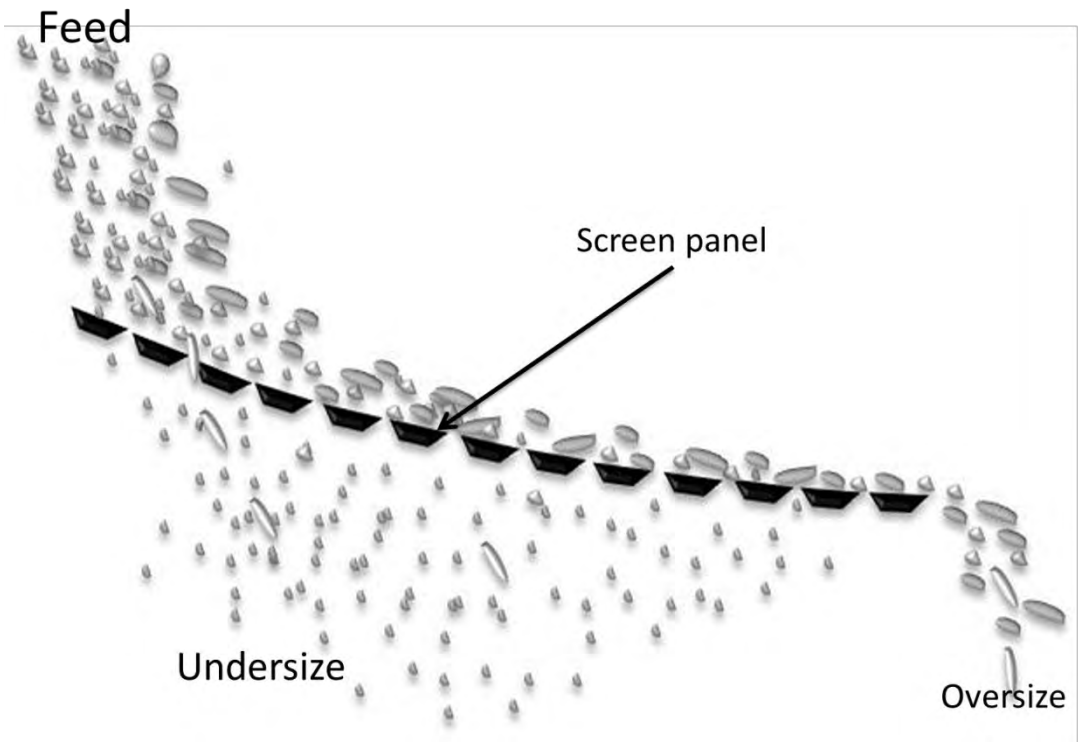

Figure 2-1 Basic screen operation principle

The screen is usually vibrated at set vibration frequency and amplitude depending on application (Wills & Napier-munn 2006). Generally, screens have found use in scalping, sizing or classifying, grading, media recovery, dewatering and desliming or de-dusting operations. Depending on application screens are operated either dry with relatively low frequency and high amplitude or wet with relatively high frequency and low amplitude (King 2001; Albuquerque et al. 2008). Separations of dry materials by screens and sieves are generally attempted down to about 75 microns (Gupta & Yan 2006). Fine

and wet screening is generally attempted at sizes below 5 mm to 45 um (Wills & Napier-munn 2006).

The screening process involves random movement of particles through which particles finer than the screen aperture have to stratify and eventually pass through the aperture (Subasinghe et al. 1990; Soldinger 1999). The rate of stratification of finer particles depends on variables such as the screen angle of inclination, the feed rate, the mass fraction of fines in the feed and nature of vibration employed (Ferrara et al. 1987; Subasinghe et al. 1990; Soldinger 1999). The angle of inclination aids in movement of material on the screen by providing a gentle slope. Vibration provides continued stratification of particles by lifting the material over and away from the screen towards the oversize discharge and dilating the material. At steady state operation feed is continuously supplied to the screen at a rate equal to the depletion rate. This ensures there are enough particles preventing bouncing off of particles or overclouding the screen (King 2001). The eventual particle passage through the screen aperture depends on its probability of passage (Gaudin 1939; Ferrara et al. 1987; Soldinger 1999).

2.2 Screen efficiency

The ideal design of a screen is that all particles finer than the screen aperture pass through and coarser particles are retained (Wills & Napier-munn 2006). Given the chance and the time, screens are capable of transmitting all the undersize material in the feed. In practice, however, time is a major limiting factor (Gupta & Yan 2006). Therefore, not all undersize particles transmit through the aperture. The fraction of the feed undersize that transmits through the screen aperture is the screen efficiency (King 2001). Therefore, an efficient classification device is one that is able to place the majority of the particles of a particular size to the stream they should belong for a given aperture size. It is from this placement of particles that the efficiency of each stream is determined and out of which an overall efficiency of the unit is determined. Gupta and Yan (2006) have illustrated that a screening operation does not produce a perfect separation and have expressed the efficiency of the process using equation (1), (2) and (3) where

- Efficiency based on undersize is E_u
- Efficiency based on oversize is E_o
- Overall screen efficiency is E
- Mass flow rate of solid in the feed is F_f
- Mass flow rate of solid in the overflow is F_o
- Mass flow rate of solid in the underflow is F_u
- Mass fraction of undersize in the feed is $m_{u(f)}$
- Mass fraction of undersize in the oversize is $m_{u(o)}$
- Mass fraction of undersize in the undersize is $m_{u(u)}$

$$E_o = \frac{F_o(1 - m_{u(o)})}{F_f(1 - m_{u(u)})} \quad \text{Eq (1)}$$

and

$$E_u = \frac{F_u m_{u(u)}}{F_f m_{u(f)}} \quad \text{Eq (2)}$$

Where the overall screen efficiency from mass balance of the system is given by $E = E_o \times E_u$

$$E = \frac{(m_{u(f)} - m_{u(u)})}{(m_{u(o)} - m_{u(u)})} \frac{(m_{u(o)} - m_{u(f)})}{(m_{u(o)} - m_{u(u)})} \frac{(1 - m_{u(o)})}{(1 - m_{u(f)})} \frac{m_{u(u)}}{m_{u(f)}} \quad \text{Eq (3)}$$

Wills and Napier-munn (2006) observed that formulae such as the one derived are acceptable for assessing the efficiency of a screen under different conditions, operating on the same feed. He observed that no absolute efficiency values can be given without accounting for near-mesh particles that are most difficult to screen.

2.3 Efficiency curve

Nageswararao, (1999) from his work on hydrocyclone defined classification efficiency as the recovery of the mass fraction of particle size d_i recovered to the overflow stream in relation to that size fraction in the feed. For a particular particle size distribution, the efficiency curve is drawn for all the particles indicating how each particle size class i partitions to the oversize stream. This is a graphical method used to assess and account for misplaced materials or the difficulty of separation of near size particles and to assess

separation efficiency on size by size basis (Gupta & Yan 2006). The graph can be referred to as “Tromp Curve”, or “Partition Curve”. As shown in Figure 2-2, a partition curve of a screen is drawn by plotting partition numbers, defined as the percentage of the feed reporting to the oversize product, against the geometric mean size (Wills & Napier-munn 2006) or arithmetic mean (Gupta & Yan 2006) on a logarithmic scale.

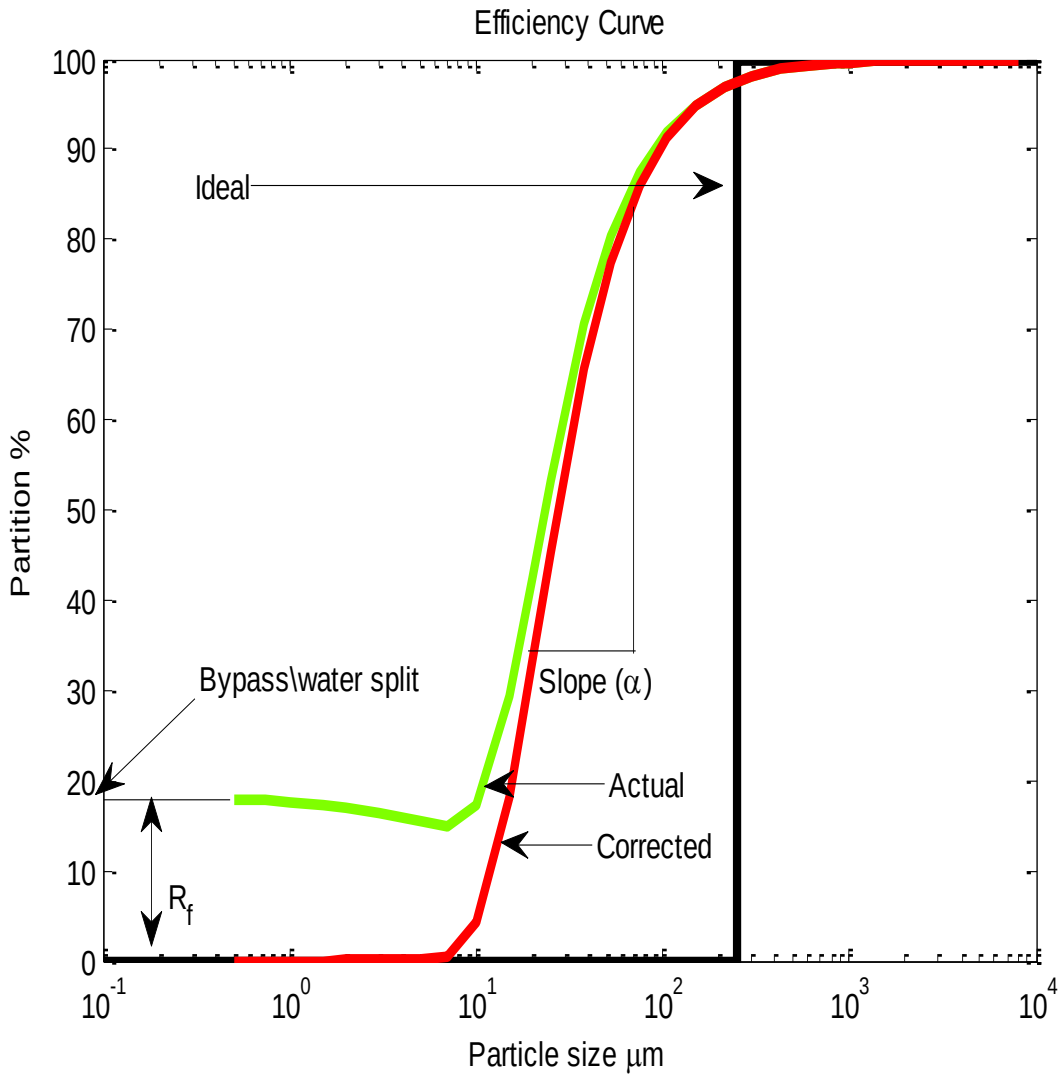

Figure 2-2 Tromp curve for a screen (from Wills & Napier-Munn, 2006:188)

The slope of the partition curve is used to assess the sharpness of separation. The steeper the slope of the partition curve, the sharper the separation. The cut size value gives a quick first glance performance indication. The closer the cut size value is to the aperture size, the more effective the screening device is. The partition curve effectively models the

screen performance (Wills & Napier-munn 2006), and has been used for simulation and design purposes (Ferrara et al. 1987; Subasinghe et al. 1989).

The efficiency curves for fine wet screen operations and hydrocyclones are far from ideal separation (Figure 2-2). Due to poor classification, there is a portion of fine size classes that bypass the classification process due to entrainment and report to the coarse stream as shown by the actual partition curve in Figure 2-2 (Austin & Klimpel 1981; Nageswararao 1999a; Mainza 2006). A corrected efficiency curve is used to account for classified material. The difference between the actual curve and the corrected curve at particle size zero along the y-axis has be termed the bypass or R_f (Austin & Klimpel 1981; Nageswararao 1999a; Nageswararao 1999b). The value of the R_f is said to approximate the water split to the coarse stream (Rogers 1982; Rogers & Brame 1985; Nageswararao 1999b; Mainza 2006). However, Austin & Klimpel (1981) observed in their work that this value need not necessarily equal the water split because the water split is bound to change for different conditions. Thus, it is from the corrected efficiency curve that partition curve properties are extracted (Rogers & Brame 1985)

2.3.1 Partition curve properties

As a measure of how effective the classification method is, some properties of the curve have been identified as important performance indicators (Gupta & Yan 2006; Wills & Napier-munn 2006). These include the sharpness of separation alpha α, the cut size d_{50}, the water split to the oversize R_f, and the fishhook parameter delta β.

2.3.1.1 Sharpness of separation

Sharpness of separation indicates how the screen places the undersize material to the undersize stream at given conditions. Gupta & Yan (2006) explains that the sharpness is calculated from the slope of the curve where a steeper slope indicates high separation sharpness. The slope is calculated from the straight section of the partitions curve where the difference of the 75% and 25% partition marks is divided by their corresponding size difference $(d_{75} - d_{25})$. Most workers modelled this parameter and have given it the

symbol alpha α (Rogers 1982; Rogers & Brame 1985; Nageswararao 1999a; Mainza 2006; Narasimha et al. 2014)

2.3.1.2 Cut size d_{50}

Particle size separation in screens does not always occur at size equal to the aperture size as seen from Figure 2-2. Separation size is measured using particle size that has a probability of 0.5 referred to as the d_{50} to report either to the coarse or fine product stream (Mainza 2006; Narasimha et al. 2014). The cut size is a good indicator of screen efficiency and a value close to the aperture size indicates good separation.

2.3.1.3 Water split (R_f)

The water split is basically the ratio of the amount of water reporting to the oversize stream to that of the feed (Austin & Klimpel 1981). The water split value has been used to estimate the amount of fines that by pass the classification process due to entrainment (Rogers & Brame 1985; Frachon & Cilliers 1999; Narasimha et al. 2014). Thus, the water split ratio can be used to assess the performance of the screen.

2.4 Effect of operating variables on screen performance

Screen performance is influenced by many variables that can be classified into operational and design. The operational variables include particle size distribution of the feed, the feed rate, feed solid concentration, ore density, and ore type (Valine & Wennen 2002; Wills & Napier-munn 2006; Gupta & Yan 2006). Design variable include vibration frequency, vibration amplitude, vibration mode, screen panel area, screen panel open area, angle of inclination, aperture type and aperture size (Gupta & Yan 2006). Most of the design variable are usually fixed for a given screen for its operational life span. Thus, most of the design variables were not discussed in this thesis. The operational variables pertinent to this thesis are discussed in the sub sections that follow.

2.4.1 Effect of feed rate

The screen feed rate is an important parameter in sizing the screen as well as efficient screen operation (King 2001). The feed rate has to be carefully determined in relation to the screen capacity and conditions under which the screen is operated on (King 2001; Gupta & Yan 2006). The residence time of particles and bed thickness on the screen is directly related to the flow rate. A high flow rate increases bed thickness and reduces the residence time (King 2001) an effect that lowers screen efficiency. However, Rogers & Brame (1985) in their work performed a series of wet screening tests on aperture sizes that ranged from 292 microns down to 111 microns where results showed otherwise. The volume percent content of solids in the feed used ranged from 37.5% down to 15.4% and feed flows from 98 l/min/m^2 to 610 l/min/m^2. Their results showed that, for a given percent solid content in the feed, there is very little influence on screen efficiency with regards feed flow increase provided the screen capacity is not exceeded.

2.4.2 Effect of feed solid concentration

One of the major efficiency driving factors in fine wet screening is the feed water content in relation to solids. The fraction of water in the feed is responsible for the efficient transmission of the undersize to the undersize stream (Valine et al. 2009). Feed solid concentration is directly related to rheological characteristics of the feed slurry (He & Forssberg 2007). Feeds with high solid concentration have reduced average inter particle distance an effect that restrict particle movement leading to agglomeration (He & Forssberg 2007; Albuquerque et al. 2008). Valine & Wennen (2002) observed that wet screen operations do not require a longer screen. A wider screen is recommended because the effect of water on screen is felt a short distance from the feed point as water quickly percolates and depletes before the solids are half way through the screen. The remaining material on the screen is conveyed to the overflow with very small amount going through the screen. This is the reason why spray water is usually employed midway through. Rogers & Brame's (1985) work showed that bypass increased with increase in feed solids concentration. Valine & Wennen (2002) note that,

from experience depending on the ore density, a feed solid concentration ranging between15- 20% solids by volume would give fairly good screen performance.

2.4.3 Effect of feed size distribution and particle shape

Particle size distribution of the feed plays a significant role in screen operations. The share of the fines, near size and coarse particles greatly affects screen performance (Standish et al. 1986; Soldinger 1999; Tsakalakis 2001). Since particles are randomly dispersed in the feed stream, stratification of fines to the screen aperture is an important step (Spottiswood & Kelly 1982; Subasinghe et al. 1990). The rate of stratification depends on the amount of fines in the feed and screen vibration (Soldinger 1999). Soldinger (1999) observed that the rate of stratification was high when fine particles are in the order of 15 - 30%. Stratification rate decreased when the amount of fine particle increased and approached zero for fine particle proportions above 60%. The most difficult particle size to screen are sizes nearing the aperture size (Wills & Napier-munn 2006). Particles of this size have a tendency to blind the screen aperture reducing the effective screen open area and separation efficiency (Tsakalakis 2001). However, Standish et al. (1986) indicated that the rate of separation of fine particles is affected more by operating conditions rather than the amount of near size particles in the feed. In fine wet screening stratification of fines through coarser particles depends primarily on the feed water content and screen operations with high water content are more efficient (Rogers & Brame 1985; Valine & Wennen 2002; Albuquerque et al. 2008; Valine et al. 2009; Pelevin & Lazebnaya 2009). Irregularly shaped particles in the feed, especially near size particles, must first orient themselves in a manner that allows them to pass through the aperture (Wills & Napier-munn 2006). If the feed contains about 15% or more of slabby or elongated particles, the efficiency begins to drop because of increased blinding of the screen cloth (King 2001). This makes shape characterisation one of the most important factors to put into consideration in screen operations or modeling.

2.4.4 Screen capacity

Spottiswood & Kelly (1982) indicated that there are two criteria used to assess screen performance, Capacity and Efficiency. Capacity is directly related to the screen area and is defined as the quantity of material fed to the screen per unit time per unit area of screen surface (Gupta & Yan 2006). Increasing screen capacity is feasible, but this is likely to be achieved at the expense of efficiency (King 2001). The capacity based efficiency is determined predominantly by the actual feed loading on the screen relative to the rated feed capacity of the screen (Mathews 1985). Feed flows in excess of or below 80% of the rated feed rate results in reduced transmission efficiency. Excess feed rate overclouds the screen reducing rate of stratification whilst under fed screens results in particles bouncing off the screen much quicker (King, 2001). Screen capacity is not necessarily fixed for a given screen but for a given set of feed conditions because the effective transmission depends on how quick undersize particles get to the screen aperture (Mathews 1985; King 2001; Gupta & Yan 2006). Screen capacity determination methods incorporate factors that describe the screen operational conditions and equation is given as

$$F_B = \frac{F_f}{AC_R} \qquad \text{Eq (4)}$$

Where, A is the screen area, F_B is the basic capacity of the screen in $t/hr/m^2$ and C_R is the correction factor dependant on operating conditions (Mathews 1985). Capacity equations such as equation (4) have mostly been developed for coarse dry screening operations whilst rate determination methods for wet screens still remain experience based.

2.4.5 Probability of particle passage

The eventual passage of the undersize depends on the chance of a particle size i to pass through a given aperture size. This theory has been well developed by Gaudin (1939) and the probability function has been modified by different scholars to simplify the screen modelling procedures (Ferrara et al. 1987; Subasinghe et al. 1989; Trumic & Magdalinovic 2011). The probability function derived by Gaudin (1939) describes unhindered particle

passage showing chance of a particle if it was dropped on the screen with no surrounding particles. Subasinghe et al. (1990) and Soldinger (1999) showed that the eventual passage of a particle is affected by the amount of undersize material in its vicinity as well as the rate at which undersize stratify and report to the screen cloth. Thus, here it can be deduced that even at high rate of stratification, undersize particles can have a reduced transmission rate due to local hindrance, an effect that can greatly reduce screen efficiency.

2.4.6 Percent open area

The overall rate of transmission of undersize particles depend on how much open area is available for particles to pass through (Wills & Napier-munn 2006). Particles may have high probability of passage; however, this may result in reduced capacity and low separation efficiency if the effective open area is very low. The effective screen open area for a fixed width and length of panel reduces as aperture size get finer (Tsakalakis 2001). This is so, because room for increased panel strength and rigidity is provided for in the design and construction of the screen (Kelley 2007). This significantly reduces the capacity of the screen to transmit undersize material to the underflow stream (Barkhuysen 2010). In fine wet screening wider screen is more efficient than a longer screen (Valine & Wennen 2002; Albuquerque et al. 2008). This is because most of the feed water percolates to the undersize by the time material is midway through the screen. Thus, in an effort to improve the capacity of fine wet screening, strides have been made to improve the width of the screen by the introduction of screen units such as the derrick screen stack sizer (Figure 2-3). The unit employs a stack of narrow screen panels with an equal feed distribution mechanism (Kelley & Mckeon 2005; Barkhuysen 2010). This system thinly spreads the feed equally on each screen panel. This reduces congestion on screen and enhances the passage of undersize particles whilst maintaining an overall high flow rate and low floor space.

Figure 2-3 Derrick stack sizer unit in operation (courtesy: Derrick corporation)

Other factors include vibration frequency and amplitude, the screen angle of inclination and bulk density. For continued stratification to take place on the screen deck, the material needs to be able to move over and away from the feed point towards the discharge end (King 2001; Wills & Napier-munn 2006). This will constantly allow fine particles to move down through the apertures while the oversize leaves through the oversize discharge point. For effective movement of material, vibration on the screen deck at an inclined position is induced, making the screen angle a critical factor. The material is lifted up and down repeatedly as it travels along the screen surface allowing the particles to reorient and stratify through the bed while at the same time presenting the particles onto the aperture several times to increase their chance of passage (Mohanty et al. 2003; Cleary et al. 2009). At larger screen angles, the particle approaching the aperture sees an effective narrow aperture opening, an effect that increases the rate of travel of material on the

screen (King 2001; Gupta & Yan 2006; Wills & Napier-munn 2006). This means at lower angles of inclination, the rate of material travel on the screen is reduced but with an increased effective aperture size. Thus, it can be seen that screen angle has a bearing on both the throughput and efficiency of the screen.

Vibrational modes for wet screening and dry screening operations differ primarily on frequency level. Fine wet screening operations are more accustomed to high frequency vibrational with low amplitude modes (Rogers & Brame 1985; Kelley & Mckeon 2005; Albuquerque et al. 2008). This allows the water to carry along with it the undersize material as opposed to low frequency and relatively high amplitude vibrational modes.

2.5 Screen models

Screen models aim to predict the size distribution and flow of the screen products, which in turn give a performance curve. Models in the literature can be classified as phenomenological models that incorporate theory of the screening process, empirical models based on experimental data, and numerical models based on computer solutions of Newtonian mechanics (Wills & Napier-munn 2006).

2.5.1 Model types

2.5.1.1 Phenomenological Models

Phenomenological models are models based on the theory of particle passage through a screening surface (Wills & Napier-munn 2006). Within the phenomenological models two different approaches, the kinetic and probabilistic, have been used to represent screening operations. The probabilistic approach is an approach based on the probability of a particle passing through the aperture of the screen (Subasinghe et al. 1989). On the other hand, the kinetic approach defines the screening performance as a rate process that varies with the distance along the screen and depends on the amount and particle size distribution of the material being processed (Ferrara et al. 1987; Subasinghe et al. 1990).

2.5.1.2 Empirical Models

Empirical models aim to predict performance curve using an equation that relates to the experimental data (Rogers & Brame 1985). More frequently these kind of empirical models are used by screen manufacturers (Wills & Napier-munn 2006). There are a number of different formulations of these models. From experimental data, mathematical relations are derived using linear regression methods to predict screen performance curve (Karra 1979).

2.5.1.3 Numerical Models

The particle flow is modeled by means of Discrete Element Method (DEM) at a particle scale. In other words it is a numerical method for computing the motion and effect of a large number of small particles. An explicit numerical scheme is used to trace the motion of individual particles in a system according to their mutual interaction (K. J. Dong et al. 2013).

2.5.2 Existing screen models

2.5.2.1 The Ferrara et al. (1987) Model

This section refers to the model developed by Ferrara et al. (1987). According to Ferrara et al. (1987), there are two (crowded and separate) distinct process conditions that exist on a screen with each condition involving two rate processes; the kinetics of particle passage through space and the dependence of probability of passage on the particle to aperture size ratio. In their approach, they developed a screen model that was composed of four factors. First factor described the initial feed conditions that included the ore properties and size distribution. The next factor described parameters that characterised the screen process system. The third factor described the screen dimensions, and the last described the screen operation results (oversize partition curve). Crowded conditions exist when a critical feed rate (F_c) is exceeded. That is to say, the rate of passage of particles in contact with the screen cloth equals the rate at which this layer is replaced. With these conditions existing, a constant mass flow rate is achieved where the mass of passing particles of size range i is proportional to a constant K_i and

to the feed mass fraction (m_{iL}) of particles with size d_i as expressed in equation (5).

$$-\frac{dF_{iL}}{dL} = K_i m_{iL} \qquad \text{Eq (5)}$$

F_{iL} is the feed rate at a position L along the screen length. In their derivation, the feed rate F_f to the screen (at $L = 0$) was regarded as a function rather than a constant which complicated their derivation. A function for kinetic through space was then developed as in equation (6)

$$F_f\left[\int_0^a m_{jf}\frac{1}{\chi_j}({E_{oiL}}^{\chi_j} - 1)dd_j + \int_a^{\infty} m_{jf}\, ln\, E_{oiL}\, dd_j\right] = -K_i L \qquad \text{Eq (6)}$$

The constant K_i was also derived for the eventual passage of the particles through the aperture of size a. The eventual passage of a particle under crowded conditions depends on the probability of a particle reaching the screening surface through stratification and the probability that the particle will pass through the screen. Ferarra et al used the probability function derived by Gaudin (1939) to express the crowded screening as a function of kinetic and probability expressed in equation (7).

$$F\left[\int_0^a m_{jf}\frac{1}{\chi_j}({E_{oiL}}^{\chi_j} - 1)dd_j + \int_a^{\infty} m_{jf}\, ln\, E_{oiL}\, dd_j\right] = -K_{50}\, 2^{\sigma}\left(1 - \frac{d_i}{a}\right)^{\sigma} L \qquad \text{Eq (7)}$$

Where the variable i represents the particle size under kinetic study and the variable j represents the generic particle size of the screen particle population, whose distribution affects the kinetics of the particle of size class i.

Ferrara et al. also modeled the separate condition screening regime with a notion that in this regime, there is no particle to particle interaction. The relation for this system was given as shown in equation (8).

$$-\frac{dF_{iL}}{dL} = S_i F_{iL} \qquad \text{Eq (8)}$$

Where the kinetic constant S_i was derived theoretically by applying the probability theory as a function of the passage probability P_i and n as the

number of times a particle is presented to the screen. The equation derived is shown in equation (9)

$$E_{oiL} = exp\left[-S_{50}\, 2^{\sigma}\left(1 - \frac{d_j}{L_A}\right)^{\sigma} L\right] \quad \text{Eq (9)}$$

Separate conditions rarely occur and equation (9) is only applicable when these conditions are known to exist.

Crowded conditions occur from the feed point to the critical distance $L_c$and separate conditions occur from the critical point to the screen discharge point a distance L_s where total screen efficiency is given in equation (10).

$$E_{oiL} = E_{oiL_c}.E_{oiL_s} \quad \text{Eq (10)}$$

Ferrara et al. (1987) showed the significant of the constants K_{50} and σ. They showed that K_{50} has the same characteristics as the basic capacity of the screen. The constant depends mainly on the aperture size, the screen open area, particle shape screen surface type, angle of inclination and screen vibration conditions. The dimensionless parameter σ affects the particles probability of passaged and has been shown by Ferrara et al. to depend on screen surface type, slope and vibration conditions.

The assumptions made in this model were that there is perfect mixing in material flow as well as plug flow through the aperture. With these two assumptions, at steady state, the initial feed conditions can be thought to be constant at the initial feed point $(L = 0)$ and there after vary with screen length. In this work the initial feed rate was considered as an unknown function that could not be evaluated. Had the feed rate been considered to be a constant at $L = 0$, the model derivation would have been simplified to a more palatable function for process simulation. The model was specifically developed for coarse sized material. The model involves iterative solving for partition numbers by first inputting guessed constant values. Thus, the output is generally dependent on the initial values supplied to the equation.

2.5.2.2 Subasinghe et al. (1990) Model

This section refers to the model developed by Subasinghe et al. (1990). In this model Subasinghe et al. developed a model that describes screening

process as a process involving two first order processes occurring concurrently, the rate of stratification through the bed and rate of passage through the screen aperture. In this model, at a given screen length, the mass M_i of size less than the screen aperture stratifies to the bottom to form a bottom layer B_i in contact with the screen surface out of which a mass of Q_i passes through the aperture (Subasinghe, et al., 1990). The stratification process is represented as

$$\frac{dM_i}{dL} = -k_{s,i}M_i \quad \text{Eq (11)}$$

The rate of passage as;

$$\frac{dQ_i}{dL} = k_{p,i}B_i \quad \text{Eq (12)}$$

The rate of accumulation on the screen surface is the given as

$$\frac{dB_i}{dL} = k_{s,i}M_i - k_{p,i}B_i \quad \text{Eq (13)}$$

Where k_s and k_p are rate constants for stratification and passages respectively. Equations (11) and (13) were combined and integrated to yield the partition number in equation (14).

$$E_{oi} = \frac{\left[k_{s,i}e^{-(k_{p,i}L)} - k_{p,i}e^{-(k_{s,i}L)}\right]}{k_{s,i} - k_{p,i}} \quad \text{Eq (14)}$$

When one of the rate constants is much greater than the other equation (14) reduces to a first order equation of the form;

$$E_{oi} = e^{-(k\,L)} \quad \text{Eq (15)}$$

Where $k = k_{s,i}, k_{p,i}$.

According to Subasinghe et al (1990)., the rate of passage constant depends on size of the particles i and tends to zero as particle size approaches the aperture size. The stratification constant depends on the prevailing environment at a particular point of the screen and the variation is rather complex. This model has been developed for dry screening and it is only valid for particle sizes below a given aperture size. The model predicted the screen performance with reasonable accuracy. However, the model involves determining the two screen constants of each particle size at each particle

size, a strenuous process. It involves iterative solving for constants values. Thus, the constants' output is generally dependent on the initial values supplied to the equation.

2.5.2.3 Trumic & Magdalinovic (2011) Model

The discussion of the model developed by Trumic & Magdalinovic is based on the work published in 2011. In this section a screen model, from a single experiment, by fitting two points predicts the screen performance based on the residence time of material on the screen.. From this approach, the rate of passage of the underflow is given in equation (16).

$$\frac{d(m_{it})}{dt} = -K_p k m_{it} \qquad \text{Eq (16)}$$

Where m_{it} is the mass fraction of particles of size class i on the screen at time t, k is the rate constant and K_p is the change of the probability of the screening coefficient. From dependence of probability on the ratio of particle to aperture Trumic & Magdalinovic (2011) produced a first order model of the form shown in equation (17)

$$E_{uit} = \frac{kt}{1 + kt} \qquad \text{Eq (17)}$$

In this model, the kinetic constant (k) for a particular screen can be determined from a single experiment and be used to predict the screen performance at different operating conditions of the same screen. This model was developed for dry screening process and has no variables pertinent to fine wet screening. The model bases screen performance on screening duration. It is not practical to determine the residence time of a given size class on the screen and relate that to performance. In a continuous screen operation, for a first order rate process, Standish & Meta (1985) pointed out that screen length is used as the basis of calculations while for batch processes time can be measured and be used (Standish 1985). On this account, this model can be thought to be a batch screen process model.

2.5.2.4 Rogers (1982) Model

Rogers, (1982) developed an empirical classification function for wet screens in the size ranges of 522 – 1252 um using a derrick MS-3 high frequency vibrating screen. The screen was arranged in such a way that the slurry was continuously recirculated from the sump through a pump on to the screen and back to the sump where samples where cut. The data was used to develop a classification function based on the function developed by Hatch & Mular (1978). Rogers proposed that the Hatch & Mular function had high alpha values and the reduced performance curve did not start from zero at fine particle sizes. The classification function developed was a function of the alpha α, the corrected cut size d_{50C}, and the particle size d_i as shown in equation (18).

$$E_{oi} = \left[1 + \left(\frac{d_{50C}}{d_i}\right) exp\left\{\alpha\left(1 - \left(\frac{d_i}{d_{50C}}\right)^3\right)\right\}\right]^{-1} \quad \text{Eq (18)}$$

The model is independent of screen conditions and the author claims excellent performance approximation at the studied conditions. This model was validated by the data produced by Rogers & Brame (1985) where good agreement between the experimental data and the model prediction was observed. The model was empirically developed for prediction of corrected and reduced partition curves. However, this model is specific to the conditions at which it was developed, particularly the screen aperture size and the material used. It was developed for a wet screen process but does not capture how the changes in feed conditions affect the screening process at various levels.

2.5.2.5 The Karra (1979) Model

Karra (1979) developed an empirical model that factors in the deviations of operating condition of the screening process from the standard as used in the determination of the basic capacity of the screen. The model can be used to size screens. Using regression method and a normalised partition curve by plotting E_{oi} against d_i/d_{50C} Karra took an empirical approach and related the efficiency to the size ratio as shown in equation (19).

$$E_{oi} = 1 - exp\left[-0.693\left(\frac{d_i}{d_{50C}}\right)^{5.846}\right] \quad \text{Eq (19)}$$

In equation (19) Karra (1979) showed that the screen efficiency curve is controlled by the particle to cut size ratio whilst the exponent was fixed. The Karra model was empirically developed and is specific to dry screening. The model predicts reduced performance curve without capturing most of the factors that affect screen performance discussed earlier in this chapter.

2.5.2.6 The Subasinghe et al. (1989) Model

This section reviews the empirical model developed by Subasinghe et al. (1989). In their model, Subasinghe et al. developed a model that gives an overall behaviour of the material on the screen without the need to describe the effects of the vibrating system. This model was developed using data collected from two different vibrating screens operated at varying parameters. Using Spottiswood & Kelly's, (1982) approach, Subasinghe et al. described the mass fraction retained for a given screen length using equation (20).

$$m_{iL} = (1 - P_i)^{n_T} \quad \text{Eq (20)}$$

Where n_T is the number of attempts of a particle to go through the aperture and P_i is the probability of passage of particles of size class i. Values of n_T were back calculated using the expression in equation (21).

$$n_T = \frac{ln(m_{iL})}{ln(1 - P_i)} \quad \text{Eq (21)}$$

The probability of passage P_i was given by equation (22).

$$P_i = \frac{[(\mathrm{L_A} + t)cos\theta - t - d_i](\mathrm{L_A} - d_i)}{(\mathrm{L_A} + t)^2 cos\theta} \quad \text{Eq (22)}$$

$\mathrm{L_A}$ is the screen aperture size and t is the screen wire thickness, whilst θ is the screen's angle of inclination. The values were plotted against the particle to aperture ratio at various screen lengths (L= number of apertures) as shown in Figure 2-4.

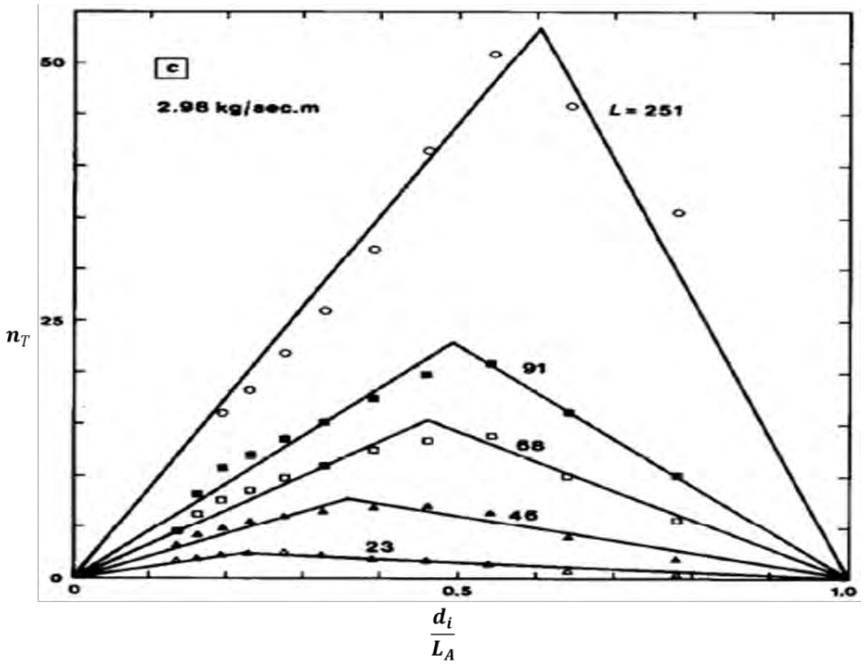

Figure 2-4 Plot of number of attempts of passage verse $\frac{d_i}{L_A}$ at different screen lengths (Subasinghe, et al., 1989).

From Figure 2-4 two constants (K_1 and K_2) were realised of the form shown in equation (23).

$$n_T = \mathrm{K_1}\frac{\mathrm{d_i}}{\mathrm{L_A}} \qquad \text{For } \frac{\mathrm{d_i}}{\mathrm{L_A}} < \left(\frac{\mathrm{d_i}}{\mathrm{L_A}}\right)_{\mathrm{t}}$$
$$n_T = \mathrm{K_2}\left(1 - \frac{\mathrm{d_i}}{\mathrm{L_A}}\right) \qquad \text{For } \frac{\mathrm{d_i}}{\mathrm{L_A}} > \left(\frac{\mathrm{d_i}}{\mathrm{L_A}}\right)_{\mathrm{t}} \qquad \text{Eq (23)}$$

Where $\left(\frac{d_i}{L_A}\right)_t = \frac{K_2}{K_1+K_2}$ $K_1, K_2 > 0$

K_1 and K_2 are gradients of the lines in Figure 2-4 and meet at the transition point $\left(\frac{d_i}{L_A}\right)_t$. Subasinghe et al defined the gradients as:

$$K_1 = c_1(L)^{\tau_1} \quad \text{and} \quad \mathrm{K_2} = \mathrm{c_2(L)^{\tau_2}} \qquad \text{Eq (24)}$$

Where c_1, c_2, τ_1 and τ_2 are empirical constants defining the systems. Equation (25) was obtained by combining the equations (20), (21), (23) and (24).

$$ln\, E_{oiL} = c_x(L)^{\tau_x}\left(1 - \frac{d_i}{L_A}\right) ln(1 - P_i) \qquad \text{Eq (25)}$$

An equation to evaluate screen performance without taking into account the initial feed conditions but predict results for different particle size distribution at various screen lengths and systems ($x = 1\ or\ 2$).

The model shows that screening operation depends mainly on the particle to aperture ratio and that the sharpness of separation depends on the screen length. However, this empirical model was developed for dry screening operations and it does not give insight on the screening mechanism in relation to wet screening.

2.5.2.7 Mahonty et al. (2003) Model

Mahonty, et al., (2003) developed an empirical wet screen model that can be used to predict the partition curve from coal screening operation using a pansep linear screen. The model shown in equation (26) was developed using linear regression method using the Karra (1979) model as a basis.

$$E_{oi} = 1 - \frac{1}{\{1 + exp[-c(a - d_i)]\}^{\alpha}} \qquad \text{Eq (26)}$$

Where c and α are fitted constants.

To develop this model, Mahonty et al., conducted experiments on a linear screen using the conventional setup (Karra 1979; Rogers & Brame 1985; Trumic & Magdalinovic 2011). The test works were conducted on the 180 x 400 um, 100 x 400 um and 50 x 150 um aperture sizes with respective cut sizes targets of 250, 150 and 45 microns. Even though these effects were observed, the developed model has constant exponents specific to ore type used. The model has not been tested using other linear screens of different capacity and aperture size using a different ore type is not proven. Though the study stressed the importance of feed rate, volumetric flow rate, screen linear speed and spray angle on the performance of the linear screen, the study could not demonstrate how sensitive the model is to variations in these factors. More importantly, the model was developed for a linear screen, this screen design and screening mechanism is significantly deferent from the vibrating screens.

Modeling approaches using physical scenario simulations with aid of a computer programs such as DEM have been attempted. Using DEM, the

manner in which particles flow on a vibrating banana screen have been studied using different range of vibrational frequency to investigate its effect on screen performance (Cleary et al. 2009; Chen & Tong 2010). Cleary, et al., (2009) investigated the effect of particle speed on the screen in relation to screen efficiency. This study showed that fast flowing particles, induced by high vibrational frequencies, produce a loosely expanded bed on the screen panel. Due to high particle velocity on the screens, the residence time of particle on the screen and the probability of passage for the particles through the aperture is greatly reduced and consequently the efficiency. As a limitation, Cleary, et al., did not validate this scenario with real life screen operations. Chen & Tong (2010) also studied the influence of vibration frequency, amplitude and angle on the performance of the screen and the observations are in agreement with that of Cleary, et al., (2009). The work showed that at a given screen angle, screening efficiency increases with vibrating frequency to around 60% (Figure 2-5) after which the efficiency reduces as the frequency increases. In a similar manner, the screening efficiency increased with amplitude to around the same value after which efficiency reduced with further increase in vibration amplitude. The study further showed that angle of vibration has less influence on the screen performance as compared to frequency and amplitude.

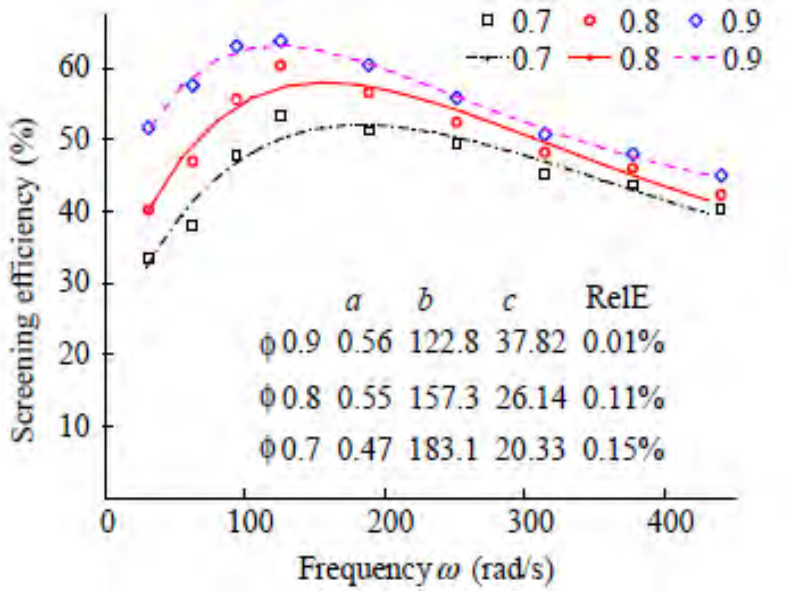

Figure 2-5 Influence of vibration frequency on screen efficiency (Chen & Tong, (2010))

Cleary, et al., (2009) and Chen & Tong, (2010) through their DEM simulation studies have shown just how important vibration parameters are for effective and efficient screening operation. Thus, vibration effect should have some influence on the partition properties. However, DEM simulations have not showed the influence of vibration on the partition curve properties explicitly.

2.6 Discussion

Literature has shown that screening efficiency is dependent on many variables. These variables can be grouped into operational and design variables. Design variables include vibration amplitude, vibration frequency, vibration mode, angle of inclination, aperture type and aperture shape. Design variable will not affect screening operation in a routine plant operation because they are mostly constant for a particular screen, but are important factors in screen design and selection (K. J. Dong et al. 2013; H. Dong et al. 2013). Operation variables include feed rate, feed solid concentration, feed particle size distribution, ore density, and ore type. Thus, for any reasonable prediction, a model should therefor include the influence of some of these factors.

A number of screen models have been developed. The basis for most of the developed screen models has been that the feed fraction of a given size class change along the screen length. In the development process,

proportionality constant related to the model has been determined experimentally. Most of the model formation involved the probability of particle passage through the screen aperture. Literature has shown that in developing the screen models, the device can be considered as a rate process unit. Using the probability approach one can determine how the operating and design variable influence the performance as indicated by the partition curve properties.

2.7 Project aim

Despite all these models existing with very good predication of screen performance on the data that they were developed on, most models have limitations with regards to predicting performance outside the conditions developed on. There is no data available for fine wet screening for apertures from 150 um down to 45 um. The screen theory to help in developing mechanistic models that can be universally used is still in its infancy evidenced from the large number of existing empirical models. Even models that had their initial development stage mechanistic, their end results have been empirical.

This study primarily aimed at developing a screen partition model that is able to predict screen performance taking into account condition changes in the operation of fine wet vibrating screen. The modelling aimed at providing a set of equation(s), with satisfactory physical meaning of the process to give a reasonable fit to any specific data set. The model can be systematically adjusted to provide meaningful performance expectations over a broad range of screen configurations and operating conditions.

The secondary objective was to generate a fine wet screening data set through experiments that will provide meaningful insight on the performance of a wet vibrating screens for particle size below 600 um and apertures size ranging from 45 – 150 um.

2.8 Hypothesis

To guide this work, it was hypothesised that;

- For fine wet screening operations, increased feed water content and reduced feed rate result in improved screen efficiency. This is because water supplied in sufficient amounts efficiently transmits the undersize to the undersize stream at relatively low feed flow rates.
- For the same operating conditions, screen performance will improve with increasing aperture size. This is because coarser aperture sizes come with increased open area a factor that enhances particle passage.
- Fine wet screen performance can be modeled using the partition curve approach because passage of different sizes have unique probability of passage under certain conditions.

2.9 Key questions

To achieve the objectives and test the hypotheses the following questions were developed.

- How does the feed rate affect the partition curve properties?
- How does the feed solid concentration affect the partition curve properties?
- For the same feed conditions, how does changing aperture size affect the partition curve properties?
- Using operating variables, can a partition curve equation be structured to describe the fine wet screen performance?

CHAPTER 3: APPARATUS

3 Experimental apparatus

3.1.1 Derrick screen

A Derrick screen pilot plant was used to perform experiments in this work. There are several vibrating screen manufacturers on the market who cater for different applications in different industries, of which Derrick Corporation and Weir Mineral are known to manufacture and supply screens for fine wet screening in mineral processing.

Derrick screens have found wider application in the fine wet screening processes. This is because of their improved screen operation principle that employs high frequency vibration at low amplitudes. The Derrick screen design requires low installation space for higher throughputs than most conventional screens. The Derrick screen panels come with high wear resistance urethane (Figure 3-1) panels that have extended panel life resulting in low operation and maintenance costs. Operation costs are reduced due reduced down times that used to be experienced with higher wear rate wire woven panels.

Figure 3-1 Single deck Derrick screen installed at Mintek

In addition to stacking the screen decks one on top of the other for improved capacity, each deck has two screen panels in series (Figure 3-1). Separation starts immediately after the material is introduced onto the first screen panel. Approximately midway through the first panel, most of the water would have percolated through leaving almost half of the screen just covered with high solid concentrated slurry. Figure 3-2 shows the pilot plant in operation during experiments performed at low flow rates and feed solids concentration of around 50 $wt\%$.

Figure 3-2 Slurry feed through the first panel

At this point, separation is minimal and the slurry still contains a significant amount of fines that can be misdirected to the oversize unless water is added. The slurry falls onto a rubber-lined trough before it is introduced onto the second panel. Water is added through sprays distributed along the length of the trough in order to repulp the material. The spray water rate can be regulated by means of a valve. The spray water facilitates continued separation to improve separation efficiency as the diluted slurry travels along the length of the second panel allowing the fines that are able to go through the aperture to do so. The screen oversize and undersize products then collect in two separate streams before reporting to a common sump for recirculation.

Other equipment used in this thesis were buckets for sampling and sample storage, standard laboratory filter pots for sample filtration and an oven for sample drying. A rotary splitter was also used for sample splitting down to manageable sizes as well as a scale for sample weighing. The Malvern Mastersizer 2000 was used for particle size distribution analysis.

3.1.2 The derrick screen rig and operation

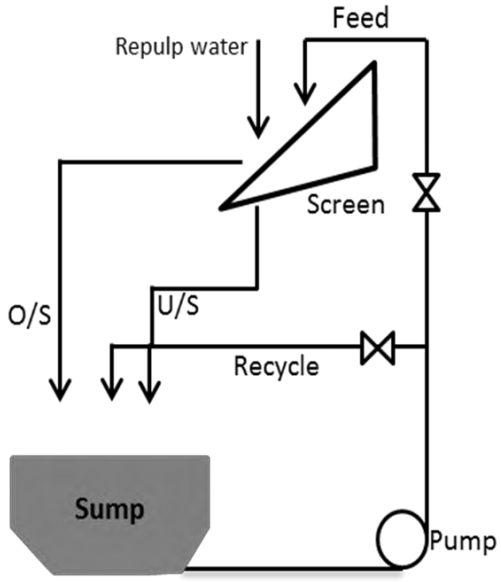

Figure 3-3 Screen rig schematic and setup picture

The test rig used in the experiment was set up at Mintek as shown in the schematic in Figure 3-3. The test plant set up consisted of two motorised units, the pump and the screen, and one sump with a feed-recycle pipe network. The circuit operation involved pumping the slurry mix from the sump to the screen surface. After separation, the undersize and the oversize are collected through separate chutes and recombined in the same sump. The sump has a volume capacity of 600 litres with a drain valve before the fixed speed pump. The flow rate was controlled using manually operated valves on the recycle and feed line valves.

The screen deck has two panels that are easy to change or replace. In this thesis, varying screen aperture sizes were used. The aperture sizes studied were 45 micron, 75 micron, 106 micron and 150 micron. Each panel had a percentage open area of 28, 30.8, 35.8 and 34.5 respectively. Each panel had a length of 0.711 meters and width of 1.080 meters. The rig ran with two panels at any instant giving a total panel area of 1.54 square meters. The rig is operated with a fixed speed pump that ran at its highest capacity. Due to limitations of the pump volumetric flow, high dry tonnes flow rates were not attainable at low feed percent solids because they required very high volumetric flows. The pump ran as high as 36 m^3/h. This equates to 37 tph at 60 $wt\%$ solids and 13 tph at 30 $wt\%$ solids. This allowed only two flow rates

at 30 $wt\%$ solids concentration. This pilot plant design is a well-accepted procedure in the field and has been used by other authors (Karra 1979; Ferrara et al. 1987; Trumic & Magdalinovic 2011) for similar studies.

CHAPTER 4: METHODOLOGY

4 Methodology

4.1 Introduction

The purpose of this chapter is to provide a description of the experiments performed to collect data for model development and validation, which is the main outcome of this thesis. A lot of care is required when data are collected for model development. The data was required because the findings from various researchers considered in the literature survey gave results for data whose aperture sizes were coarser than the sizes looked at in this thesis.

4.2 Objective

The objective of the experimental work was to collect data for model development and validation. To achieve the prescribed objective, tests were performed with the screen operated at different aperture sizes, different feed flow rates and different feed solids concentration

4.3 Sample preparation

The sample used was a UG2 and chromite ore blend. The chromite ore had an 80 percent passing 75-micron particle size distribution and did not require further size reduction for the experiments. The actual particle size distribution for the chromite ore was not measured but the d80 value was given as supplied by Mintek. The UG2 ore was visually very coarse and was crushed using a short head cone crusher (Figure 4-1) and screened to minus 600 µm size range.

Some 800 kg of screened UG2 ore and 1070 kg of chromite ore were blended using a mechanical blender as shown in Figure 4-1. The two ore types were emptied into the blender hopper at the same time. The mechanical blender allowed spreading the ore thinly on a flat concrete bay for easy mixing. The blend was further mixed with shovels after which cone and quartering was used to apportion the sample into different lots.

Figure 4-1 Sample preparation

Sampling across randomly selected cones was conducted to check for consistency in particle size distribution across the different lots. Five different cones were selected randomly across the bay and three different sub-samples were collected from each of these for particle size distribution measurements. The results in Figure 4-2 show that the blending was satisfactory and produced a similar particle size distribution from the randomly selected portions. The blended ore sample was then packaged in small pockets of masses ranging between 45 and 50 kg for easy handling during experiments.

The aim of this experiment was to generate the data for use in model development and validation. The variables considered included screen aperture size, feed solids concentration and feed flow rate. To ensure that the model development was robust, the minimum and maximum points taken were at the lowest and the highest possible values that the system can handle in terms of feed $wt\%$ solids and feed volumetric flow rate.

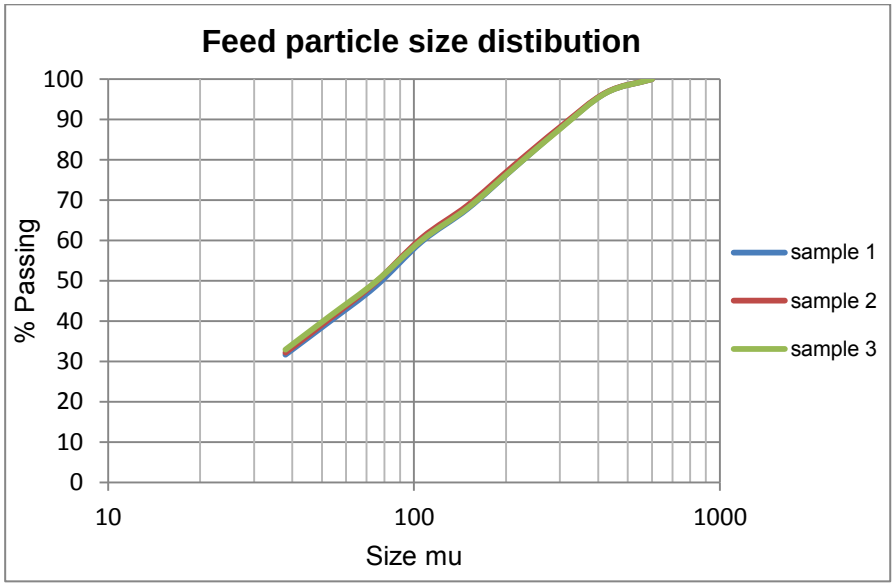

Figure 4-2 Feed particle size distribution

The key performance variables were varied using four different apertures to assess their effect on the efficiency of the screen. The matrix of the experimental variables is discussed in the next section.

4.4 Experimental matrix

Due to lack of fine wet screen data and a large number of permutations needed to cover the range of operating conditions for the screen variables chosen, a full factorial experimental design was used to carry out the test work. When choosing the experimental variables, the pump capacity influenced the choice of the feed flow rate range chosen to a greater extent than did screen area. The feed solid concentration was chosen for a range that is more realistic in everyday plant practices. The ranges were 9 to 35 tph for the feed flow rate and 30 to 60 $wt\%$ solids for the feed solids concentration. The full factorial experimental design is shown in Table 4-1 for each aperture size.

Table 4-1 Experimental Matrix

Run	1	2	3	4	5	6	7	8	9	10	11	12	13	14	15
Rate (tph)	35	30	25	19	13	25	19	13	9	19	16	13	9	13	9
wt% solids	60	60	60	60	60	50	50	50	50	40	40	40	40	30	30

The matrix in Table 4-1 shows the order in which the experiments were performed. The runs were not randomised due to sump capacity limitation and time, and material constraints. This is because the procedure involved adding water to the sump every time a sample was taken, an effect which could have meant either diluting or concentrating the slurry every time a new random condition was to be tested. Logistically, it was more efficient to start with a high concentration slurry and slowly dilute it as samples were taken. The variables shown in Table 4-1 were used for all four aperture sizes tested.

4.5 Test Procedure

4.5.1 Operation of Rig

At start-up of the experimental procedure a predetermined amount of water was fed into the sump. Compressed air was introduced into the sump in order to prevent settling once ore was added. One pocket of pre-packed sample bag was emptied into the sump. The recycle line valve and feed line valve were both set to half open. The screen was switched on. The fixed speed pump was then started and the rest of the remaining pre-weighed sample were added to make up the slurry to the required solids concentration after which the compressed air supply was discontinued. Using half sump capacity as a starting point gave enough room for spray water addition to the sump and make up water when dilution was required at change of feed solids concentration. The system was allowed to run for about 15 to 20 minutes to allow for conditioning and steady state to be achieved. Conditioning allowed for the sample to properly get mixed and stabilize the system before sampling could commence. The water line feeding the sprays on the screen was opened and set to a fixed volumetric flow rate of 20-litres per second (l/s). This was enough to allow repulping of the slurry in the trough before the material traversed the second panel.

The spray water was only turned on during sampling. Apart from preventing excessive dilution of the slurry in the sump during each set experimental run, sampling with spray water running simulated normal screen operation conditions. A period of four seconds was allowed from the time spray water was introduced to sampling the oversize and undersize samples. The time

was adjudged to be sufficient for the water to have produced a well-mixed slurry across the entire length of the second screen panel.

During operation, water was added every time a sample was cut and the feed in the sump gradually got diluted. Thus, to maintain the solids concentration, constant monitoring was done by cutting a sample from the recycle line to check the solids concentration using a 1 litre can and weighing to get the pulp density. Dry sample ore was added if a significant reduction was noted from the measurements. Using this procedure ensured that sampling was performed at a fairly constant feed solids concentration. Sampling was then performed using the procedure described in the next section. The shutdown procedure involved switching off the pump and turning on the compressed air line in the sump before shutting down the screen.

4.5.2 Sampling

Before sampling could start, the observed variables had to be adjusted to the required conditions. The feed flow rate was adjusted using the feed and recycle line valves and the installed flow meter. Prior to all this, the correct apertures size panels would first be installed. Once the solids concentration and the feed flow rate were set to the required conditions, spray water was introduced after which sampling was undertaken. Samples were taken simultaneously from the oversize and undersize streams using buckets. The entire streams were diverted into the sampling buckets and time taken to sample was recorded for flow rate calculation. After cutting the oversize and undersize samples, the spray water supply was discontinued. For each set value of solids concentration, a feed sample was taken from the recycle line while the feed line valve was closed. This made cutting of the feed sample easier and avoided compromising the sample quality. This procedure was repeated for each aperture size.

4.5.3 Sample processing

Processing of the sample involved weighing the sampled material to obtain wet weights prior to filtering. The samples were then filtered and left in ovens to dry overnight The dry samples were then weighed to obtain the dry solid mass and water mass. The dried samples were de-lumped using steel rods

and screening through a 1 mm sieve before the bulk samples were split down to packets of masses ranging between 200 and 300 grams. The split samples were packaged and stored in preparation for particle size analysis.

Sizing of the samples was done using a Malvern particle sizing instrument called the Mastersizer 2000 (Rawle & U. K. 2003). For this exercise, the split sample was emptied in a stirred beaker with water in it for thorough mixing. A sample of about 3 ml was carefully sampled and added to the sample dispersion unit. The measured results were used to generate partition numbers and plotted as presented in the next chapter.

CHAPTER 5: RESULTS AND DISCUSSION

5 Results

The chapter focuses on the results obtained from experiments. The results of the experimental procedure given in Chapter 4 are given. The analysis of these results was performed to prepare the results for modeling which is the main focus of this study. The discussion of results is mainly concerned with factors contributing to the modeling of fine wet screens.

5.1 Raw data obtained from experiments

The raw data obtained from each of the test included the feed mass flow rate, the flow rate of the oversize and the undersize. It also included the feed solids concentration, the solids concentration of the oversize and undersize streams, the particle size distribution of the feed, oversize and undersize. Table 5-1 shows an example of the mass flow data obtained from each test.

Table 5-1 Mass flow results for 106 um aperture at 50wt% solids

Flow results				
Flow meter rate (t/h)	Sample	feed rate (t/h)	o/s rate (t/h)	u/s rate (t/h)
25	A	23.84	12.96	10.88
	B	26.97	14.69	12.28
19	A	19.73	9.03	10.71
	B	19.89	7.76	12.13
13	A	17.19	7.10	10.08
	B	12.29	2.22	10.07
9	A	12.40	4.52	7.89
	B	10.16	1.78	8.39

The first column of Table 5-1 shows the set feed flow rates, whilst the second column shows the sample type row of either the A sample or the B sample. The actual feed rate is shown in the third column which is the sum of columns 4 and 5, the oversize and undersize mass flows respectively. Table 5-2 shows the feed distribution data for the feed stream, undersize stream and oversize stream at various feed rates at a feed solid concentration of 50 $wt\%$ presented as percent passing.

Table 5-2 Particle size distribution data for 106 micron aperture 50wt% solids

Sieve	Feed	25 tph u/s	25 tph o/s	19 tph u/s	13 tph u/s	13 tph o/s	9 tph u/s
850	100.0	100.0	100.0	100.0	100.0	100.0	100.0
600	99.9	100.0	100.0	100.0	100.0	100.0	100.0
425	99.4	100.0	99.8	100.0	100.0	99.8	100.0
300	98.9	100.0	98.9	100.0	100.0	98.9	100.0
212	93.6	100.0	97.6	99.3	100.0	97.6	100.0
150	84.3	100.0	68.8	97.3	99.3	73.5	99.1
106	74.6	96.7	56.1	92.7	94.9	55.0	94.0
75	65.5	89.5	46.4	85.3	87.6	43.9	85.6
53	57.1	80.5	40.4	75.4	76.3	37.1	75.3
38	49.0	68.7	35.6	64.5	66.1	32.7	64.3
25	39.2	56.5	31.2	50.7	53.0	27.7	50.7
20	34.5	49.4	28.7	43.9	46.6	25.3	44.1
15	29.1	41.3	25.5	36.4	39.1	22.3	36.8
10	22.7	32.4	21.6	27.8	30.6	18.7	28.3
7	18.0	25.5	18.3	21.7	24.2	15.7	22.2
5	14.1	19.6	15.1	16.8	18.8	12.9	17.1
3	9.0	13.1	10.8	10.7	11.6	8.7	10.7
2	5.8	8.4	7.4	7.0	7.3	5.8	6.7
1.5	4.0	5.7	5.2	5.1	4.9	4.1	4.6
1	2.2	3.0	2.9	3.2	2.6	2.2	2.4
0.75	1.2	1.5	1.5	2.1	1.3	1.2	1.3
0.5	0.0	0.0	0.0	1.0	0.0	0.0	0.0

5.2 Mass balancing

Prior to performing any analysis, the data was subjected to mass balancing. Mass balancing was done on both solids and water in order to provide information on how the feed splits to the two streams. Table 5-3 shows how the material split to each stream with the feed solid concentration set at 60

$wt\%$ on a 106 micron aperture for the A sample. The measured feed solid concentration at the set conditions after drying the feed sample was found to be 58 $wt\%$ solids. However, the reconstituted feed solid concentration from the two product streams was found to be around the set value of 60 $wt\%$ solids. Table 5-3 gives an example of mass balanced size distribution numbers for the product stream at different set feed rates.

Table 5-3 Mass balanced particle size distribution for 106 micron at 60wt% solids

Size	Balanced	Actual	Balanced	Actual	Balanced	Actual	Balanced	Actual	Balanced	Actual	Balanced	Actual	Balanced	Actual	Balanced	Actual	Balanced	Actual
	Feed		U/S tph		O/S tph		U/S tph		O/S tph		U/S tph		O/S tph		U/S tph		O/S tph	
			10.63	11.38	20.28	19.54	10.30	12.28	18.08	16.10	8.30	8.99	14.53	13.84	4.89	6.20	8.00	6.69
1400	0.01	0.02	0.01	0.00	0.01	0.00	0.01	0.00	0.01	0.00	0.01	0.00	0.01	0.00	0.01	0.00	0.01	0.00
1000	0.01	0.02	0.01	0.00	0.05	0.04	0.01	0.00	0.03	0.02	0.01	0.00	0.01	0.00	0.01	0.00	0.01	0.00
850	0.01	0.01	0.00	0.00	0.07	0.07	-0.01	0.00	0.14	0.15	0.00	0.00	0.00	0.00	0.00	0.00	0.00	0.00
600	0.04	0.05	0.01	0.00	0.36	0.35	-0.06	0.00	0.98	1.04	0.02	0.00	0.14	0.11	0.00	0.00	0.22	0.21
425	0.24	0.40	0.16	0.00	1.42	1.26	0.01	0.00	2.36	2.35	0.19	0.00	0.35	0.15	0.15	0.00	0.60	0.45
300	0.77	1.19	0.50	0.08	4.75	4.33	0.35	0.03	3.62	3.30	0.59	0.00	0.81	0.22	0.36	0.03	2.71	2.38
212	2.50	2.32	0.49	0.66	31.39	31.57	0.01	0.43	16.91	17.33	1.12	0.03	2.64	1.55	0.13	0.31	11.38	11.56
150	3.95	3.88	3.43	3.51	11.42	11.50	2.59	2.04	7.24	6.70	1.86	0.09	5.11	3.34	0.49	0.91	18.53	18.94
106	6.10	5.93	6.07	6.23	6.50	6.67	5.61	5.54	7.19	7.13	2.99	0.84	13.35	11.20	2.79	3.16	19.46	19.83
75	7.99	7.86	8.22	8.34	4.66	4.78	8.13	8.13	6.48	6.48	7.26	7.35	16.20	16.29	7.70	8.10	10.33	10.73
53	9.05	9.04	9.44	9.45	3.54	3.56	9.61	9.54	5.61	5.54	9.90	10.79	10.24	11.12	10.67	10.87	3.86	4.05
38	8.91	8.88	9.30	9.33	3.41	3.44	9.55	9.49	5.07	5.01	10.91	12.59	6.34	8.01	11.00	11.43	2.97	3.40
25	10.67	10.54	11.11	11.24	4.36	4.50	11.32	11.32	6.47	6.47	14.78	18.40	6.58	10.19	13.90	15.02	3.22	4.34
20	5.24	5.14	5.43	5.53	2.46	2.56	5.58	5.70	3.63	3.76	5.45	5.58	3.09	3.22	5.84	5.77	2.22	2.16
15	6.16	6.05	6.36	6.47	3.18	3.29	6.53	6.69	4.46	4.61	6.56	6.88	4.00	4.31	7.04	7.12	2.68	2.76
10	7.57	7.46	7.81	7.93	4.15	4.27	7.92	8.07	5.95	6.10	8.40	9.11	5.46	6.18	8.84	9.11	3.53	3.80
7	5.70	5.57	5.87	6.00	3.37	3.51	5.92	6.08	4.77	4.93	6.06	6.43	4.49	4.86	6.37	6.45	2.93	3.01
5	4.88	4.82	5.01	5.07	3.14	3.20	5.04	5.11	4.14	4.21	5.09	5.28	4.11	4.30	5.30	5.25	2.72	2.67
3	6.42	6.35	6.56	6.63	4.36	4.42	6.60	6.67	5.53	5.60	6.50	6.57	5.54	5.61	6.72	6.47	3.79	3.54
2	4.08	4.04	4.16	4.19	2.93	2.97	4.17	4.20	3.60	3.63	3.93	3.78	3.56	3.41	4.08	3.79	2.55	2.26
1.5	3.13	3.98	3.17	2.32	2.50	1.64	3.18	2.33	2.86	2.00	3.00	2.01	2.88	1.88	3.06	1.98	2.32	1.25
1	2.47	2.58	2.51	2.40	1.83	1.72	2.52	2.41	2.20	2.08	2.31	2.03	2.19	1.90	2.37	2.00	1.64	1.27
0.75	1.71	1.38	1.83	2.17		0.23	2.22	2.75	0.23	0.76	1.22	1.07	1.17	1.01	1.26	1.07	0.88	0.68
0.5	1.91	1.52	2.06	2.45		0.14	2.71	3.48	0.04	0.81	1.35	1.18	1.28	1.10	1.39	1.17	0.96	0.74

The first columns provide information about the particle size in the feed stream; the next two columns provide information about the undersize stream distribution whilst columns four and five provide information about corresponding distribution in the oversize stream. The columns that follow provide information as described above for the next set feed rate. For this data, the set feed rate were 35, 30, 19 and 13 tph respectively.

5.3 Partition Curves

It has been shown that the amount of material going onto a screen has a degree of impact on the performance of the screen (Rogers & Brame 1985; Valine & Wennen 2002). Valine and Wennen (2002), in their work showed that the feed rate greater than the determined screen capacity results in increased misdirection of fines to the oversize stream. Rogers & Brame (1985) performed wet screen experiments on aperture sizes ranging from 111um to 292um where they found that the feed rate had no significant influence on the performance of the screen provided the screen capacity was not exceeded. The works showed sharpness of separation and cut size values do not get affected by the feed rate change. To assess these effects partition curves have been used.

Partition curves are used to conveniently present the efficiency of a separation device on a size-by-size basis. The curve shows the percentage of a given size reporting either to the oversize or undersize in relation to the amount of that size in the feed. Thus, to assess the efficiency of the Derrick screen, test results were used to generate partition curves for each data set. In line with the variables considered in this work, partition curves properties were sought from the respective curves in order to assess the influence of every variation of the variable on screen efficiency. An example of the partition curve from experimental results is given in Figure 5-1.

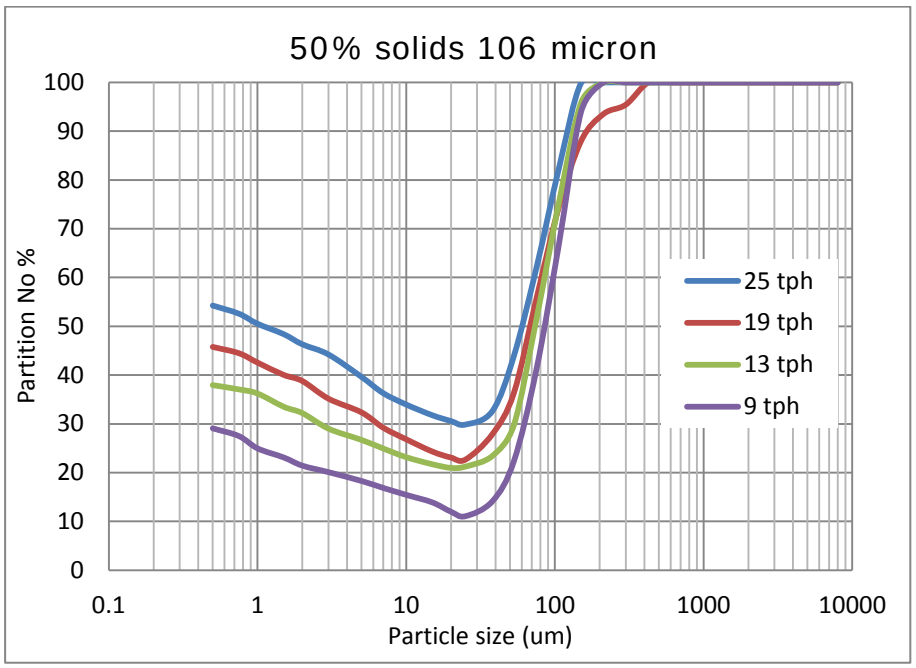

Figure 5-1 Screen partition curve for 106 um aperture at 50 wt% solids in feed

It can be seen that the partition curves exhibits a fish-hook behaviour. This behaviour has been observed in most fine classification works and reasons for this behaviour have well been covered (Austin & Klimpel 1981; Rogers 1982; Rogers & Brame 1985; Nageswararao 2000; Kraipech et al. 2002; Nageswararao & Medronho 2014; Kuang et al. 2014; Dueck et al. 2014). In this work, it is noted that the screen performance improves with reducing feed rate as seen in Figure 5-1. Figure 5-1 shows that as the feed rate increases, the amount of fines reporting to the oversize increases. This is supported by Table 5-3 where it is shown that the solids mass split to the oversize increases with increasing feed rate. This increase is coupled with the increase of the amount of water reporting to the oversize stream as shown in Table 5-3. This trend is general across different solids concentrations and aperture sizes. The distinguishing effects are that; as the solids concentration increases the fish-hooks increase in size for the same feed rate. However, for the same feed rate, the fish-hook effect decrease as the aperture size is increased from 45 microns to 150 microns.

For the same variables, screen performance was plotted for conditions at different feed solids concentration at a fixed feed rate. An example of the performance results is shown in Figure 5-2 for different aperture sizes at 13 tph.

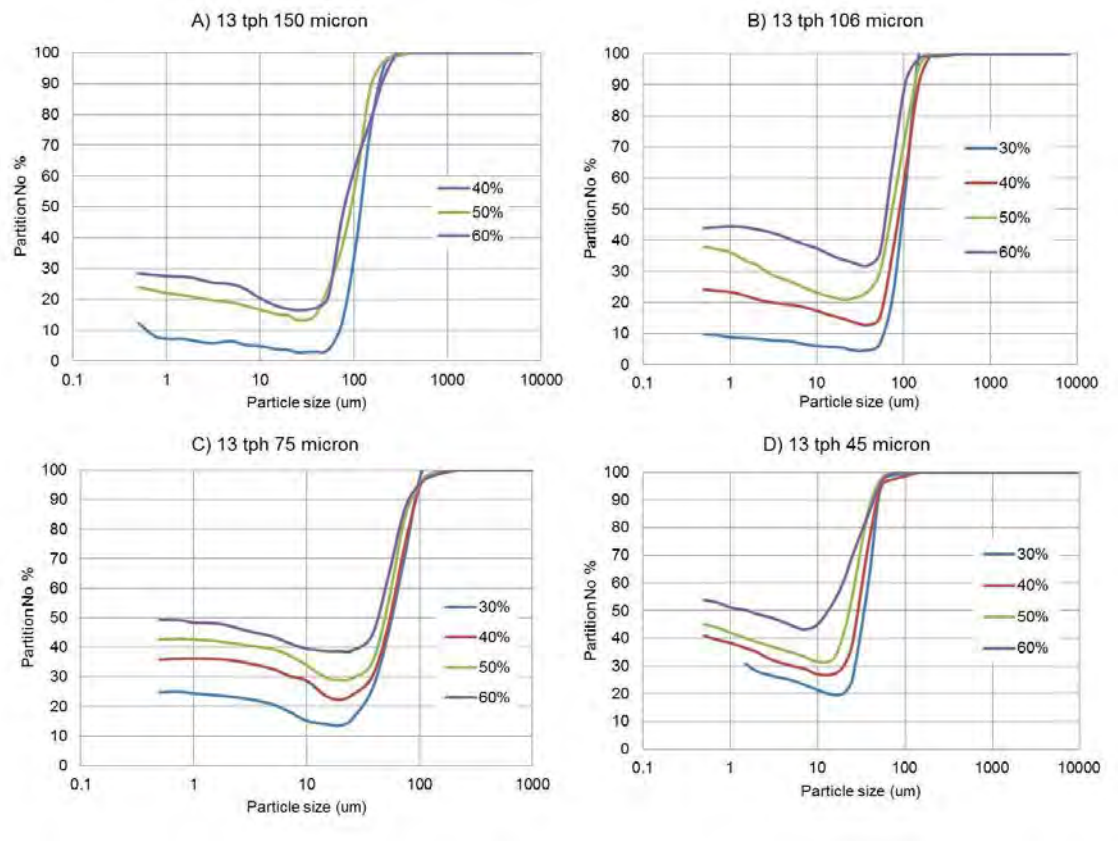

Figure 5-2 Screen performance at different aperture sizes

It can be observed that the feed solid concentration has a significant influence on the performance of the screen. There is an increased amount of fines reporting to the oversize stream at 13 tph as the $wt\%$ solids are increased from 30 to 60 for all four apertures sizes shown Figure 5-2. The amount of fines to the oversize stream is more pronounced at finer aperture size. This can be seen for example, at 40 $wt\%$ solids the fishhook rise from 12% to 41% in Figure 5-2 A through to D as the aperture size gets finer. There is also a curve shift to the left as the feed solid concentration increases, a result that affects the cut size and the sharpness of separation. To quantify the screen performance in a manner that gives performance indicator values, the partition curve properties are extracted from the curves in the next section using the Whitten model in equation (27) (Napier-Munn et al. 2005).

$$E_{oi} = 100 - C\left[\frac{\left(1+\beta\beta^{*}\frac{d_i}{d_{50c}}\right)(exp(\alpha)-1)}{exp\left(\alpha\beta^{*}\frac{d_i}{d_{50c}}\right)+exp(\alpha)-2}\right] \qquad \text{Eq (27)}$$

In equation (27), C is the water split ratio to the undersize stream, β is the fishhook parameter that represent the size of the hook at particle sizes finer than 45 micron known as beta and β^* is the maximum fishhook value attainable (equal to 1). The other variables are as discussed in Chapter 2. The partition curves were first corrected then reduced as shown in Figure 5-3 and Figure 5-7 respectively.

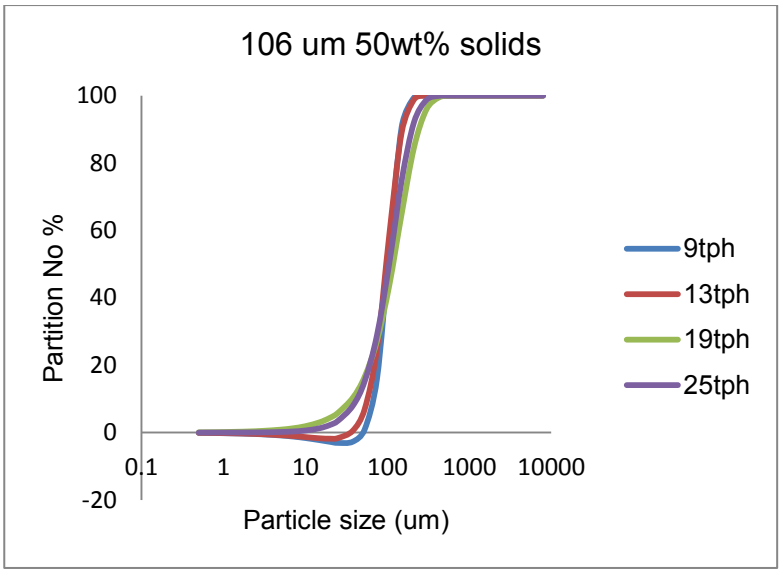

Figure 5-3 Corrected partition curve for 106 microns at 50 wt% solids

The trends observed in Figure 5-1 are still holding in Figure 5-3 where the curves shift to the left as the feed rate is increased. However, Figure 5-3 clearly shows the difference in the slope for each condition visually. The sections that follow quantifies the fine wet screen performance in relation to partition curve properties.

5.4 Influence of feed variables

The influence of feed rate on screen performance has been illustrated in Figure 5-1 and Figure 5-3. It can be seen that the curve shifts systematically with increasing feed flow rate and feed solids concentration affecting the cut size, the sharpness of separation and the water recovery to the oversize. As has been shown that the amount of material going onto a screen has a degree of impact on the performance of the screen (Rogers & Brame 1985; Valine & Wennen 2002); Valine and Wennen (2002), in their work explained that the feed rate greater than the determined screen capacity results in increased misdirection of fines to the oversize stream. To ascertain this for

model development, partition curve properties where extracted from the experimental data using the Whitten partition model (Napier-Munn et al. 2005). The model was fitted to the data where the partition curve properties such as the alpha, water split and beta were extracted. The influence of the feed on these properties is discussed in the next subsections. For this work, the particle size distribution was held constant for all test works due to scope limitations.

5.4.1 Influence of feed rate on cut size

A particle size value that corresponds to the 50% partition mark is referred to as the cut size value, most often as the d_{50}. It indicates the value at which separation occurs and is used as a screen performance indicator (Gupta & Yan 2006). This value correlates well with the sharpness of separation where a high value (closer to aperture size) indicates high performance and high sharpness of separation. Figure 5-4 shows a plot of the cut size against the feed rate. It is observed that as the feed increases from 13 tph to 35 tph at a feed solid concentration of 60 $wt\%$, the cut size value decreases on a 75 micron aperture. There is a sharp decrease when the feed rate is increased from 19 tph to 25 tph.

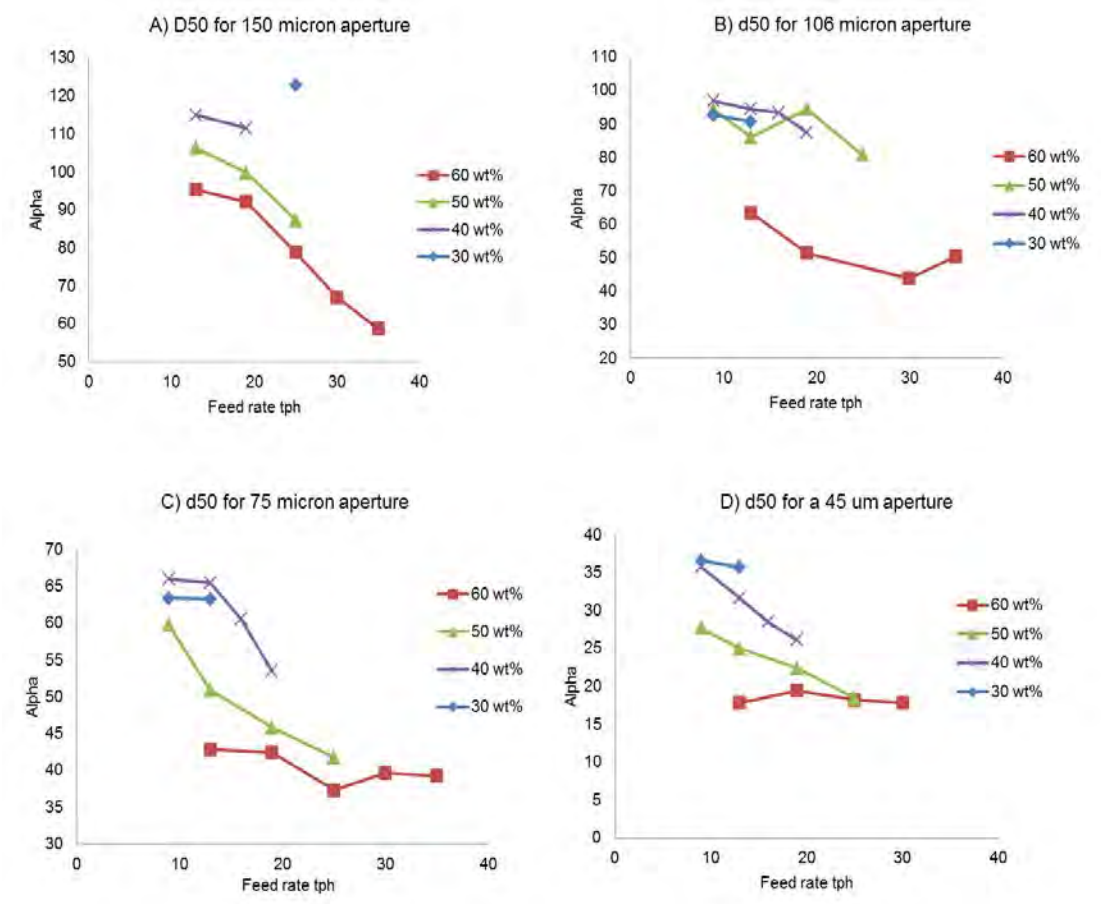

Figure 5-4 Influence of feed rate on cut size

Decreasing the feed rate from 13 tph to 9 tph and reducing the solids concentration, it can be observed in Figure 5-4 – C that the cut size value is stable at 30 and 40 $wt\%$ solids. The cut size decreased when the feed rate was raised from 13 tph and any further rate increase from the point forward showed reduced cut size value. This was observed both at feed solids concentrations of 40 $wt\%$ and 50 $wt\%$. The influence of feed observed on the 75 microns aperture is general across all the four apertures investigated as shown in Figure 5-4 – A through to D.

5.4.2 Influence of feed solids concentration on cut size

To ascertain the influence of the feed solids concentration a plot of the cut size against the concentration was constructed in Figure 5-5 on a 45 micron aperture for feed rates of 9 tph through to 19 tph.

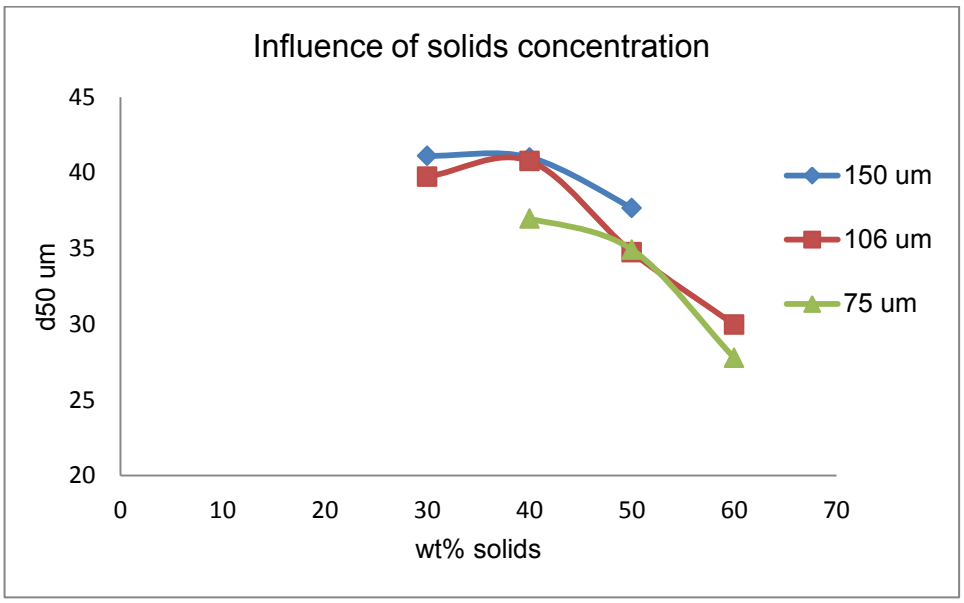

Figure 5-5 Influence of solids concentration on cut size at 45 micron screen aperture

In Figure 5-5, it is observed that the cut size gets finer as the solids concentration increases indicating poor screen performance. The cut size decrease is sharper as the solids concentration increases beyond 40 $wt\%$ solids in feed for all the feed rates shown. This shows that the feed solids concentration has a significant influence on the performance of the screen. Even though in Figure 5-4 results have shown decreasing cut size with increased feed rate, the cut size decrease in Figure 5-5 is sharper with increased feed solids concentration.

5.4.3 Influence of aperture size on cut size

To assess the influence that the aperture size has on performance, experimental results are shown for the same feed rate at the same feed solids concentration at different aperture sizes in Figure 5-6.

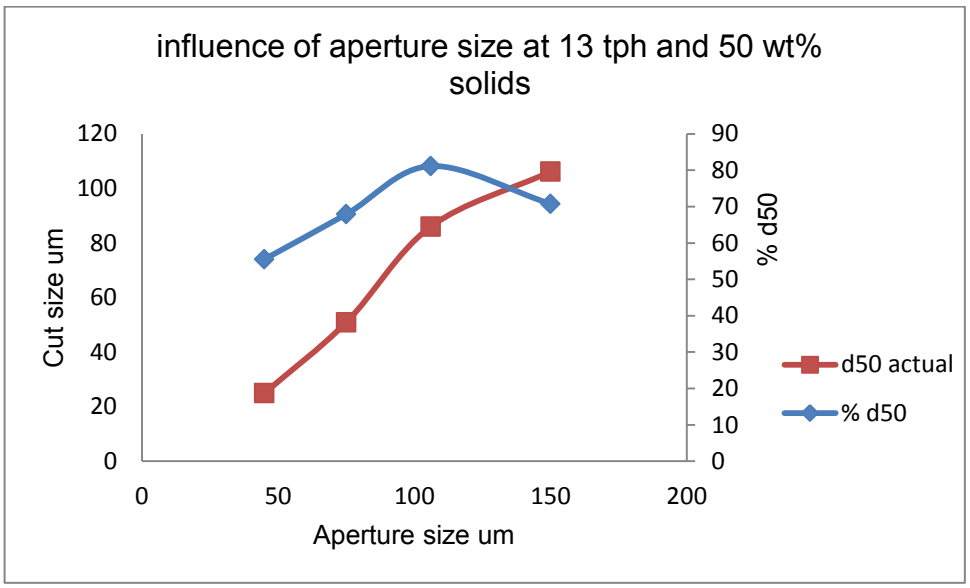

Figure 5-6 Influence of aperture size on cut size

Using a feed rate of 13 tph and a feed solids concentration of 50 $wt\%$ solids the results are plotted using two Y-axes. The red line is a plot of the primary axis on the left of the graph showing the actual cut size for each aperture size. It can be seen that the cut size increases with increasing aperture size. However, this is not a good indication because each cut size is relative to the aperture size used. To properly compare the influence of the aperture, the cut size are plotted as a percentage of the of the aperture size using the secondary axis where it is seen that; the cut size improves as the aperture size is increased from 45 microns to 106 microns for the same feed rate. As the size is increased from 106 microns to 150 microns, the cut size reduce. This is also observed from the actual cut size curve where the linear increase of cut size with aperture size is distorted at 106 microns aperture size. The reason of this behaviour at this stage is unclear.

5.5 Influence of feed variables on alpha

Sharpness of separation, designated by the symbol alpha (**α**), has been measured and reported in different ways. One of the common ways to measure sharpness of separation is to find what has been termed the imperfection (Wills & Napier-munn 2006), it describes the slope of the partition curve for particles sizes that correspond to the 25% and 75% partition marks. A steeper slope indicates high sharpness of separation. Because the partition curve is *S* shaped, the slope is usually determined as

an instantaneous slope tangential to the point taken from. It is usually taken along the region where the curve is mostly linear. For this work, to assess how the feed variables influence the sharpness of separation the alpha values were extracted from the partition curves by fitting the Whitten model to data. High alpha values indicate improved sharpness of separation and lower values indicate low sharpness of separation.

5.5.1 Influence of feed rate on the sharpness of separation

The corrected partition curves for a 106 micron aperture screen at 50 $wt\%$ solids are reduced and plotted for feed rate of 9, 13, 19 and 25 tph, and whose corresponding alpha values shown in Figure 5-7 are 4.4, 3.3, 1.6 and 1.8 respectively.

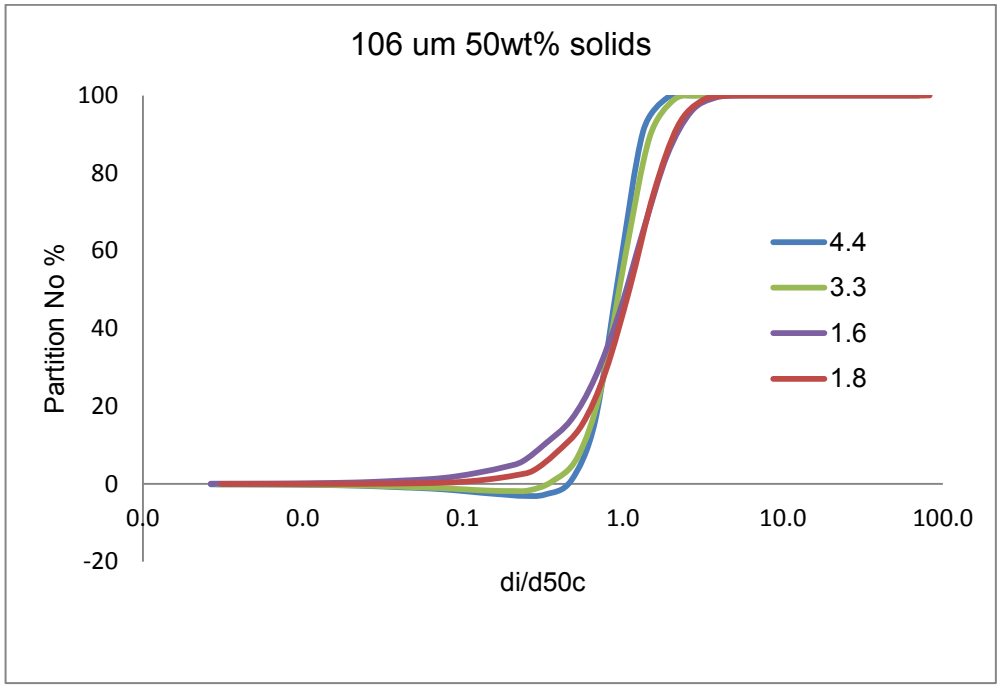

Figure 5-7 Reduced partition curve showing how alpha relates to sharpness of separation

From Figure 5-7 it can be seen that the sharpness of separation merges at as the feed rate increase from 19 to 25 tph where the sharpness of separation was both low and very close at 1.8 and 1.6 respectively. The sharpness initially reduced with increasing feed rate. The alpha results for the rest of the 106 micron aperture are plotted against the feed rate at different feed solids concentration in Figure 5-8.

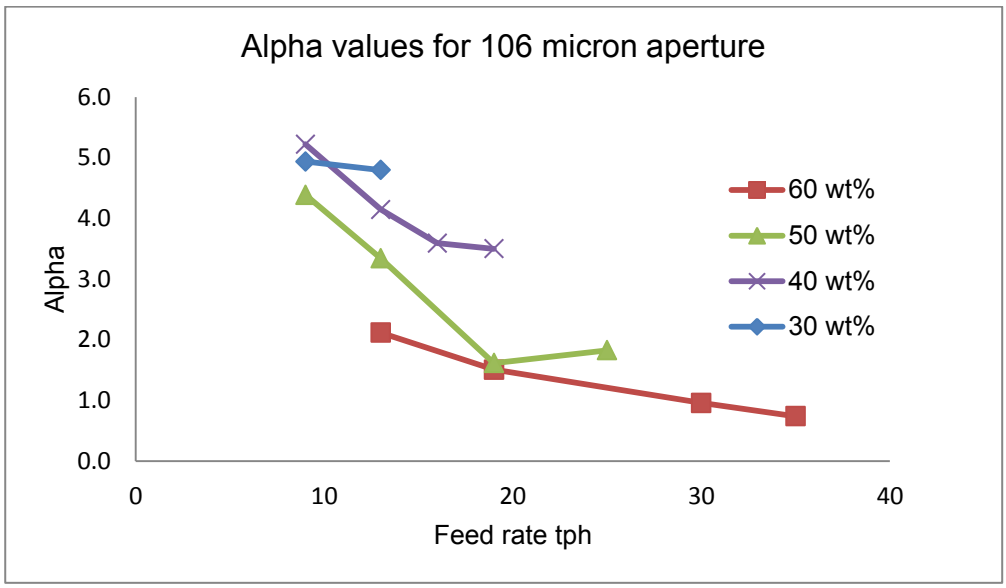

Figure 5-8 Influence of feed rate on alpha

The results show that there is a sharp decrease of the sharpness of separation as the feed starts to increase. A point is reached where a further increase in the feed rate has very little or no influence on separation sharpness. This point could be thought as the point at which the screen capacity is exceeded and any excess feed material bypasses to the oversize giving rise to increased fish hook size on the partition curve. This is the general observation across all the apertures used in this thesis.

5.5.2 Influence of feed solids concentration on alpha

The influence of feed solids concentration was assessed by plotting the alpha values at a specific feed rate against feed solids concentration. An example is shown in Figure 5-9 where the feed rates considered are 9, 13 and 19 tph on a 75 micron aperture size. For all the flow rates, results show a steady decrease of the alpha values as the feed solids concentration increased. When the feed concentration is increased beyond 50 $wt\%$ solids the curve becomes shallow for the 13 and 19 tph feed rates. The slope of the 19 tph curve is more shallow than 9 and 13 tph curves even though the 13 and 19 tph curve eventually merge at 60 $wt\%$ solids. This shows that increasing the feed solids concentration reduces the sharpness of separation. Just as seen in Figure 5-8, Figure 5-9 also shows there is a point beyond which the sharpness of separation is not affected with increasing feed solid

concentration. This effect can also be related to loading capacity of the screen as discussed earlier.

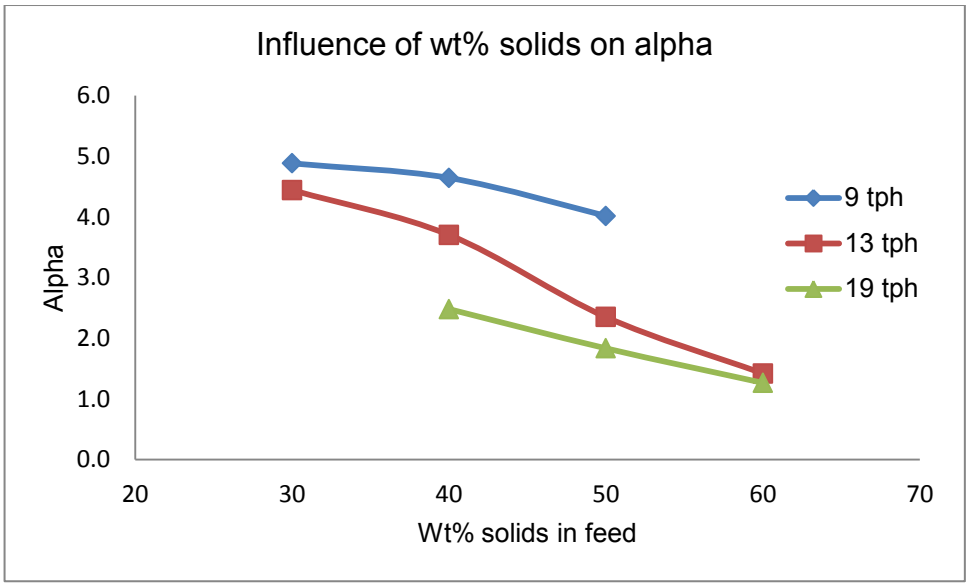

Figure 5-9 Influence of feed solids concentration on alpha at 75 micron screen

5.5.3 Influence of aperture size on alpha

The influence of aperture size on alpha was assessed by plotting the alpha for a specific feed rate at a specific feed solid concentration against the aperture size. An example is shown in Figure 5-10 where the plot was done at a feed rate of 13 tph and a feed solids concentration of 40 $wt\%$. Results show that as the aperture size increased from 45 microns through to 150 microns, the alpha values increased linearly. These results show that the coarser the aperture the sharper the separation.

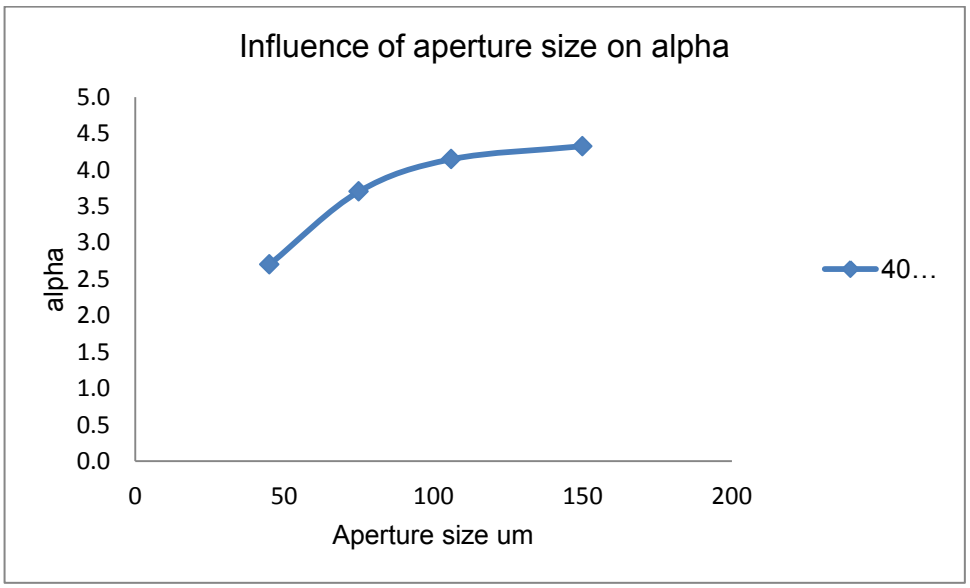

Figure 5-10 Influence of aperture size on alpha at 13 tph

For the same feed rate of 13 tph, the results are plotted at 40, 50 and 60 $wt\%$ solids against the aperture size in Figure 5-11.

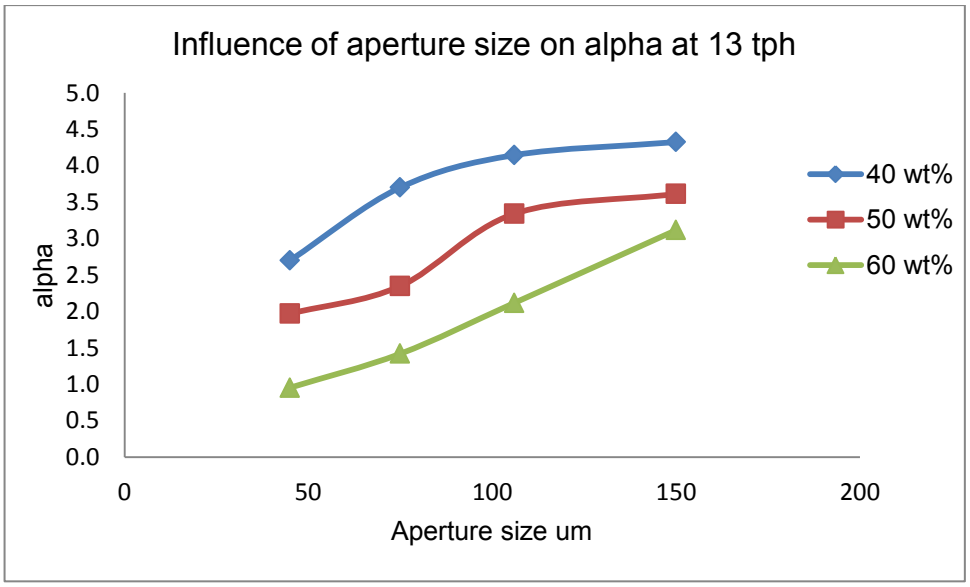

Figure 5-11 Influence size of aperture with varying feed solids concentration on alpha

Results generally show a linear relationship of the alpha values with increasing aperture size. The results also show that the alpha values decrease with increasing solids concentration a trend observed in Figure 5-9. This indicates that coarser screens have sharp separation at all conditions in comparison to the finer screens.

5.6 Influence of feed variables on water split

Wet screening performance, as seen from the above two sections, is primarily dependent on the amount of water in the feed (Valine & Wennen 2002). This makes the water recovery (water split) to the respective product stream an important performance indicator for a wet screen process.

5.6.1 Influence of feed rate on water split

Owing to this effect, an assessment of effect of the feed conditions on the oversize water split ratio was plotted in Figure 5-12. Results for a 13 tph feed rate are plotted for different apertures at a feed solid concentration of 50 $wt\%$. It can be seen that the fraction of water that reports to the oversize increases with increasing feed rate. The oversize water split ratio, however, is more for finer aperture sizes than it is for the coarser. At low flow rate, 9 tph in this case, the oversize water split ratio seemed larger for the 45 micron aperture but as the feed continued to increase, the water split ratio for a 45 micron reduced to slightly below that of the 75 micron aperture size. This could be due to errors during experiments, however, the trend still holds where an increased feed gave an increased oversize water split ratio.

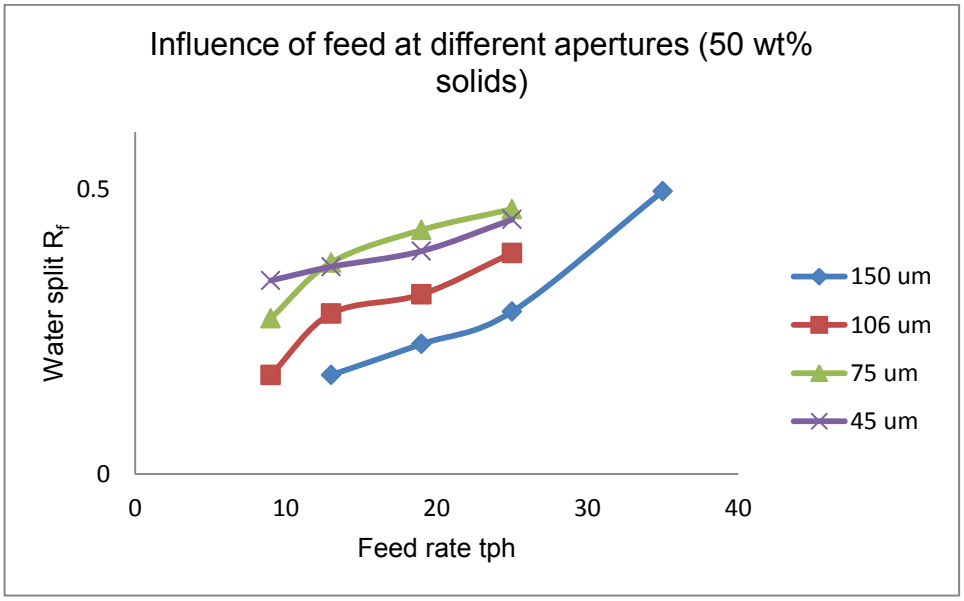

Figure 5-12 Influence of feed at different aperture sizes and at 50 wt% solids on water split

5.6.2 Influence of feed solids concentration on water split

Using the oversize water split ratio, an assessment of the effects of the values of the water split ratio were plotted against the feed solids

concentration at a specific feed rate and aperture size. An example is shown in Figure 5-13 where results for a 75 microns aperture size are plotted at feed rates of 9, 13, and 19 tph. The results show that as the feed solids concentration increases, the percentage of water that report to the oversize increases. The increase in the oversize water split ratio is more pronounced as the feed rate increase at the same feed solid concentration.

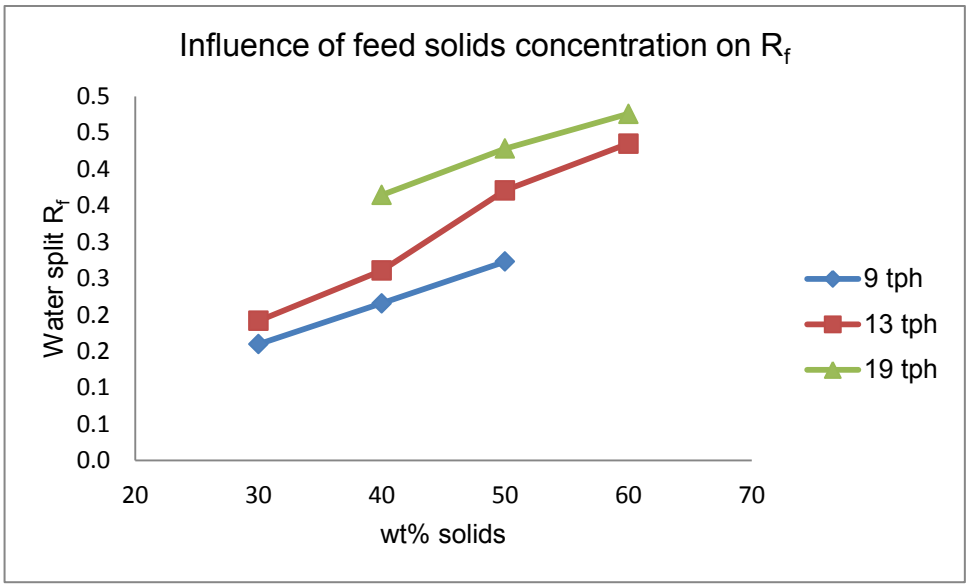

Figure 5-13 Influence of feed solids concentration on water split at 75 micron aperture

At this point, it can be deduced that, reduced solids concentration in the feed translates in improved screen performance and reduced fines carryover to the oversize stream. Water as it percolates through the pore spaces between the particles and the screen aperture drags with it the undersize particles (Valine et al. 2009). Due to the fact that water, in the slurry mixture, has the lowest viscosity, its percolation rate is relatively high (Valine et al. 2009) as compared to the undersize particles. Thus, as water is percolating, dragging undersize particles along, the undersize particles tend to lag behind in the percolation path. It can be postulated that, a point is quickly reached where the lagging particles are completely separated from the water. Because most of the water has gone through, the bed tends to shrink reducing the percolation path. The particles that lagged behind fill the pore spaces adhering to the coarse particles and any amount of water and fines that did not pass through are trapped and conveyed to the oversize stream (Valine et al. 2009). The effect appears to be more pronounced at 45 um aperture size

(Figure 5-12 and Figure 5-13) than at 150 um aperture size. This could be due to the fact that, as the aperture gets finer, an effect similar to filtration gradually takes effect when the screen load increase and feed water reduce. Thus, as has been suggested by many researchers (Rogers & Brame 1985; Nageswararao 1999b; Austin & Klimpel 1981; Valine & Wennen 2002), the amount of water in the feed is a vital variable and most importantly the split ratio to the two product streams. It has been reported that the amount of water split ratio to the oversize stream approximates the percentage recovery of fines to that stream (Austin & Klimpel 1981; Rogers & Brame 1985).

5.7 Influence of feed variables on beta

Beta is used to quantify the extent of the fishhook in the Whiten equation. It controls the initial rise of the hook in the partition curve. Results from this work exhibited the fishhook behaviour, to quantify this effect, the beta (β) parameter was extracted from the Whitten model.

5.7.1 Influence of feed rate on Beta

The influence of feed rate on beta is shown in Figure 5-14 where plots A, B, C and D corresponds to aperture sizes of 150, 106, 75 and 45 microns respectively. Generally the beta value increase with increased feed rate. Figure 5-14 – A shows that the beta value higher at increased feed solids concentration. This signifies an increased fishhook. Figure 5-14 – C and D show that at feed concentration of 60 $wt\%$, the beta values reduces to zero. This behaviour is not expected and there is no proper explanation as to why this is the case. However, one can postulate that the fishhook rises are too high for the Whitten Beta parameter to quantify. Partition results showed increased fishhooks as the aperture size got finer. Generally, as the feed rate and the feed solids concentration increase, the fishhook increases but the extracted beta parameter abruptly lowers to zero at these high feed condition values.

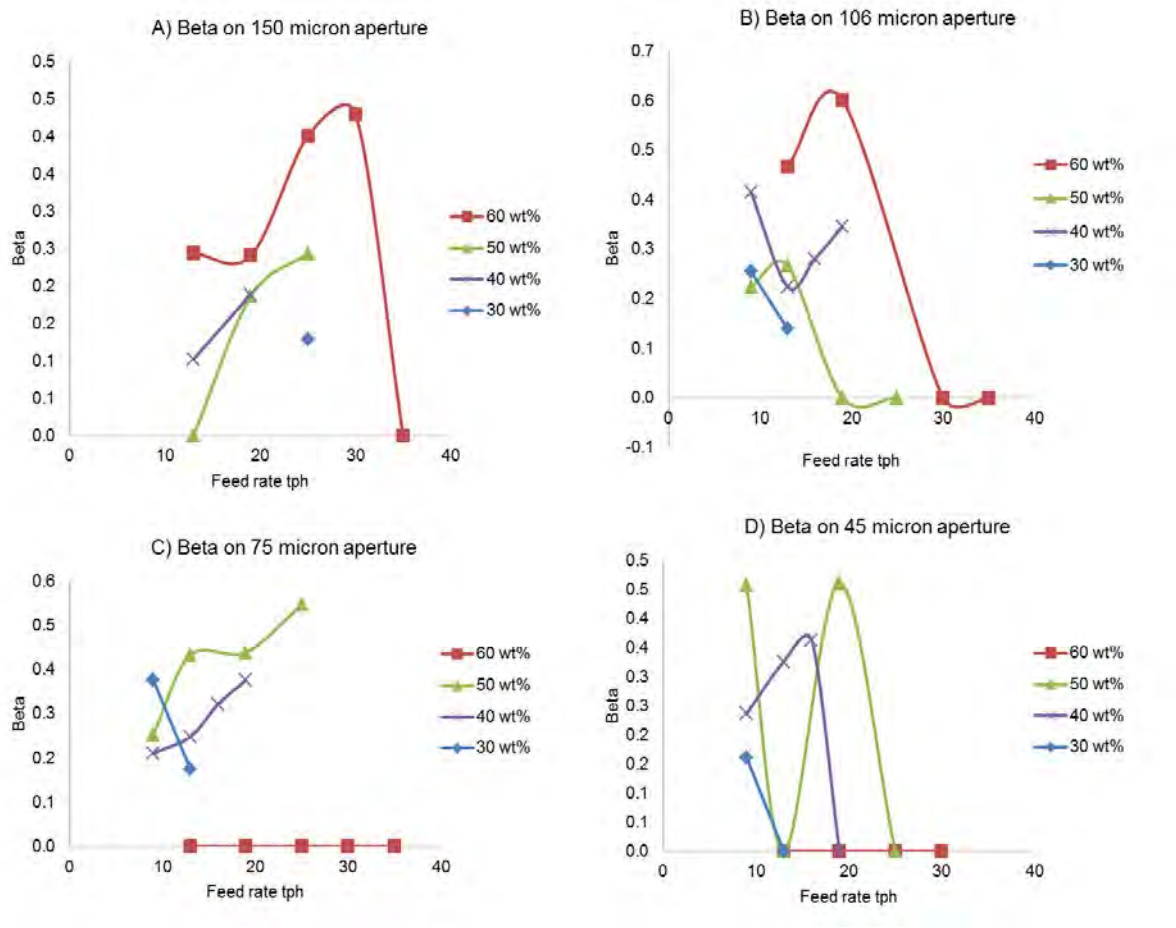

Figure 5-14 Influence of feed rate on beta at varying aperture size

5.7.2 Influence of feed solids concentration on Beta

A plot of Beta against the feed solid concentration in $wt\%$ is shown in Figure 5-15 at 13 and 19 tph mass flow rates. The Figure 5-15 A,B and C show the plots for aperture sizes of 150, 106 and 75 microns respectively. It can be seen that in Figure 5-15 A the beta values increase with increasing feed solids concentration for feed rate of 19 tph. For the 13 tph beta value lowers to zero before it can rise to about 0.29 as the solids concentration is increased. Figure 5-15 B shows the same behaviour at 106 micron aperture. Figure 5-15 C shows an initial increase of the beta values as solids concentration is increased from 30 to 50 $wt\%$ beyond which the values drop to zero.

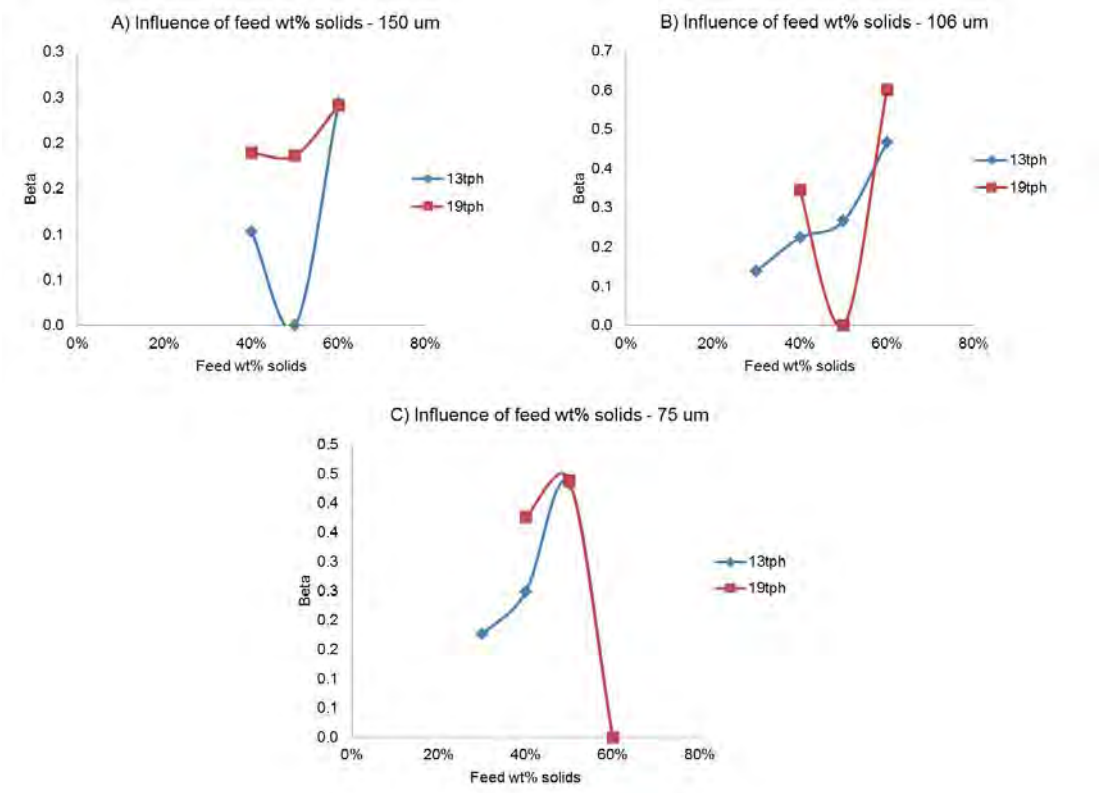

Figure 5-15 Influence of feed solids concentration on Beta

5.8 Summary

From the experimental results and discussion, it was observed that the feed flow rate, the feed solid concentration and the aperture size affect the performance of fine wet screen. It has been noted that increasing feed rate simultaneously reduces the cut size and the sharpness of separation of the screen whilst at the same time increase the oversize water split ratio. This is a triple retrogressive effect on the performance of the screen. The same can be said for increased feed solids concentration. Similar trends have been observed on all the four screen apertures considered in this thesis. With regards to the aperture size, results have shown that there is an accompanied increase of the cut size as the aperture size increase. However, the percentage cut size seemed to increase at low aperture size then decreased as the aperture size increased from 106 micron to 150 micron. These effects are considered in the screen modeling process that follow in Chapter 6.

CHAPTER 6: MODEL DEVELOPMENT

6 Introduction

The main focus of this thesis is to develop a model for fine wet screening and this chapter discusses the model development and validation performed to fulfil the main aim of the study. In the previous chapter, results have shown that feed rate and feed solids concentration influence the performance of the screen. This chapter uses these results in the development of a fine wet screen model that responds to key changes in operating conditions. The approach used is a combination of mechanistic and empirical modelling.

6.1 Screening as a Rate Process

Screening process is a complex process because of the random nature of particle movement. This makes screen modeling process complex, the main reason why the process is dominated by empirical models. Where mechanistic models have been attempted, the screening process has been described as a rate process by many researchers (Ferrara et al. 1987; Subasinghe et al. 1990; Trumic & Magdalinovic 2011). Ferrara et al., (1987) described the dry screening as a two first order rate processes. They described the two processes as kinetic rate of travel of particles through space and the probability of particles passing through the aperture. Using Gaudin's (1939) probability function, the chance of particle passage through the aperture was well described by Ferrara et al., (1987). The chance that a particle will pass through a given aperture depends on the size of the particle with fine particles having a greater chance than coarse particles. Subasinghe et al., (1990) also described the screen process as two rate process involving the rate of particle stratification through the bed and the rate of particle passage through the screen aperture. Soldinger, (1999) described the dry screen process as a two first order rate process with the first being stratification of particles through the bed and the second being the rate at which particle pass through the aperture. The rate of passage has been emphasised to primarily depend on the particle to aperture ratio which is a prime factor that determines probability of a particle passing through the

screen (Gaudin 1939). Trumic & Magdalinovic, (2011) simplified the probability (P) of a given particle size (d_i) passing through a given aperture of size a as;

$$P = 1 - \left(\frac{d_i}{a}\right)^2 \quad \text{Eq (28)}$$

However, as observed from the experimental results in this study, passage is also influenced by the solids concentration where diluted feed resulted in sharper separation. The rate at which a given particle reports to a product stream depend on the rate of change of that size fraction with respect to the screen length (Ferrara et al. 1987; Subasinghe et al. 1990) shown in equation (29);

$$-\frac{dm_i}{dL} \quad \text{Eq (29)}$$

or equation (30) where the rate of change of the mass fraction of that particle size is with respect to the screening time (Soldinger 1999; Trumic & Magdalinovic 2011).

$$-\frac{dm_i}{dt} \quad \text{Eq (30)}$$

Owing to the fact that screen length and width (W) play a major role in designing an efficient screen (Valine & Wennen 2002; Albuquerque et al. 2008; Valine et al. 2009), the width, length and feed solids concentration (s) have been incorporated in the model development. King, (2001) showed that a wider screen carries high loads with a thinner bed while Rogers and Brame, (1985) showed that higher feed solids concentration leads to high undersize carryover to the oversize stream an effect that lowers the screen performance.

Thus, the rate of change of mass fraction on the screen, the feed rate, the screen width, the particle to aperture ratio and the amount of water (w) in the feed combined with all other design variables have a significant impact on the performance of the screen and must be considered in the modeling process. In this work, design variables were held constant and only operational variables (feed rate, solid concentration and aperture size) were varied.

6.2 Modeling

The modeling approach taken in this work considers the screen process to depend on the rate of change of mass fraction with respect to position on the screen for a given feed rate, screen width, particle to aperture ratio and the amount of water in the feed. The Modeling approach focused on deriving an expression that predicts the partition curve and its properties for various operating conditions.

6.3 Partition Model

The model approach in this thesis is represented by Figure 6-1 where the system is regarded as a black box. Figure 6-1 shows that as the mass fraction on the screen changes, whether the particle size of class i will report to the oversize or undersize, depend on the probability of that size, the feed solid concentration, aperture size and the screen width. The driving force is the feed rate of size i.

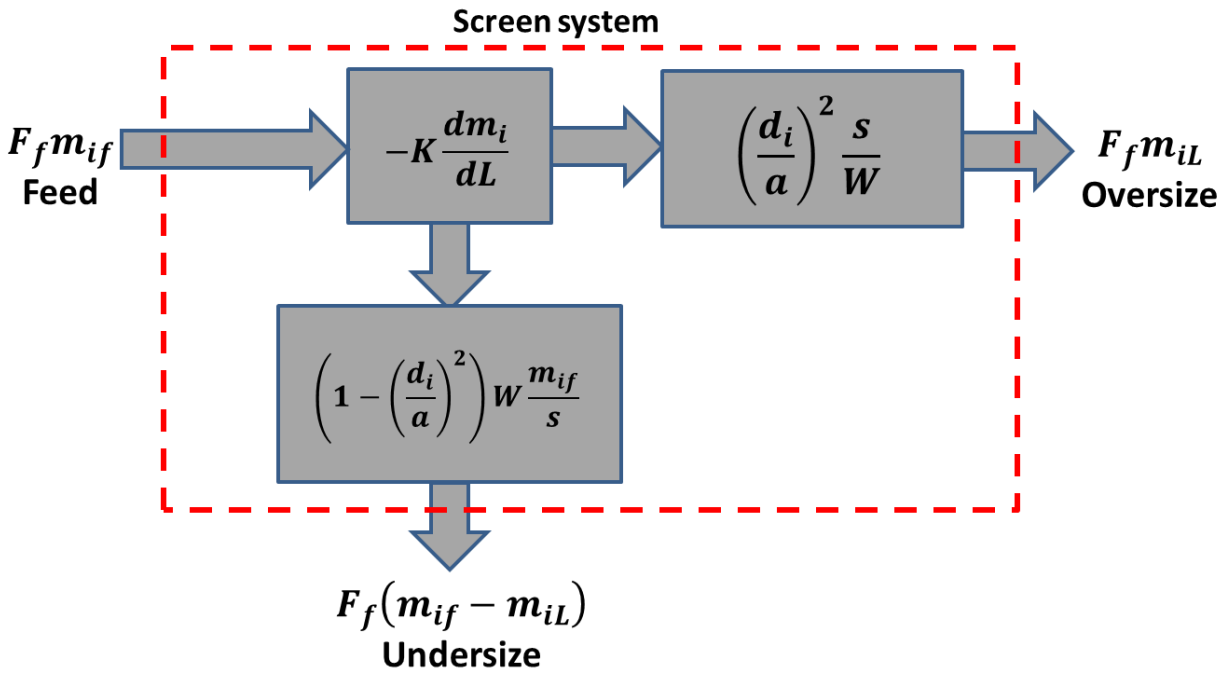

Figure 6-1 Screen system show product recovery

In this model approach recovery to the oversize of a feed mass whose fraction m_{fi}, associated with a particle size d_i depends on the rate of change of the mass fraction on the screen as given by equation (29). The initial mass fraction in the feed changes from m_{if} to a mass fraction of m_{iL} at any point

along the screen length L such that the product of m_{iL} and the feed rate F_f is the mass of size i remaining on the screen. This rate of mass fraction change depends on the particles probability of passage (equation (28)), the screen width and solids concentration in the feed. Using equation (28) the probability that a particle will report to the oversize can be expressed using equation (31).

$$P = \left(\frac{d_i}{a}\right)^2 \quad \text{Eq (31)}$$

Thus, the mass of feed remaining on the screen at every point along the screen length can be obtained by combining equations (29) and (31) to obtain equation (32).

$$F_f m_{iL} = -\left[\left(\frac{d_i}{a}\right)^2 \frac{s}{W}\right] K \frac{dm_{iL}}{dL} \quad \text{Eq (32)}$$

where K is a kinetic rate constant. Introducing a feed rate term f_L at any point on the screen as well as rearranging and introducing integrals with the integration limits 0 and L from the feed point to the discharge point yields equation (33).

$$F_f \int_0^L dL = -\left[\left(\frac{d_i}{a}\right)^2 \frac{s}{W}\right] K \int_{F_f m_{if}}^{F_o m_{io}} \frac{df_L m_{iL}}{f_L m_{iL}} \quad \text{Eq (33)}$$

where m_{io} is the mass fraction of size i in the oversize stream and total oversize flow rate is F_o . Integrating equation (33) yields the expression in equation (34).

$$F_f L = -\left[\left(\frac{d_i}{a}\right)^2 \frac{s}{W}\right] K \, ln \frac{F_o m_{io}}{F_f m_{if}} \quad \text{Eq (34)}$$

The partition number to the oversize is represented by the expression in equation (35).

$$E_{io} = \frac{F_o m_{io}}{F_f m_{if}} \quad \text{Eq (35)}$$

Taking this into account and rearranging equation (34) gives the form shown in equation (36).

$$E_{ioA} = exp\left(-\frac{F_f LW}{\left(\frac{d_i}{a}\right)^2 sK}\right) \quad \text{Eq (36)}$$

Where LW is the total screen area but instead, the actual open area $A_o(m^2)$ is used because it is the actual area that transmits the undersize. The kinetic constant K to be fitted is taken as a reciprocal, a manipulation which has no effect on the significance of the fitted value but gets rid of the error in a case where $K = 0$.

Equation (36) is the general form of the model developed in this thesis to represent the partition number for fine wet screening. However, the model does not capture all the factors that influence screen performance. These were incorporated using empirical modeling approaches. The empirical approach was also taken in modifying the equation so that it can predict the trends observed in the experimental results. The sections that follow describe how the factors were incorporated.

6.4 Empirical modifications to general form

To produce the fine wet screen model for predicting the screen performance under different operating conditions, the general model form was modified using empirical approaches. To capture the influence of feed rate and feed solids concentration the exponents x and y were introduced as shown in equation (37).

$$E_{io} = exp\left(-\frac{{F_f}^x A_o K}{\left(\frac{d_i}{a}\right)^2 s^y}\right) \qquad \text{Eq (37)}$$

The values of the exponents x and y were then determined empirically using Matlab (R2013a) curve fitting tool (cftool). The values of x and y were determined by initially setting the value of the kinetic constant K to 1. This was done as an initial step to ascertain the sign of the exponents on the feed rate and the feed solids concentration. Fitting results given in Table 6-1 show that the sign of the exponent x was consistently negative for all values of the feed rate. The value of y was consistently positive and constant for a given feed solid concentration.

Table 6-1 Values of x and y on a 106 micron aperture

Feed rate tph	Wt% solids	x values	y values	R^2
9	50	-0.3355	0.6797	0.8809
13	50	-0.4416	0.6797	0.6947
19	50	-0.4702	0.6797	0.5254
25	50	-0.5302	0.6797	0.1388

The representation of the partition curve from these results is shown in Figure 6-2. The results in Table 6-1 allowed giving x and y the values of -1 and 1 respectively whilst the rest of the unaccounted for condition are taken care of in the value of K that is to be fitted against the results for varying conditions at a particular aperture size in later section.

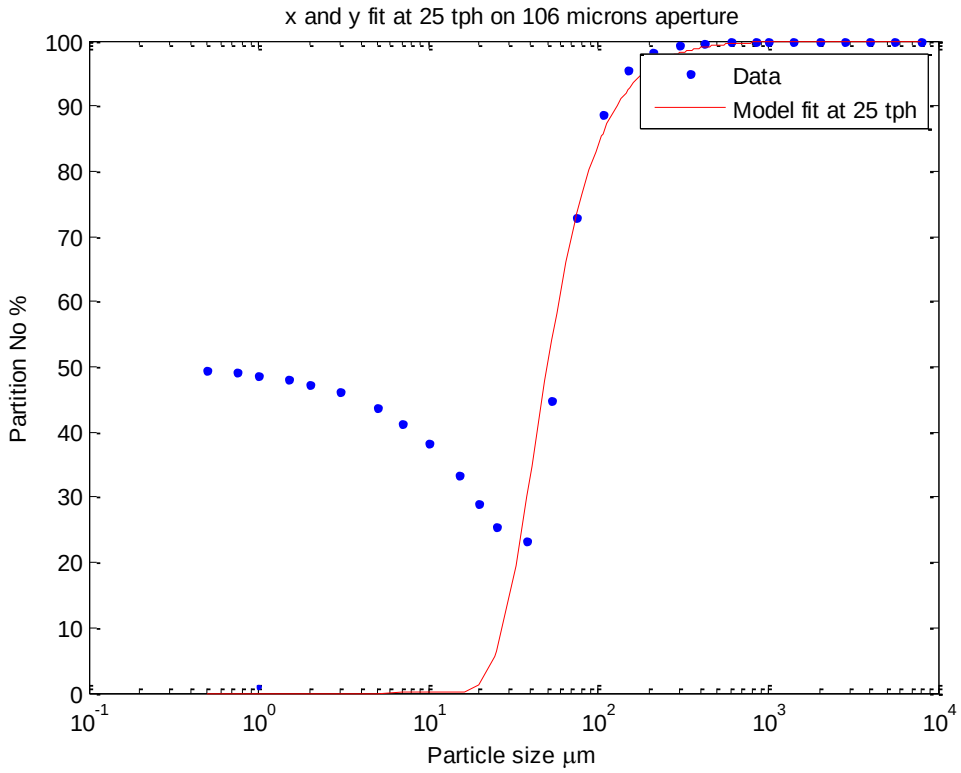

Figure 6-2 Fitting x and y with Matlab curve fitting tool

The probability function given by Trumic & Magdalinovic, (2011) in equation (28) implies that for as long as the ratio $\left(\frac{d_i}{a}\right)^2$ remains constant, the chance of a given particle to go through a given aperture will remain the same. However, experimental results have shown that for the same particle size, the amount that report to the product stream depends on the operating conditions. Thus, the probability of a particle to pass through a given aperture

size can be thought to be changing with changing operating conditions. To account for this change, a dimensionless parameter alpha (α) is introduced in place of the value of 2 in equation (31) which can be fitted against feed conditions. The significance of alpha (α) is discussed in the later section of this thesis. Equation (31) is rewritten as

$$P = \left(\frac{d_i}{a}\right)^{\alpha} \quad \text{Eq (38)}$$

Equation (37) is thus written as

$$E_{io} = exp\left(-\frac{A_o K}{F_f s \left(\frac{d_i}{a}\right)^{\alpha}}\right) \quad \text{Eq (39)}$$

The constant K has units of $\frac{ton}{hr.m^2}$ and alpha (α) is a dimensionless number. Equation (39) has only two constants that require fitting, K and alpha (α). An average value of K can be used though other researchers have shown that the kinetic constant depends on varying conditions (Ferrara et al. 1987). The fitted results are plotted in Figure 6-3. Figure 6-3 shows the model is able to predict the performance curve at given conditions except for the bypass. The bypass material or the undersize carryover to oversize stream has been described as the material that is not available for classification (Austin & Klimpel 1981; Rogers 1982; Nageswararao 1999a). To assess screen performance, corrected or reduced partition curves have been used where corrected cut size values have been deduced (Karra 1979; Rogers 1982; Firth & Hart 2008).

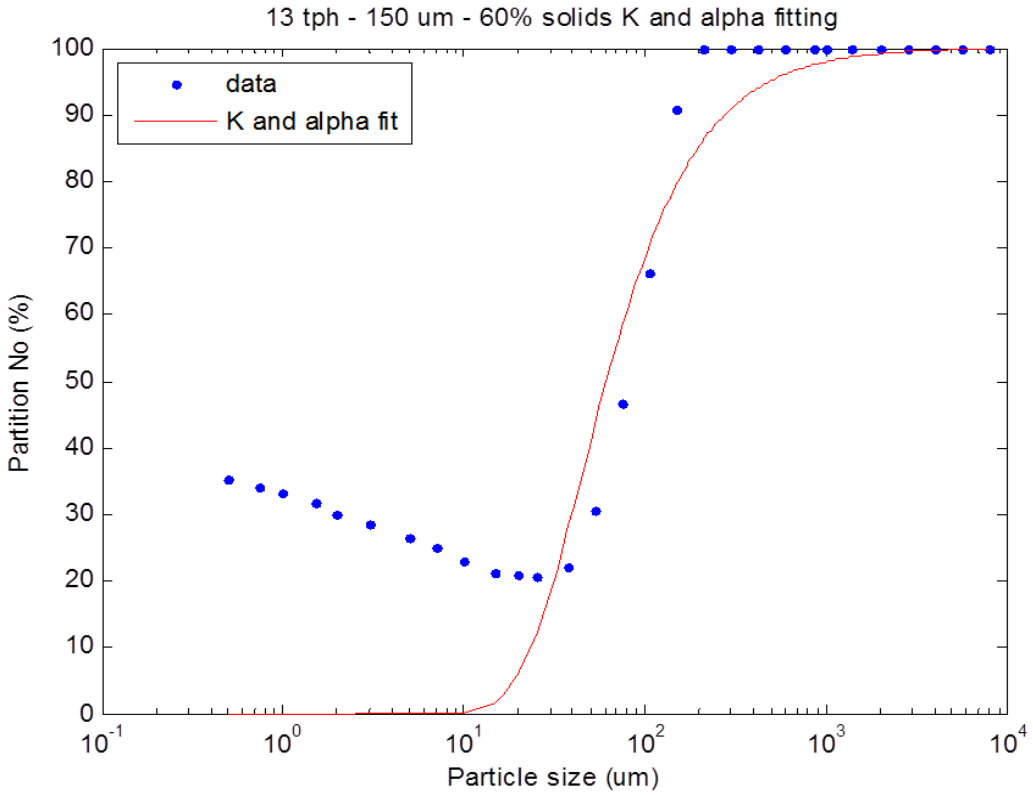

K	Alpha(α)	SSE	R^2	Adjusted R^2	RMSE
3.247	1.245	9558.764	0.7315	0.72161	18.815

Figure 6-3 Fitting alpha and K

The model developed in this work is able to predict the performance of the screen for the conditions covered in the experimental work and generate the actual partition curve (Figure 6-3). There is no need to perform the correction to get the corrected curve. However, the form given in equation (39) does not account for the by-pass and the fishhook, which is important for fine wet screening. The next section gives a description of the approach to incorporate the by-pass and the fishhook.

6.5 Bypass Partition Model

The bypass in classification has been reported to generally represent the water split to the oversize stream at the point where the partition curve intersects the y axis (Austin & Klimpel 1981; Nageswararao 1999b; Mainza 2006; Narasimha et al. 2014). In this study, the amount of bypass has mainly been attributed to changing feed conditions. High flow rates and high feed

solids concentrations were shown to have pronounced fishhook and high carryovers of fines to the oversize stream. An expression given in equation (40) was developed to account for the fishhook effect and the bypass fraction.

$$E_{iob} \propto \frac{\delta F_f}{\omega} \emptyset\left(\frac{d_i}{a}\right) \qquad \text{Eq (40)}$$

Where delta (δ) is a proportionality constant, omega ($\omega = 1 - s$) is water weight fraction in the feed and $\emptyset\left(\frac{d_i}{a}\right)$ is a function that relates the conditions to aperture size and particle size. The formation in the Karra, (1979) model was adopted as the basis to incorporate the fishhook and bypass as shown in equation (41).

$$E_{iob} = \frac{\delta F_f}{\omega} exp\left[-\left(\frac{d_i}{a}\right)^{\alpha}\right] \qquad \text{Eq (41)}$$

Where E_{iob} is the fishhook partition number for a particle of size i. The constant delta δ has units of tph^{-1} and can be fitted for given conditions. The alpha value is the same as determined in equation (39). A plot of the fishhook using equation (41) compared against experimental data is shown in Figure 6-4.

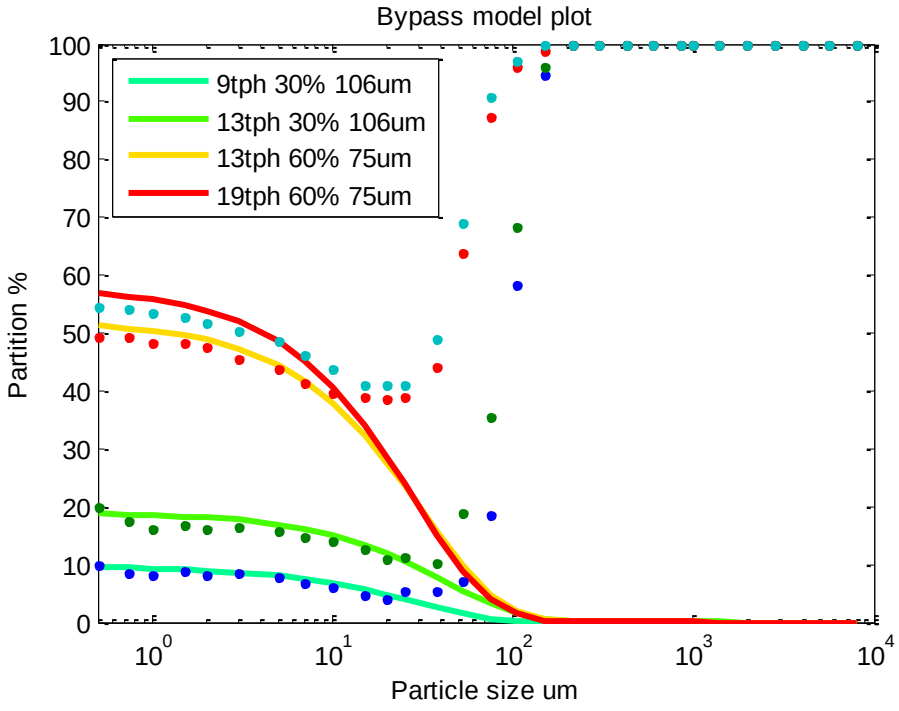

Figure 6-4 Fishook model against data

Figure 6-4 shows that the model for the fishhook part of the partition curve gives good prediction that match experimental data very well. From this approach, it was observed that equation (41) accounts for the particles that do not undergo true classification and equation (39) for particle reporting to the oversize due to true classification. Thus, to predict the overall screen process performance equation (39) and equation (41) are combined as shown in equation (42).

$$E_{io} = exp\left[-\frac{A_o K}{F_f s\left(\frac{d_i}{a}\right)^{\alpha}}\right] + \frac{\delta F_f}{\omega} exp\left[-\left(\frac{d_i}{a}\right)^{\alpha}\right] \quad (42)$$

Further trials with Matlab cftool showed that the bypass model fits data more precise if the exponential function is raised to alpha rather than just the probability function. This allowed for equation (42) modification to

$$E_{io} = exp\left[-\frac{A_o K}{F_f s\left(\frac{d_i}{a}\right)^{\alpha}}\right] + \frac{\delta F_f}{\omega}\left[exp\left(-\frac{d_i}{a}\right)\right]^{\alpha} \quad \text{Eq (43)}$$

6.6 The Alpha model

Alpha is a key performance indicator for classification devices that employ a partition curve as a measure of separation efficiency. It is one of the properties of the partition curve which indicates the sharpness of separation. This is common in evaluating the performance of vibrating screens and hydrocyclones (Wills & Napier-munn 2006). An equation was developed for predicting how the value of alpha varies with operating conditions. The alpha calculated independently using the equation developed can be used in the main equation given in equation (43). Most researchers have developed alpha models where good fits have been accomplished with regards to the systems they investigated (Rogers & Brame 1985; Mainza 2006; Narasimha et al. 2014). A dimensional analysis approach has been used to develop relationships for alpha (Narasimha et al. 2014). In this work, a dimensional analysis approach was adopted to develop an equation for alpha from the experimental data. Using the Buckingham pi theorem, three dimensionless terms shown in equation (44) were obtained. These terms were taken from the design and operating variables that were shown to have influence on the sharpness of separation from literature and experimental data. One of the

parameters used in the process of obtaining the dimensionless terms is the slurry viscosity (μ). The influence of viscosity on performance of the screen used in this work was assessed in terms of solids concentration (He & Forssberg 2007). The viscosity values used were obtained from Muzanenhamo (2014) who worked on a similar ore type as in this thesis. Thus, the viscosity was considered in the process of obtaining the terms as well as the mass (kg) of undersize (M_u) material in the feed. To account for solids concentration, the slurry pulp density (ρ_p) was used in place of the weight percent solids in the feed.

$$\pi_1 = \alpha\frac{a^2}{A_o}, \quad \pi_2 = \frac{F_f}{\mu {A_o}^{0.5}}, \quad \pi_3 = \frac{{\rho_p}^2 {A_o}^3}{{M_u}^2} \qquad \text{Eq (44)}$$

The three dimensionless terms were combined to form the function in equation (45). Equation (45) is a three dimensional function that requires a more advanced and rigorous process to determine the relationship.

$$\alpha\frac{a^2}{A_o} = \emptyset\left(\frac{F_f}{\mu {A_o}^{0.5}}, \frac{{\rho_p}^2 {A_o}^3}{{M_u}^2}\right) \qquad \text{Eq (45)}$$

To simplify the modeling process, the terms π_2 and π_3 were grouped together to form another dimensionless term where the function reduced to equation Eq (46), a more convenient function.

$$\alpha\frac{a^2}{A_o} = \emptyset\left(\frac{{\rho_p}^2 F_f {A_o}^{2.5}}{\mu {M_u}^2}\right) \qquad \text{Eq (46)}$$

Equation (46) has two term function and the function ∅ can take any form depending on data type. Most of the alpha data appeared to follow a linear relationship and thus equation (46) was linearized to the form shown in equation (47).

$$\alpha = k_1\left(\frac{{\rho_p}^2 F_f {A_o}^{3.5}}{\mu a^2 {M_u}^2}\right) + k_2\left(\frac{A_o}{a^2}\right) \qquad \text{Eq (47)}$$

Using Matlab equation Eq (47) was regressed for each aperture size studied to determine the values of the constants k_1 and k_2.To show the goodness of fit for the alpha model, the R^2 values for the alpha model in relation to the fitted alpha values are tabulated in Table 6-2 for each aperture size.

Table 6-2 R^2 values for alpha model against fitted values at different aperture sizes

Aperture size	Alpha model correlated	R^2
150 um	α_{150}	0.7014
106 um	α_{106}	0.7303
75 um	α_{75}	0.9520
45 um	α_{45}	0.8892

The R^2 values show that there is a consistent goodness of fit except at 75 um aperture where an improved correlation was observed. A plot showing the correlation between the predicted and fitted alpha values on an aperture size of 75 um is shown in Figure 6-5.

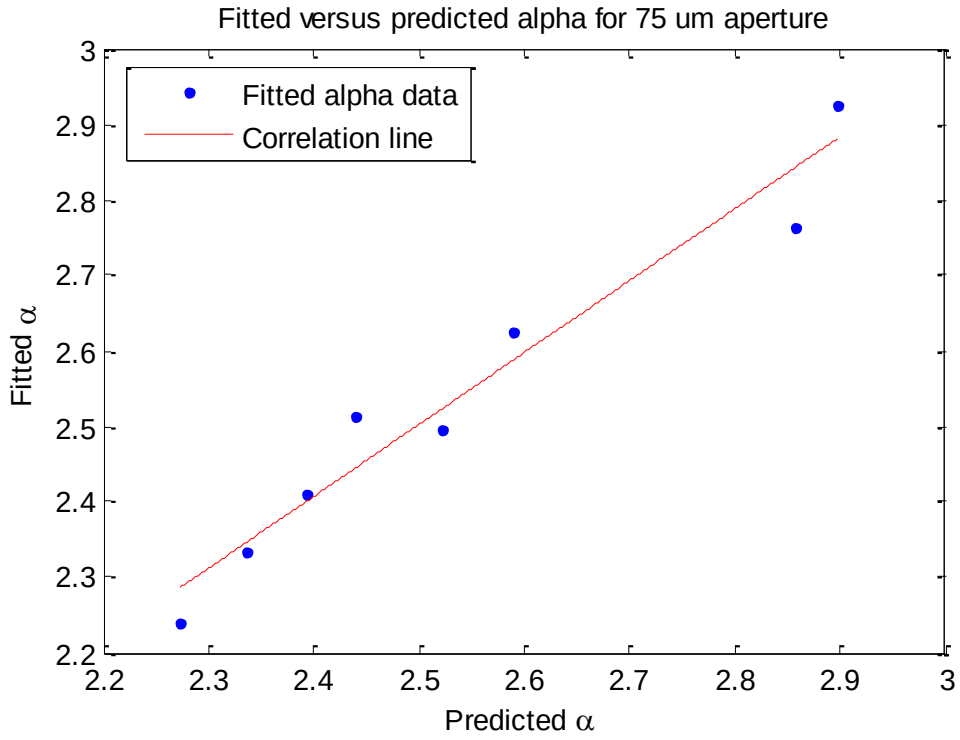

Figure 6-5 Fitted versus predicted alpha values for 75 um aperture

The alpha model can be used together with equation (43) and excludes the need to fit the alpha values to use the model for everyday plant operations and simulations. It can also be used to provide starting alpha values where fitted values a preferred.

6.7 Model constant

To assess the significance of the constants α, K and δ arbitrary values for each constant were fed into equation (43) while all other variables were held constant.

6.7.1 Significance of the alpha value

The sharpness of separation value is a partition curve property that is used in classification as an indicator of goodness of separation (Wills & Napier-munn 2006). Using a 106 um aperture size, 30 $wt\%$ feed solids concentration, 9 tph feed rate, a K value of 3.567, and a β value of 1.3638, the alpha value was arbitrarily varied from 0.5 to 3 as shown in Figure 6-6.

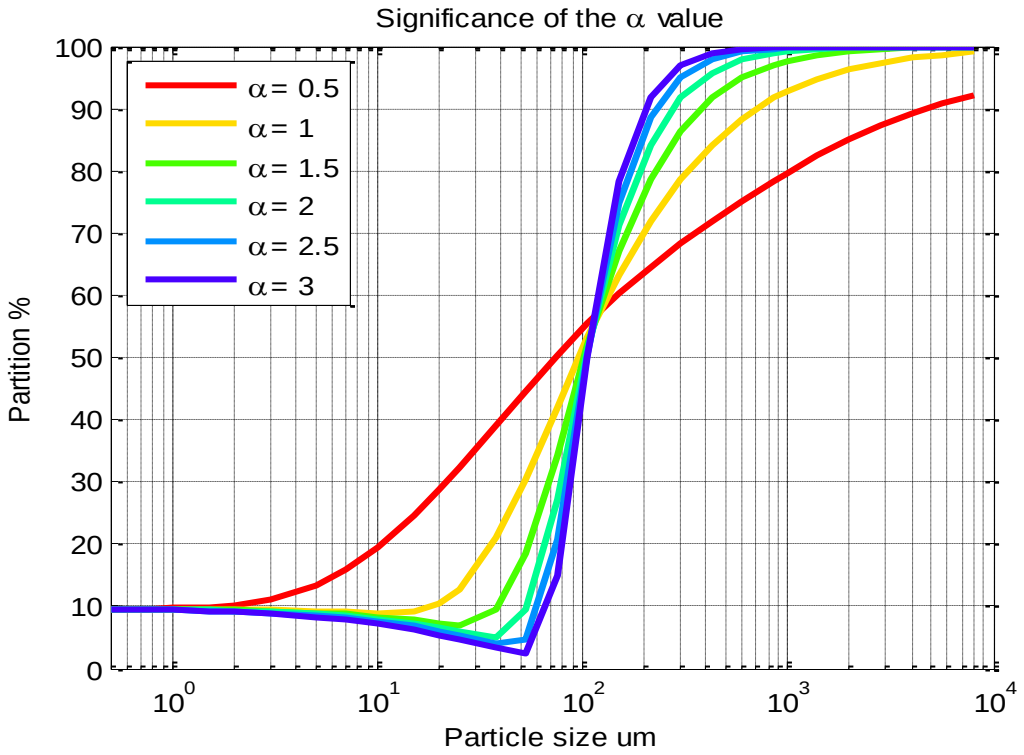

Figure 6-6 Significance of the alpha value

Figure 6-6 illustrates that the alpha value is primarily responsible for the sharpness of separation. Increase in the alpha value results in increase in the sharpness of classification. In the illustration shown in Figure 6-6 the alpha value of 0.5 corresponds to low sharpness of separation and the value of 3 to a fairly sharp separation. Mostly this value has been deduced from corrected and reduced partition curves where a high alpha value shows sharper separation and a low value indicating shallow separation (Austin & Klimpel

1981; Rogers 1982; Rogers & Brame 1985; Frachon & Cilliers 1999; Nageswararao 1999b; Kraipech et al. 2002). However, in this work there is no need to adopt the approach of using reduced partition curves because the behaviour of alpha at different operating conditions is captured by equation Eq (47). Figure 6-6 shows that for different alpha values, the curves converge at the value equal to the aperture value on the x-axis and on some value above 50% mark on the y-axis depending on the feed conditions. This is because equation (43) predicts the screen performance and the cut size value encountered in practice are such that d_{50} is usually less than the aperture size. The alpha values for 75 micron aperture were plotted in Figure 6-7 for different feed conditions captured from equation (43).

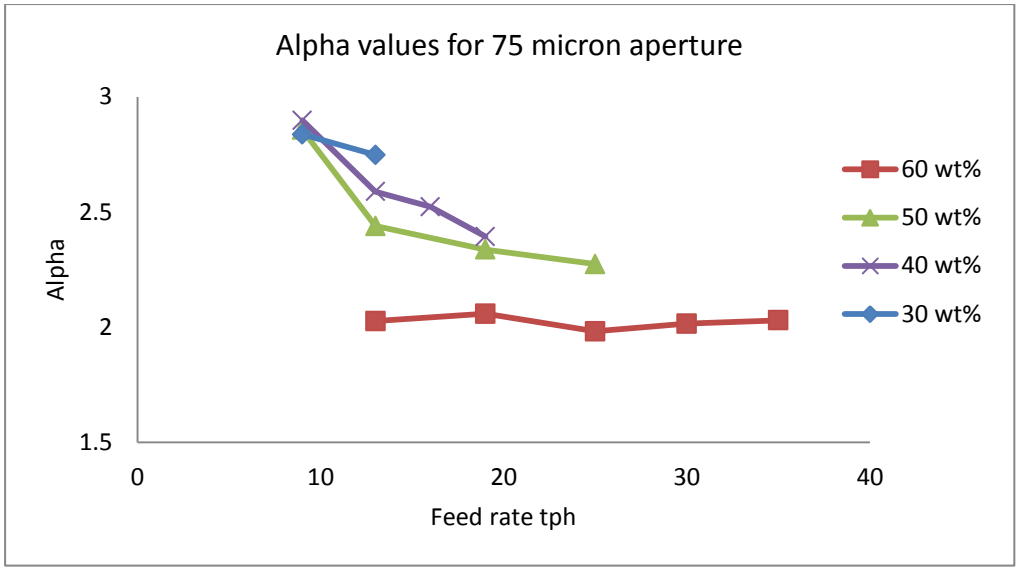

Figure 6-7 Alpha values plotted for a 75 um aperture screen panel

It can be seen that the alpha values decreases with increasing solids concentration in the feed. At low feed solids concentration alpha decreases with increasing feed rate. This shows that feed conditions have a significant influence on the sharpness of separation and equation (43) captures this very well. Ferrara et al. made similar observations for a parameter defined as σ in their model (1987). It was shown that σ affects the probability of passage and that the value was dependent on screen type, slope and vibration conditions.

6.7.2 Significance of the K values

K values were varied between 1 to 7 to assess its influence on the partition curve and the results were plotted in Figure 6-8 it was observed that the

partition curve shifted to the right with increasing K values indicating that the constant had an influence on the cut size.

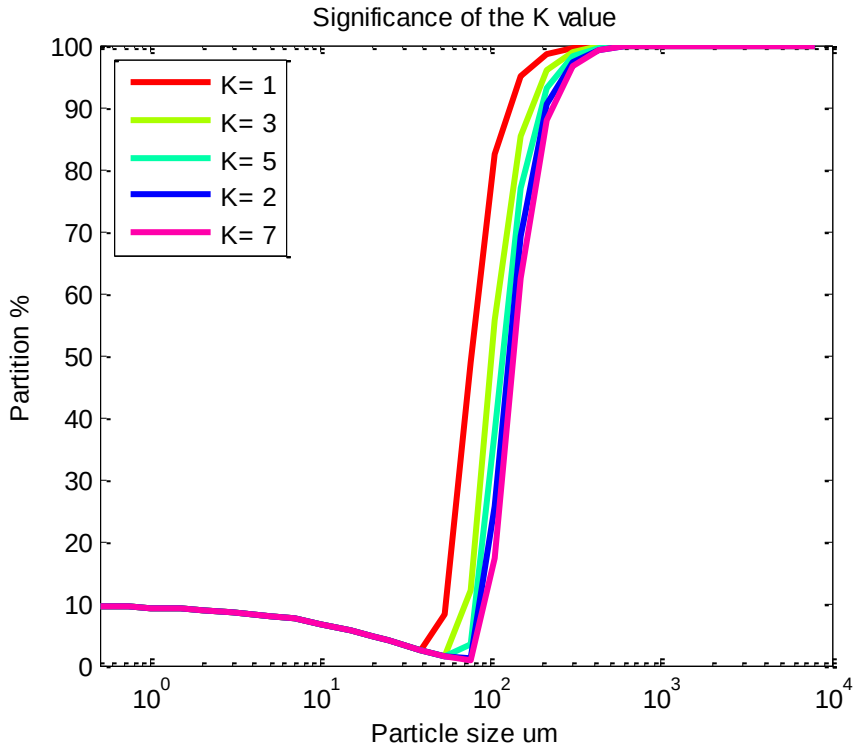

Figure 6-8 Significance of the K value

The value of K seem to have no effect on the sharpness of separation nor on the bypass. For equation (43) to be dimensionally consistent K would have the units of $\frac{ton}{hr.m^2}$ which would be taken as a mass flux. A similar observation was made by Ferrara et al. (1987) where the constant was related to the screen basic capacity. Just like the constant in the model developed by Ferrara et al. (1987) the value of K in this work exhibited the same trend. The value depends on solids concentration, aperture size, the screen open area, and screen vibration conditions.

6.7.3 Significance of the delta value

The partition curve obtained from the experiments exhibited the fishhook behaviour. To account for this a term was incorporated in the model with a parameter termed delta. The influence of delta on the partition curve was evaluated using the same conditions that were applied to assess the effect of parameters α and K. The delta values were varied between 0 and 2 whilst holding all other variables constant and results plotted in Figure 6-9. It was

observed that increasing the delta value resulted in the fishhook becoming more pronounced.

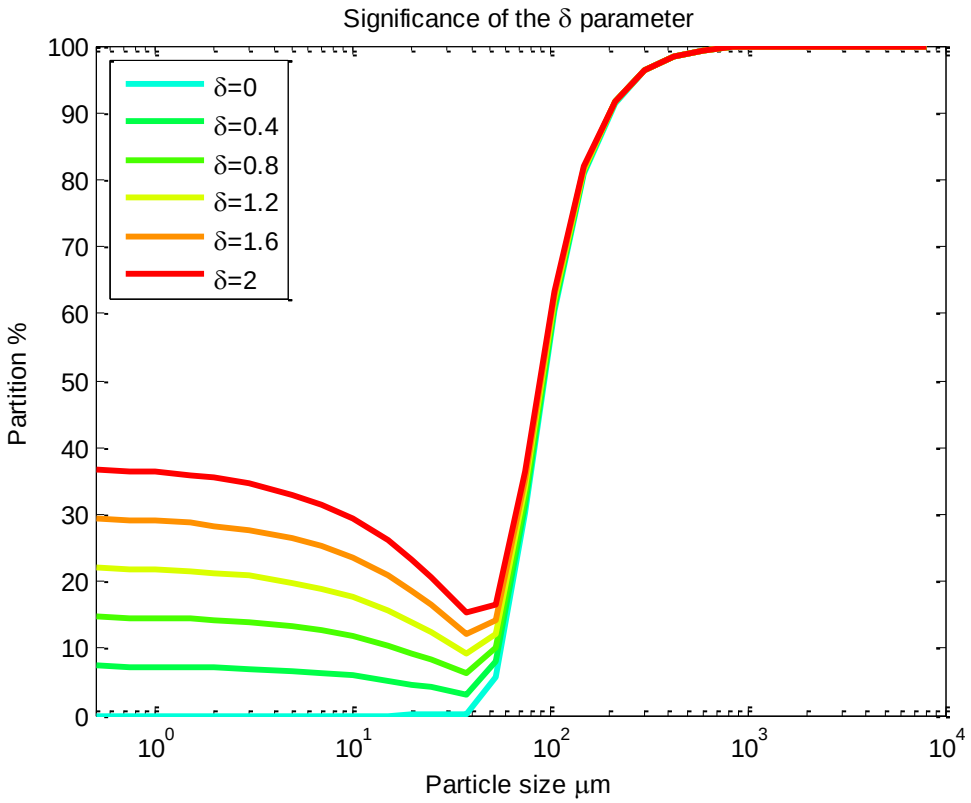

Figure 6-9 Significance of the delta value

It can be noted that when delta is zero (0), the fishhook disappears and the second part of the model can be ignored. This parameter does not capture the beta parameter in the Whitten model but predicts the fishhook effect in the current model well.

6.8 Statistical justification

To assess the model's goodness of fit, statistical parameters have been used as measures of goodness of fit in model developments (Mainza 2006). The Sum of Squares due to Error (SSE) shows the total deviations of the model response from the measured values. The smaller the SSE value the better the fit. The R-squared (R^2) is a statistical value that measures how good the correlation is between the measured values and the fit response. The R^2 value is usually adjusted in relation to the fitted coefficients. A value closer to one indicates good correlation. The Root Mean Squared Error (RMSE) also known as the standard error, measures the error due to random components

in the data and the smaller the value the smaller the fit error. These statistic parameters are used to assess the goodness of fit of equation (43) in this thesis.

Using a Matlab code developed for this work, the parameters in equation (43) were all fitted to data for each screen aperture and studied feed conditions. The results in Figure 6-10 show good correlation in the ability of equation (43) to predict screen performance. Each one of the four graphs show the model in red against the data for each aperture at a feed rate of 13 tph and feed solids concentration of 50 $wt\%$.

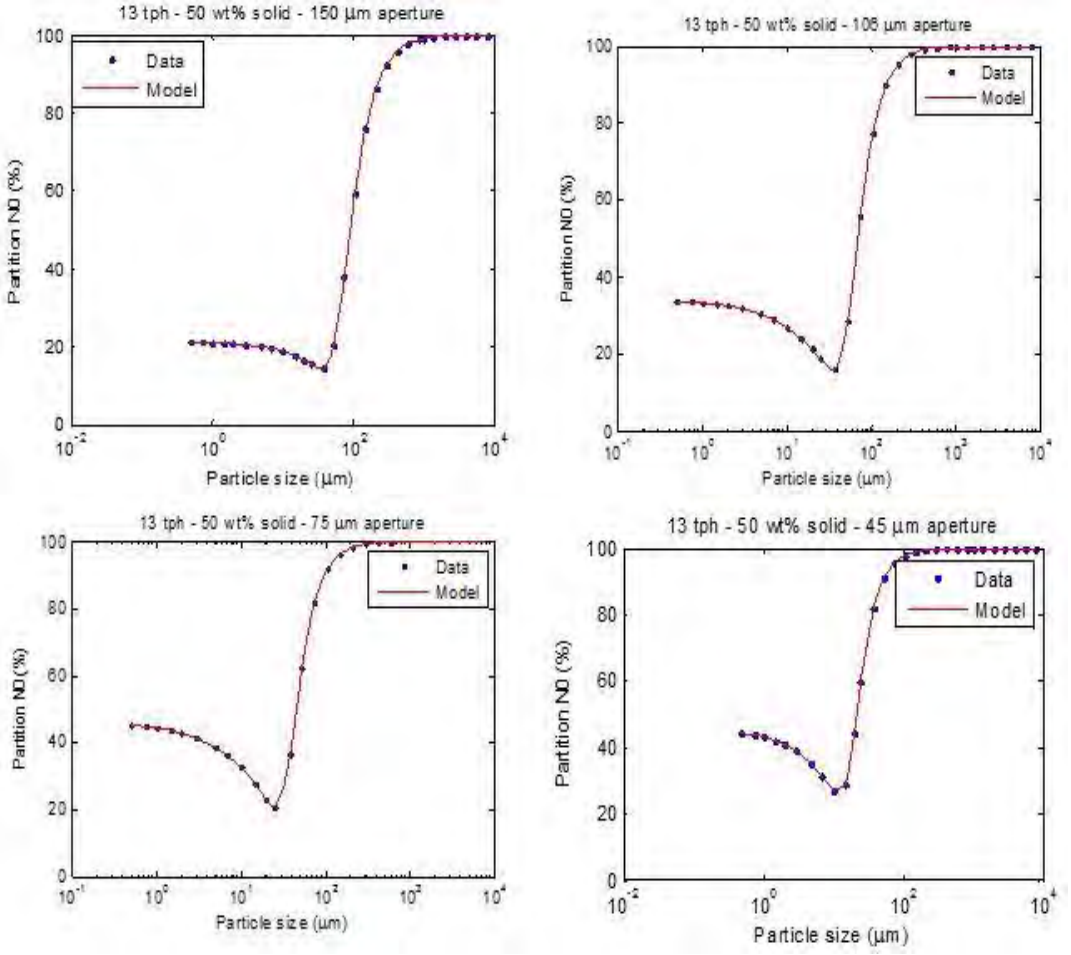

Figure 6-10 Correlation between the predicted and the observed partition values

Figure 6-11 shows the corresponding residual plot of the model against data for the conditions in Figure 6-10. It can be seen that there is a good agreement between the observed data and the predicted results at these feed conditions with most of the residuals below 5%. The corresponding statistical values are tabulated in Table 6-3. The statistical values were

obtained at a confidence level of 95% where it was seen that the deviation is not so significant from the observed values.

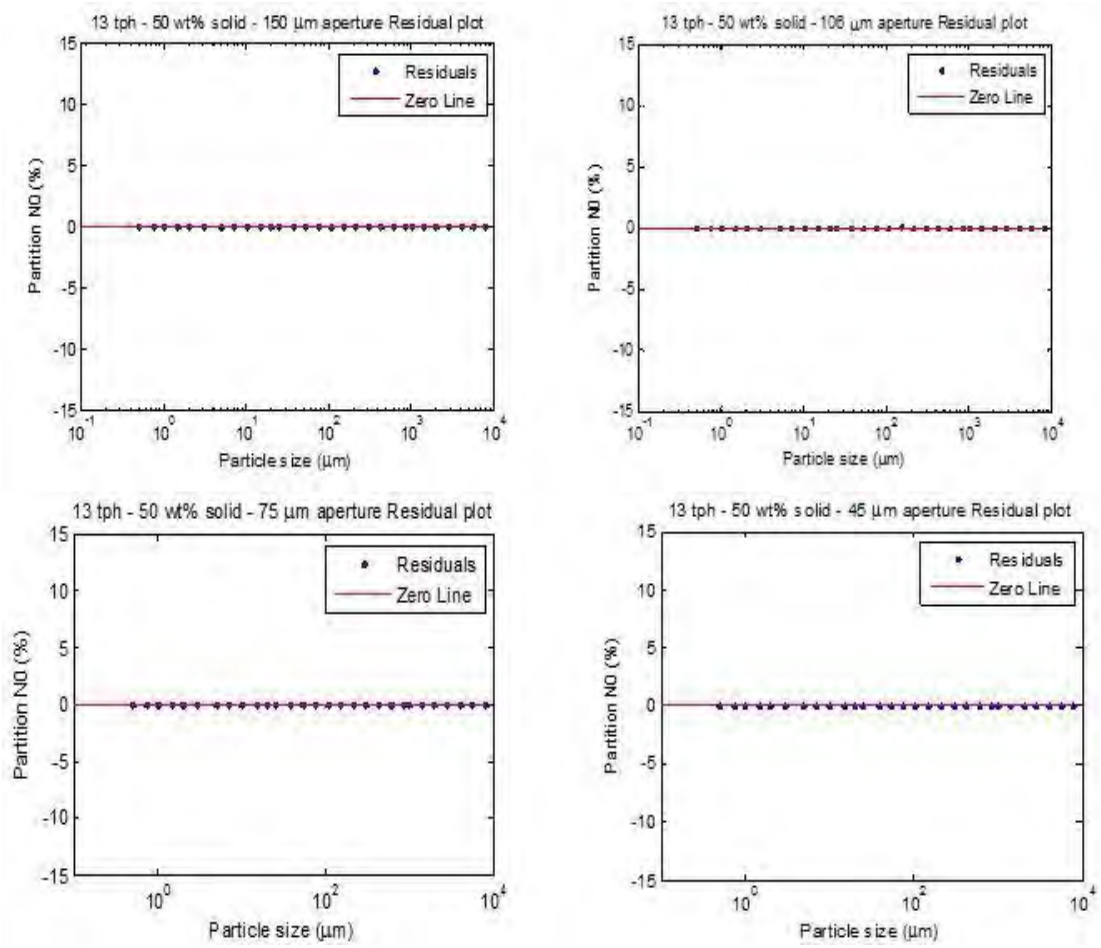

Figure 6-11 Residual plot for various aperture at 13 tph and 50 wt% solids

The fit results for all conditions are generally in good agreement with the data and all R^2 values are above 0.9. At the fitted parameters, the model was also tested to see how well it predicts the cut size value with changing conditions. The results showing the correlation of the model to all feed conditions studied are plotted in Figure 6-12. The predicated cut size values were in good agreement with the measured data with the R-squared value of 0.9817 and the RMSE value of 4.18.

Table 6-3 Operating conditions and statistical values

Aperture (um)	Feed (tph)	$Wt\%$ solids	α	K $\left(\frac{ton}{hr.m^2}\right)$	δ (tph^{-1})	R^2	SSE
150	13	50	2.641	1.511	1.270	0.9993	24.09
106	13	50	2.518	3.432	1.316	0.9999	0.019
75	13	50	2.605	3.316	1.770	0.9999	0.020
45	13	50	2.373	2.777	1.745	0.9999	0.018

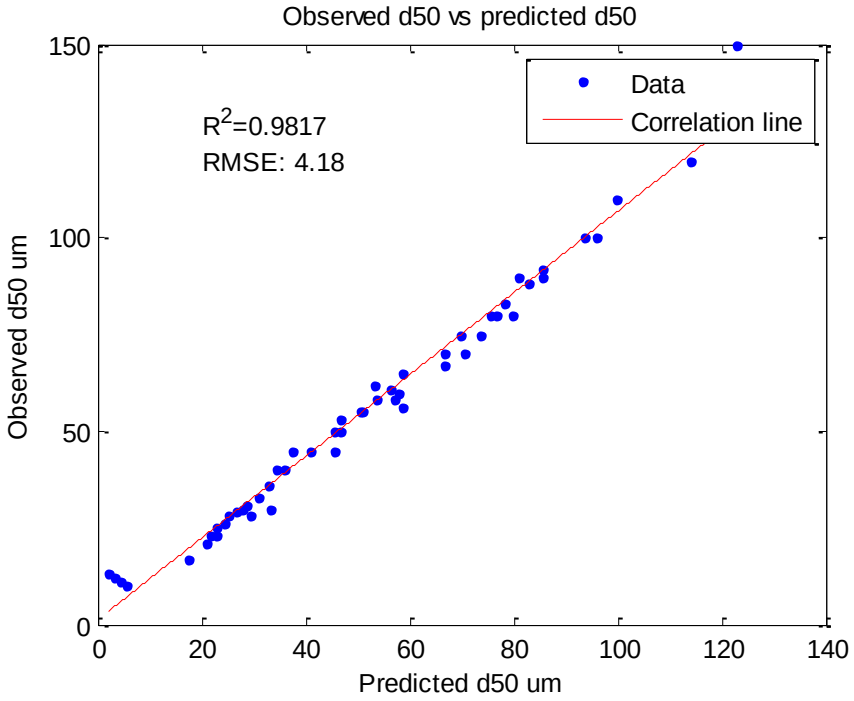

Figure 6-12 Comparison of observed d50 against predicted values

The cut size residual plot in Figure 6-13 also shows good correlation between the measured and the predicted values.

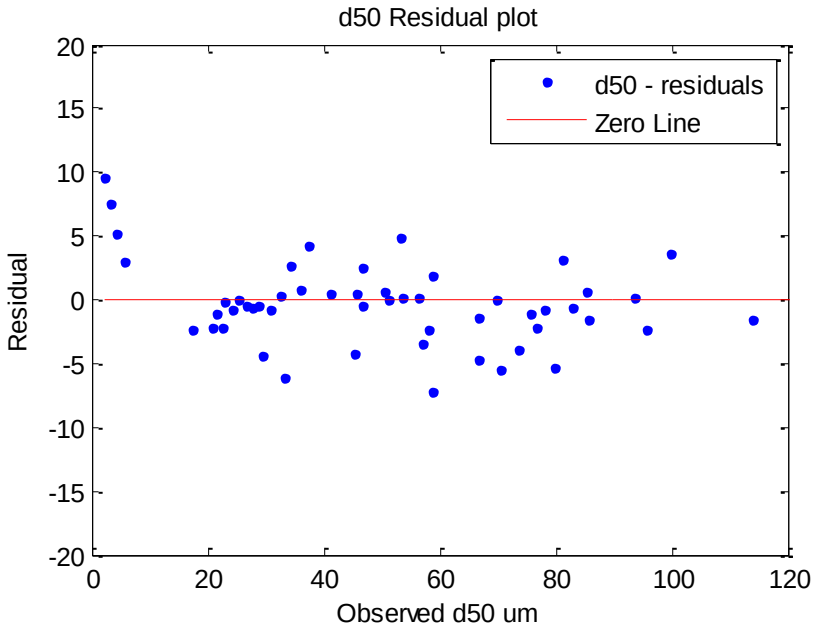

Figure 6-13 Residuals against observed d50 values

The appendix shows all the results from the test work and the model coded in Matlab can be used to obtain the results that provide the corresponding statistic parameters.

6.9 Cut size model

The cut size is one of the most important partition curve properties used to assess plant performance. Cut size models have been developed to characterise and predict the performance of the classifying units including hydrocyclones (Mainza 2006; Narasimha et al. 2014) and screens. In this study, apart from general model discussed from section 6.3 to section 6.5, a cut size model was developed. The approach involved using dimensionless terms obtained from factors that affect the cut size for fine wet screening. The approach used to develop the cut size model is discussed in section (6.6). Four dimensionless terms were obtained as shown in equation (48).

$$\pi_1 = \frac{a^2}{A_o}, \quad \pi_2 = \frac{F_f}{\mu {A_o}^{0.5}}, \quad \pi_3 = \frac{{\rho_p}^2 {A_o}^3}{{M_u}^2}, \quad \pi_4 = \frac{{d_{50}}^2}{A_o} \qquad \text{Eq (48)}$$

The dimensionless terms were combined and rearranged to yield equation (49)

$$\frac{d_{50}}{a} = \emptyset\left(\frac{{\rho_p}^2 F_f {A_o}^{2.5}}{\mu {M_u}^2}\right) \qquad \text{Eq (49)}$$

Equation (49) was linearized and rearranged to yield k_x and k_y in equation (50) for d_{50}. k_x and k_y are fitting parameters.

$$d_{50} = k_x \left(\frac{{\rho_p}^2 a F_f {A_o}^{2.5}}{\mu {M_u}^2} \right) + k_y a \qquad \text{Eq (50)}$$

Regression was used to determine the fitting parameters k_x and k_y for each aperture size studied and the respective values are given in Table 6-4. Table 6-4 also shows the goodness of fit where the cut size adjusted R^2 values in the region of 71 – 75% were obtained indicating a reasonably good fit.

Table 6-4 R^2 values for predicted against d50 values at different aperture sizes

Model	k_x	k_y	R2	R2-Adjusted
${d_{50}}^{150}$	1.04×10^{-1}	0.16	0.7697	0.7441
${d_{50}}^{106}$	3.48×10^{-2}	0.47	0.7597	0.7196
${d_{50}}^{75}$	2.58×10^{-2}	0.43	0.7814	0.7450
${d_{50}}^{45}$	1.42×10^{-2}	0.34	0.7867	0.7511

6.10 Correlations for the K and δ

Correlations were developed for the fitting parameters K and δ based on the aperture size, feed rate and feed solid concentration using linear regression method in Matlab. The correlations for δ and K are shown in equations (51) and (52).

$$\delta = 2.169 + 0.959s - 0.044F_f - 0.0071a \qquad \text{Eq (51)}$$

$$K = 0.444 + 3.32s + 0.168F_f + 0.01a \qquad \text{Eq (52)}$$

The values calculated with the correlation would provide starting values in the fitting process. Comparison of the fitted and calculated K and δ values are given in Figure 6-14 and Figure 6-15 respectively. It can be seen that there is a bit of scatter in the results. However, the calculated values would still be reasonable stating points. The calculated K and δ values from the correlation functions in equations (51) and (52) provide a guide for stating values in the fitting procedure. This is due to the large scatter observed in Figure 6-14 and Figure 6-15.

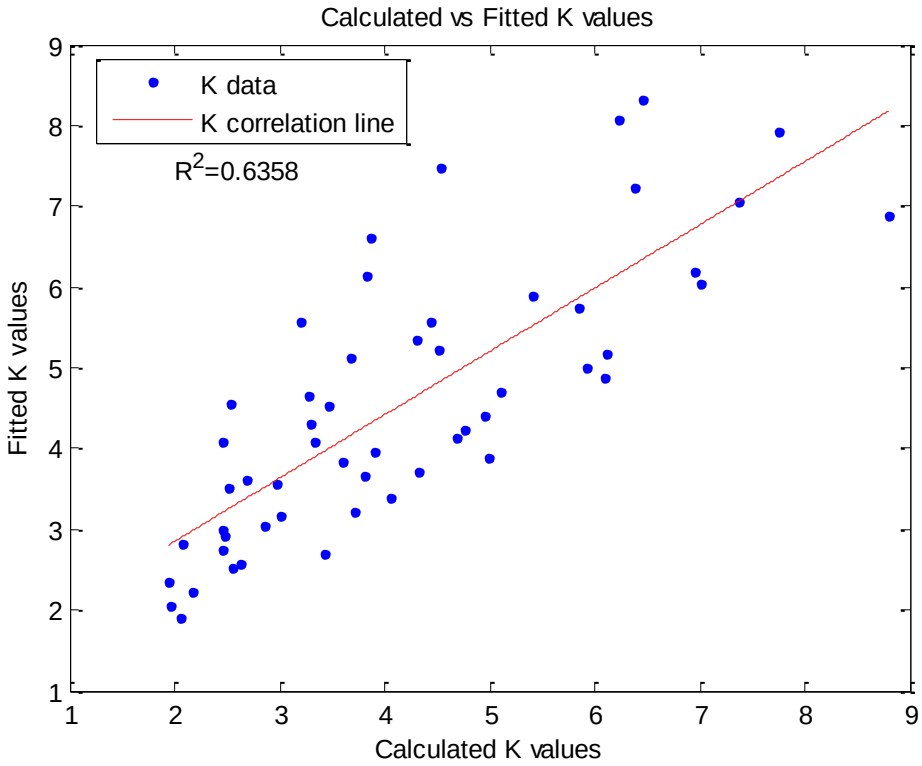

Figure 6-14 Calculated versus fitted K values

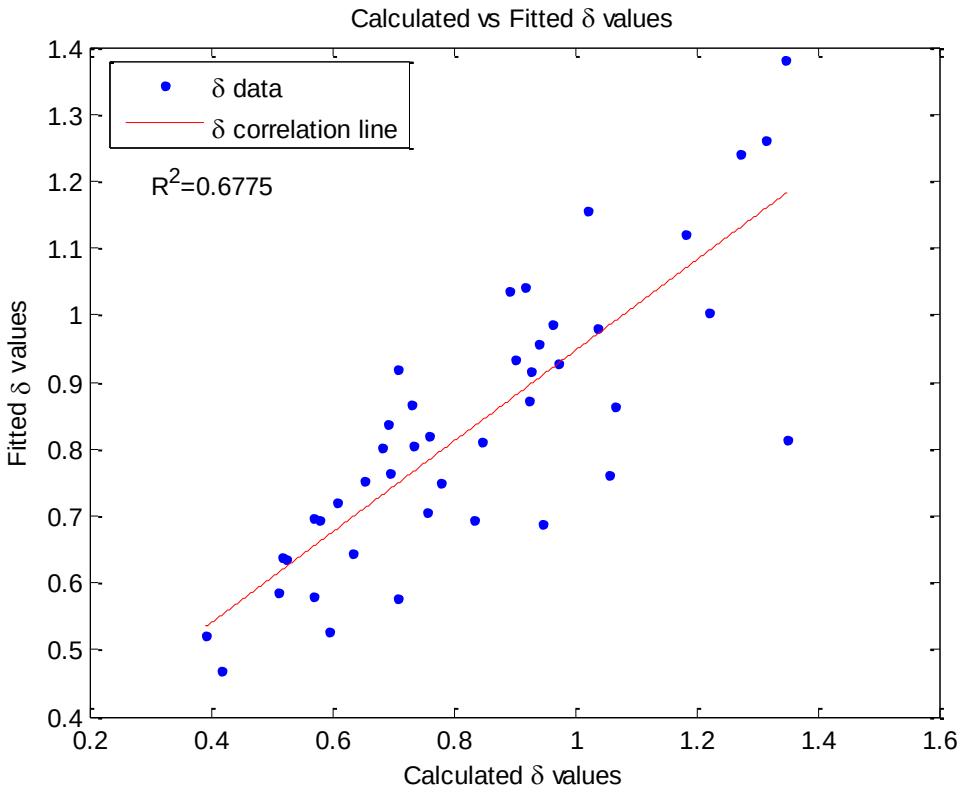

Figure 6-15 Calculated versus fitted delta values

Figure 6-16 shows the partition curve obtained by calculating the alpha, delta and K values using equations Eq (47) (51) and (52) and inserting the values into equation (43) at all four apertures. For 13 tph and 50 $wt\%$ feed solids concentration it can be seen that the model prediction is well correlated and the cut size value is well matched.

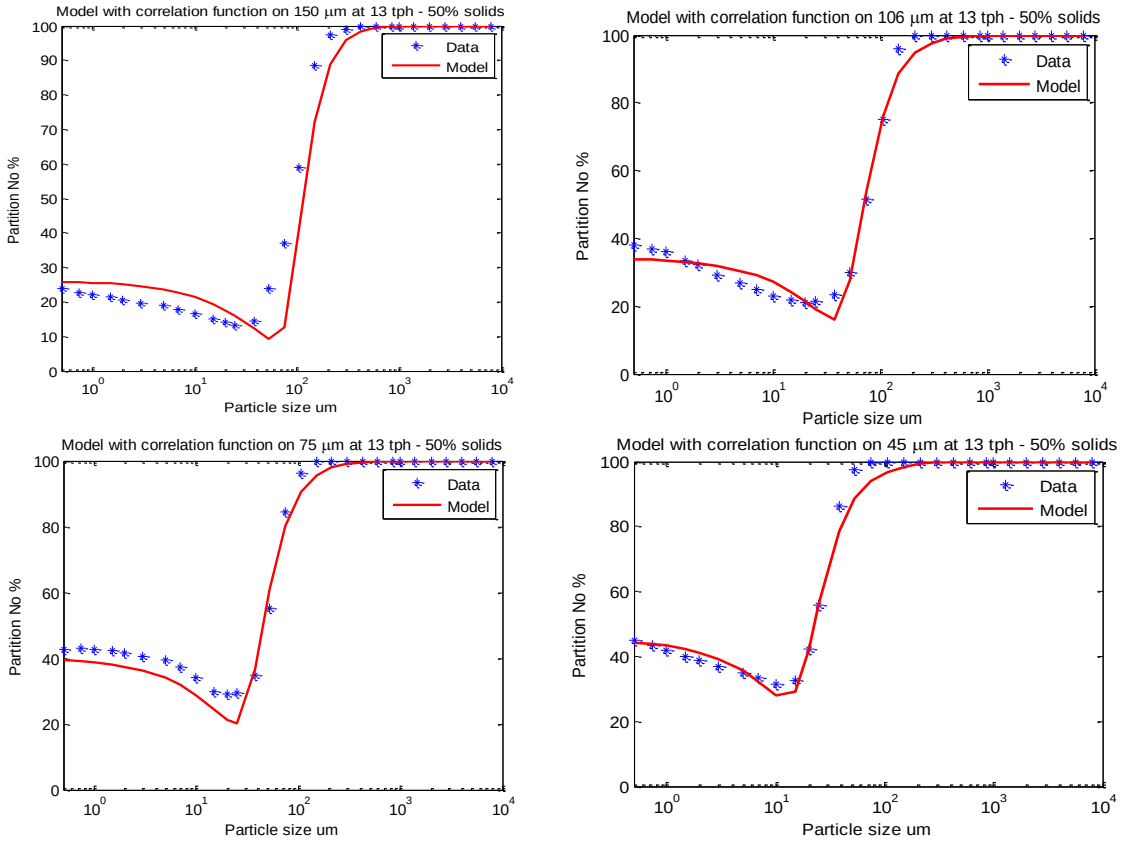

Figure 6-16 Model with correlation function versus observed data at 13 tph and 50 wt% solids

The R^2 values between the observed data and the model were all greater than 0.9900 indicating good prediction from correlation functions. The R^2 values and calculated fitting parameters are tabulated in Table 6-5 at corresponding conditions of the partition curve shown in Figure 6-16.

Table 6-5 Calculated fitting parameters from correlation functions

Aperture (um)	Feed (tph)	$wt\%$ Solids	α	δ (tph^{-1})	K $\left(\frac{ton}{hr.m^2}\right)$	R^2
150	13	50	2.484	1.003	4.086	0.9767
106	13	50	2.465	1.316	3.843	0.9931
75	13	50	2.421	1.536	3.672	0.9929
45	13	50	2.201	1.749	3.506	0.9921

6.11 Summary

A phenomenological fine wet screen model using the partition curve was developed. The model was developed using a rate process approach combined with empirical methods. The model has shown good correlation with data. The dimensionless terms comprised of factors that affect screen performance were obtained. The terms were rearranged and linearized to yield the alpha model and the cut size model. Independent equations were developed for α and d_{50}. The α model can be used to calculate the starting values for the main model equation and the cut size model provides an independent value. Correlation functions for K and δ fitting parameters were also developed to provide starting values for the fitting process. The testing performed shows that the model captures all the key properties of the partition curve. Inputs from correlation functions also captured the partition properties very well.

CHAPTER 7: CONCLUSIONS AND RECOMMENDATIONS

7 Introduction

This chapter presents the main conclusion from the study. Prior to discussing the main conclusions the main observations from the test work and model development are given.

7.1 Outcomes

7.1.1 Observations from test work

The test results have shown that fine wet screening performance deteriorate with increasing feed flow rate and feed solids concentration. The results were quantified in terms of the partition properties. Increasing the feed rate at a specified feed solid concentration reduces the cut size. The cut size reduction is more significant with increasing feed solid concentration. It has also been shown from experimental results that increasing the feed rate and the feed solids concentration resulted in reduced sharpness of separation. The sharpness of separation reduced more sharply with increased feed solids concentration. The tests performed at different aperture size for the same feed size distribution have shown that water recovery to the oversize increased with reduction in aperture size and the fishhook became more pronounced.

7.1.2 Modeling

The partition model was developed in two parts based on the trends observed from experimental results. One described the partition curve and the other describing the bypass. The model produced three parameters that required empirical fitting. Two parameters are unique to each part of the overall model where the K parameter is unique to the partition model and the δ parameter is unique to the bypass model. The alpha (α) parameter which measures the sharpness of separation is a parameter common to both the

partition model and the bypass model. A cut size model was developed using the dimensional analysis approach. Dimensionless terms were obtained based using factors that affects the screen performance. The term were combine and linearized to obtain a cut size model. Using the same approach, the alpha model was developed to describe the sharpness of separation at given conditions. The test showed that the model captures the partition curve properties reasonably well

7.1.2.1 The fine wet model

The model in this thesis comes with the following advantages;

- The model is able to predict the entire partition curve including the fishhook
- The model takes away the need to correct and reduce the partition curve for use in simulations
- The model predicts well the expected bypass on a size-by-size basis a feature that most models avoid through a corrected and reduced partition curve

7.1.2.2 Limitation of the model

The models main limitations are;

- The model was developed on a single particle size distribution. However, this is easily corrected by re-calibrating the coefficients of the alpha model using a simple linear fitting technique with additional data.
- The model is limited to wet screen processes. However, as a starting point, the model can easily be adjusted to cover dry screening by getting rid of the bypass model.

Even with these limitations, the model's potential to be used in wet screen simulation processes still remains good.

7.2 Conclusions

The objectives of this thesis were to investigate the effect of major factors that affect the efficiency of a fine wet screen and develop a model that

employs these factors as inputs to predict the partition curve. The main conclusions drawn from the study are given in the subsections that follow;

7.2.1 Test works

- Test results showed that sharpness of separation improves with reduced feed rate and reduced solid concentration leading to improved screen efficiency.
- The feed rate to the screen and solids concentration has a significant influence on the performance of the screen. The screen performance deteriorates with Increase in the feed rate and the solids concentration.
- Water recovery to the oversize increases with increase in feed flow rate and feed solids concentration.
- Cut size improves with reduced feed rate and reduced solid concentration.
- Screen performance in relation to the partition curve properties improves with increased aperture size.

7.2.2 Modeling

- A fine wet screening model that can be used to predict the performance for different feed conditions and screen aperture sizes was developed using the partition curve approach. The model takes into account the probability of particle passage. The model comprises of one main equation for predicting the partition numbers for the entire partition curve and the other for predicting the bypass. The model has sub models for predicting the sharpness of separation (α) and the cut size (d_{50}). The sub models gave good fit results. The partition curve properties are well captured in the model at varying operation conditions.
- Correlations for K and δ have been developed for calculating starting values for the fitting process.

7.3 Recommendations

The following recommendations are drawn from this thesis;

- The model was developed based on a single particle size distribution, thus, it is recommended that mass fraction of each particle size range be considered in future modifications to give the model more flexibility.
- The water split is a critical performance indicator, thus, it is recommended that a water split model be developed based on feed conditions to the screen.
- The cut size model developed in this thesis requires further work to improve the prediction for different operating conditions.

8 Works Cited

Albuquerque, Laercio G., Wheeler, Jobe, Valine, Steven & Ganahl, Brenno, 2008. Application of high frequency screens in closing grinding circuits. In *International Mineral Processing Seminar–Gecamin*.

Austin, L.G. & Klimpel, R.R., 1981. An improved method for analyzing classifier data. *Powder Technology*, 29(2), pp.277–281.

Barkhuysen, N.J., 2010. Implementing Strategies to Improve Mill Capacity and Efficiency , with Platinum References and Case Studies . In *4th International Platinum Conference*. The Southern Institute of Mining and Metallurgy.

Chen, Y. & Tong, X., 2010. Modeling screening efficiency with vibrational parameters based on DEM 3D simulation. *Mining Science and Technology (China)*, 20(4), pp.615–620. Available at: http://linkinghub.elsevier.com/retrieve/pii/S1674526409602544 [Accessed July 31, 2013].

Cleary, P.W., Sinnott, M.D. & Morrison, R.D., 2009. Separation performance of double deck banana screens - Part 1: Flow and separation for different accelerations. *Minerals Engineering*, 22(14), pp.1218–1229. Available at: http://dx.doi.org/10.1016/j.mineng.2009.07.002.

Derrick, J.W., 1973. *Multifeed Screen Increases Recovery in Fine Coal Circuits*,

Dong, Hailin, Liu, Chusheng, Zhao, Yuemin & Zhao, Lala, 2013. Influence of vibration mode on the screening process. *International Journal of Mining Science and Technology*, 23(1), pp.95–98. Available at: http://linkinghub.elsevier.com/retrieve/pii/S2095268613000220 [Accessed July 31, 2013].

Dong, K.J., Wang, B. & Yu, A.B., 2013. Modeling of Particle Flow and Sieving Behavior on a Vibrating Screen : From Discrete Particle Simulation to Process Performance Prediction.

Dueck, J., Farghaly, M. & Neesse, T., 2014. The theoretical partition curve of the hydrocyclone. *Minerals Engineering*, 62, pp.25–30. Available at: http://dx.doi.org/10.1016/j.mineng.2013.10.004.

Ferrara, G., Preti, U. & Schena, G.D., 1987. Computer-aided Use of a Screening Process Model. In *APCOM 87. Proceeding of the Twentieth International Symposium on the Application of Computers and Mathematics in the Mineral Industries*. Johannesburg: SAIMM, pp. 153–

166.

Firth, B. & Hart, G., 2008. Some Aspects of Modeling Partition Curves for Size Classification. *International Journal of Coal Preparation and Utilization*, 28(3), pp.174–187.

Frachon, M. & Cilliers, J.J., 1999. A general model for hydrocyclone partition curves. *Chemical Engineering Journal*, 73, pp.53–59.

Gaudin, A.M., 1939. *Principles of Mineral Dressing* 1st ed., London: McGraw-Hill.

Gupta, A. & Yan, D.S., 2006. *Introduction to Mineral Processing Design and Operation* 1st ed., Oxford: Elsevier.

Hatch, C.C. & Mular, A.L., 1978. Digital simulation of a secondary crushing plant. In *Annual General Meeting of CIM*.

He, M. & Forssberg, E., 2007. Influence of slurry rheology on stirred media milling of quartzite. *International Journal of Mineral Processing*, 84(1-4), pp.240–251.

Karra, V.K., 1979. Development of a model for predicting the screening performance of vibrating screens. *CIM Bulletin*, 72(84), pp.167–171.

Kelley, C., 2007. Fine dry screening with urethane screen surfaces Case study. In *The 6th International Heavy Minerals Conference "Back to Basics."* The Southern Institute of Mining and Metallurgy, pp. 205–210.

Kelley, C.P. & Mckeon, T.J., 2005. Application of Derrick High Frequency Fine Screening Technologies in Kelsey Jig Zircon Tailings Recovery (DuPont , Starke , Florida). , pp.1–5.

King, R.P., 2001. *Modeling & Simulation of Mineral Processing systems*,

Kirk, T.A., 1984. Closed-Grinding Circuits with Vibrating Screens.pdf. In *Sixteenth Canadian Mineral Processors Operators Conference*.

Kraipech, W., Chen, W.,Parma, F.J. & Dyakowski, T., 2002. Modelling the fish-hook effect of the flow within hydrocyclones. *International Journal of Mineral Processing*, 66(1-4), pp.49–65. Available at: http://linkinghub.elsevier.com/retrieve/pii/S0301751602000121.

Kuang, Shibo, Qi, Z., Yu, A.B., Vince, A., Barnett, G.D. & Barnett, P.J., 2014. CFD modeling and analysis of the multiphase flow and performance of dense medium cyclones. *Minerals Engineering*, 62, pp.43–54. Available at: http://www.sciencedirect.com/science/article/pii/S0892687513003087.

Mainza, A.N., 2006. *Contribution to the understanding of the three-product cyclone on the classification of a dual density platinum ore*. University of Cape Town.

Mathews, C.W., 1985. Screening. In N. L. Weiss, ed. *SME Mineral Processing Handbook*.

Mohanty, M.K., Palit, a. & Khanna, N., 2003. Models for Predicting the Performance of a Linear Screen. *Coal Preparation*, 23(4), pp.213–235.

Muzanenhamo, P., 2014. *Assessing the effect of cone ratio, feed solids concentration and viscosity on hydrocyclone performance*. University of Cape Town.

Nageswararao, K., 2000. A critical analysis of the fish hook effect in hydrocyclone classifiers. *Chemical Engineering Journal*, 80(1-3), pp.251–256. Available at: http://linkinghub.elsevier.com/retrieve/pii/S1383586600000988.

Nageswararao, K., 1999a. Normalisation of the efficiency curves of hydrocyclone classifiers. *Minerals Engineering*, 12(1), pp.107–118. Available at: http://linkinghub.elsevier.com/retrieve/pii/S089268759800123X.

Nageswararao, K., 1999b. REDUCED EFFICIENCY CURVES OF INDUSTRIAL ANALYSIS FOR PLANT PRACTICE. *MINERALS ENGINEERING*, 12(5), pp.517–544.

Nageswararao, K. & Medronho, R. a., 2014. Fish hook effect in centrifugal classifiers – a further analysis. *International Journal of Mineral Processing*, 132, pp.43–58. Available at: http://linkinghub.elsevier.com/retrieve/pii/S0301751614001239 [Accessed November 6, 2014].

Napier-Munn, T.J, Morrel, S., Morrison, R. D. & Kojovic, T, 2005. *Mineral Comminution Circuits: Thier Operation and Optimisation*, Julius Kruttschnitt Mineral Research Center.

Narasimha, M., Mainza, A.N., Holtham, P.N., Powell, M.S. & Brennan, M.S., 2014. A semi-mechanistic model of hydrocyclones — Developed from industrial data and inputs from CFD. *International Journal of Mineral Processing*, 133, pp.1–12. Available at: http://dx.doi.org/10.1016/j.minpro.2014.08.006.

Pelevin, A.E. & Lazebnaya, M. V, 2009. Appllication of derrick screens in locked grinding circuit at the KMAruda mining complex concentrating plant. *mineral processing journal*, 2.

Rawle, A. & U. K., M.I., 2003. *Sampling for Particle Size Analysis*, Worcs. Available at: www.malven.co.uk.

Rogers, R.S.C., 1982. A Classification Function for Vibrating Screens. *Powder Technology*, 31, pp.135–137.

Rogers, R.S.C. & Brame, K.A., 1985. An Analysis of the High-Frequency of Fine Slurries. *Powder Technology*, 42, pp.297–304.

Soldinger, M., 1999. INTERRELATION OF STRATIFICATION AND PASSAGE IN THE SCREENING PROCESS. *MINERALS*

ENGINEERING, 12(5), pp.497–516.

Spottiswood, D.J. & Kelly, E.G., 1982. *Introduction to Mineral Processing* 1st ed., New York: John Wiley & Sons.

Standish, N., 1985. The Kinetics of Batch Sieving. *Powder Technology*, 1(41), pp.57–67.

Standish, N., Bharadwaj, A.K. & Hariri-Akbari, G., 1986. A Study of the Effect of Operating Variables on the Efficiency of a Vibrating Screen. *Powder Technology*, 48, pp.161–172.

Standish, N. & Meta, I.A., 1985. Some Kinetic Aspect of Continuous screening. *Powder Technology*, 41, pp.165 – 171.

Subasinghe, G.K.N.S., Schaap, W. & Kelly, E.G., 1990. Modelling screening as a conjugate rate process. *International Journal of Mineral Processing*.

Subasinghe, G.K.N.S., Schaap, W. & Kelly, E.G., 1989. Modelling the Screening Process : A Probabilistic Approach. , 59, pp.37–44.

Trumic, M. & Magdalinovic, N., 2011. New model of screening kinetics. *Minerals Engineering*, 24(1), pp.42–49. Available at: http://linkinghub.elsevier.com/retrieve/pii/S0892687510002396 [Accessed July 31, 2013].

Tsakalakis, K., 2001. Some basic factors affecting screen performance in horizontal vibrating screens. *The European Journal of Mineral Processing and Environmental Protection*.

Valine, S.B. & Wennen, J.E., 2002. Fine Screening in Mineral Processing operations. In A. L. Mular, D. N. Halbe, & D. J. Barret, eds. *Mineral Processing Plant Design, Practice, and Control*. Colorado: SME, pp. 917–928.

Valine, S.B., Wheeler, J.E. & Albuquerque, L.G., 2009. Fine sizing with the derrick stack sizer screen. In *Recent Advances in Mineral Processing Plant Design*. SME, pp. 433–443.

Wills, B.A. & Napier-munn, T., 2006. *Mineral Processing Technology* 7th ed., UK: Elsevier Science and Technology Books.

9 Appendix

9.1 Experimental Data

150 Micron at 60%											
Feed rate	% solids	Water in Feed	U/S Rate	%solids	water in U/S	O/S Rate	%solids	water in O/S	Total	C	Mass split
28.87	60%	19.247	16.313	0.523	14.867	12.557	0.7414	4.380	19.247	0.227565	0.565050225
25.729	60%	17.153	12.904	0.508	12.519	12.825	0.7346	4.633	17.153	0.270132	0.501535233
21.475	60%	14.317	12.821	0.529	11.414	8.654	0.7488	2.903	14.317	0.202782	0.59701979
15.011	60%	10.007	10.04	0.546	8.351	4.971	0.7501	1.656	10.007	0.16549	0.668842849
11.3033	60%	7.536	7.9086	0.551	6.456	3.3947	0.7587	1.080	7.536	0.143276	0.699671777

150 Micron at 50%											
Feed rate	% solids	Water in Feed	U/S Rate	%solids	water in U/S	O/S Rate	%solids	water in O/S	Total	C	Mass split
21.8364	50%	21.836	13.8	0.417	19.280	8.0364	0.7587	2.556	21.836	0.117049	0.631972303
14.3705	50%	14.371	9.98	0.435	12.985	4.3905	0.76015	1.385	14.371	0.096401	0.694478271

150 Micron at 40%											
Feed rate	% solids	Water in Feed	U/S Rate	%solids	water in U/S	O/S Rate	%solids	water in O/S	Total	C	Mass split
18.941	40%	28.412	13.732	0.338	26.851	5.209	0.76946	1.561	28.412	0.054931	0.724988121

150 Micron at 30%											
Feed rate	% solids	Water in Feed	U/S Rate	%solids	water in U/S	O/S Rate	%solids	water in O/S	Total	C	Mass split
19.6242	30%	45.790	16.567	0.269	44.970	3.0572	0.78846	0.820	45.790	0.017913	0.844212758

Figure 9-1 150 micron feed flow rates and solids concentration

	106 Micron at 60%									
Feed rate	% solids	Water in Feed	U/S Rate	%solids	water in U/S	O/S Rate	%solids	water in O/S	C	Mass split
30.9114	60%	20.61	11.38	0.53	10.02	19.54	0.65	10.59	0.51	0.37
28.3879	60%	18.93	12.28	0.52	11.31	16.10	0.68	7.62	0.40	0.43
22.8274	60%	15.22	8.99	0.52	8.15	13.84	0.66	7.07	0.46	0.39
12.8915	60%	8.59	6.20	0.52	5.76	6.69	0.70	2.83	0.33	0.48
9.1417	60%	6.09	4.69	0.51	4.55	4.45	0.74	1.54	0.25	0.51
	106 Micron at 50%									
Feed rate	% solids	Water in Feed	U/S Rate	%solids	water in U/S	O/S Rate	%solids	water in O/S	C	Mass split
23.84	54%	20.38	10.88	0.42	14.82	12.96	0.70	5.56	0.27	0.54
19.73	53%	17.83	10.71	0.43	14.31	9.03	0.72	3.52	0.20	0.46
17.19	52%	15.80	10.08	0.42	13.76	7.10	0.78	2.03	0.13	0.41
12.40	50%	12.48	7.89	0.41	11.42	4.52	0.81	1.05	0.08	0.36
	106 Micron at 40%									
Feed rate	% solids	Water in Feed	U/S Rate	%solids	water in U/S	O/S Rate	%solids	water in O/S	C	Mass split
19.9702	44%	25.70	9.62	0.30	22.20	10.35	0.75	3.50	0.14	0.48
14.46867	32%	30.66	7.69	0.21	28.58	6.78	0.77	2.08	0.07	0.53
10.79433	39%	16.61	6.39	0.29	15.56	4.40	0.81	1.05	0.06	0.59
5.774814	36%	10.24	3.65	0.27	9.83	2.12	0.84	0.41	0.04	0.63
	106 Micron at 30%									
Feed rate	% solids	Water in Feed	U/S Rate	%solids	water in U/S	O/S Rate	%solids	water in O/S	C	Mass split
8.671957	33%	17.46	5.41	0.24	16.75	3.27	0.82	0.71	0.04	0.62
8.50571	27%	22.47	6.19	0.22	22.06	2.32	0.85	0.40	0.02	0.73

Figure 9-2 106 micron feed flow rates and solids concentration

75 Micron at 60%											
Feed rate	% solids	Water in Feed	U/S Rate	%solids	water in U/S	O/S Rate	%solids	water in O/S	Total	C	Mass split
35.454	60%	23.636	12.1	0.739	4.280	23.354	0.5468	19.356	23.636	0.818934	0.341287302
28.306	60%	18.871	10.622	0.671	5.206	17.684	0.5641	13.665	18.871	0.724142	0.375256129
24.292	60%	16.195	9.523	0.638	5.394	14.769	0.5776	10.801	16.195	0.666923	0.392022065
16.9021	60%	11.268	7.2581	0.614	4.569	9.644	0.5901	6.699	11.268	0.594511	0.429420013
10.182	60%	6.788	4.594	0.590	3.193	5.588	0.6085	3.595	6.788	0.529646	0.451188372
75 Micron at 50%											
Feed rate	% solids	Water in Feed	U/S Rate	%solids	water in U/S	O/S Rate	%solids	water in O/S	Total	C	Mass split
22.0114	50%	22.011	9.4603	0.410	13.611	12.5511	0.599046	8.401	22.011	0.381653	0.429790927
15.1125	50%	15.113	6.7666	0.407	9.874	8.3459	0.61438	5.238	15.113	0.346625	0.447748553
12.344	50%	12.344	5.985	0.412	8.527	6.359	0.62488	3.817	12.344	0.309248	0.48485094
8.662	50%	8.662	3.2488	0.371	5.511	5.4132	0.632107	3.151	8.662	0.36372	0.375063496
75 Micron at 40%											
Feed rate	% solids	Water in Feed	U/S Rate	%solids	water in U/S	O/S Rate	%solids	water in O/S	Total	C	Mass split
18.0984	40%	27.148	8.7236	0.289	21.486	9.3748	0.62348	5.661	27.148	0.208543	0.482009459
14.3025	40%	21.454	7.3526	0.296	17.458	6.9499	0.63495	3.996	21.454	0.186247	0.514077958
10.028	40%	15.042	5.4679	0.303	12.570	4.5601	0.64846	2.472	15.042	0.164346	0.545263263
9.1421	40%	13.713	5.0789	0.305	11.598	4.0632	0.65765	2.115	13.713	0.154243	0.555550694
75 Micron at 30%											
Feed rate	% solids	Water in Feed	U/S Rate	%solids	water in U/S	O/S Rate	%solids	water in O/S	Total	C	Mass split
12.2232	30%	28.521	6.955	0.212	25.812	5.2682	0.66044	2.709	28.521	0.094969	0.568999935
7.6204	30%	17.781	4.5036	0.216	16.377	3.1168	0.689499	1.404	17.781	0.078938	0.590992599

Figure 9-3 75 micron feed flow rates and solids concentration

	45 Micron at 60%										
Feed rate	% solids	Water in Feed	U/S Rate	%solids	water in U/S	O/S Rate	%solids	water in O/S	Total	C	Mass split
29.184	42%	40.88	8.88	0.30	21.13	20.31	0.51	19.74	40.88	0.48	0.30
22.398	42%	30.72	7.82	0.31	17.16	14.58	0.52	13.56	30.72	0.44	0.35
17.123	41%	24.58	6.44	0.30	15.08	10.69	0.53	9.50	24.58	0.39	0.38
11.2595	40%	16.67	4.54	0.31	10.22	6.72	0.51	6.45	16.67	0.39	0.40
	45 Micron at 50%										
Feed rate	% solids	Water in Feed	U/S Rate	%solids	water in U/S	O/S Rate	%solids	water in O/S	Total	C	Mass split
23.68	36%	41.87	9.34	0.28	24.45	14.34	0.45	17.42	41.87	0.42	0.39
17.657	36%	31.67	7.42	0.27	20.07	10.24	0.47	11.60	31.67	0.37	0.42
12.74	41%	17.97	5.55	0.34	10.75	7.19	0.50	7.22	17.97	0.40	0.44
8.146	36%	14.36	3.81	0.27	10.40	4.34	0.52	3.95	14.36	0.28	0.47
	45 Micron at 40%										
Feed rate	% solids	Water in Feed	U/S Rate	%solids	water in U/S	O/S Rate	%solids	water in O/S	Total	C	Mass split
17.94	30%	42.56	8.22	0.20	32.79	9.72	0.50	9.77	42.56	0.23	0.46
15.622	29%	38.49	7.37	0.19	30.93	8.25	0.52	7.56	38.49	0.20	0.47
10.433	25%	30.87	5.61	0.18	25.56	4.82	0.48	5.31	30.87	0.17	0.54
9.456	11%	80.32	4.88	0.06	76.42	4.58	0.54	3.90	80.32	0.05	0.52
	45 Micron at 30%										
Feed rate	% solids	Water in Feed	U/S Rate	%solids	water in U/S	O/S Rate	%solids	water in O/S	Total	C	Mass split
10.707	20%	43.94	5.84	0.13	40.08	4.87	0.56	3.86	43.94	0.09	0.55
8.856	19%	36.79	5.02	0.13	33.99	3.84	0.58	2.80	36.79	0.08	0.57

Figure 9-4 45 micron feed flow rates and solids concentration

150 microns aperture 60wt% feed solids PSD Data										
size	35 tph U/S	35 tph O/s	30 tph U/S	30 tphO/s	25 tph U/S	25 tphO/s	19 tphU/S	19 tphO/S	13 U/S tph	13 tphO/s
8000	100.00	100.00	100.00	100.00	100.00	100.00	100.00	100.00	100.00	100.00
5600	100.00	100.00	100.00	100.00	100.00	100.00	100.00	100.00	100.00	100.00
4000	100.00	100.00	100.00	100.00	100.00	100.00	100.00	100.00	100.00	100.00
2800	100.00	100.00	100.00	100.00	100.00	100.00	100.00	100.00	100.00	100.00
2000	100.00	100.00	100.00	100.00	100.00	100.00	100.00	100.00	100.00	100.00
1400	100.00	100.00	100.00	100.00	100.00	100.00	100.00	100.00	100.00	100.00
1000	100.00	100.00	100.00	100.00	100.00	100.00	100.00	100.00	100.00	100.00
850	100.00	100.00	100.00	100.00	100.00	100.00	100.00	100.00	100.00	100.00
600	100.00	99.93	100.00	100.00	100.00	100.00	100.00	99.84	100.00	99.97
425	100.00	99.93	100.00	100.00	100.00	100.00	100.00	99.74	100.00	99.78
300	100.00	99.93	100.00	99.99	100.00	99.99	100.00	99.25	100.00	98.85
212	99.99	98.40	100.00	99.45	99.97	99.45	99.86	96.53	99.90	96.09
150	99.83	96.66	100.00	99.22	99.13	99.22	97.65	83.47	98.02	80.71
106	99.11	93.40	99.97	98.22	96.50	98.22	93.90	69.41	94.09	64.36
75	97.16	88.39	99.72	95.91	90.74	95.91	87.06	55.37	90.22	56.44
53	92.10	81.94	96.33	82.39	80.68	82.39	80.84	50.07	81.96	51.46
38	82.78	73.75	92.16	77.84	69.30	77.84	70.94	45.40	72.95	47.12
25	51.83	50.30	79.78	67.50	54.08	67.50	57.73	40.59	63.00	42.53
20	44.49	44.78	68.84	59.98	47.12	59.98	48.88	36.53	53.42	37.98
15	36.22	38.12	54.34	50.80	39.18	50.80	39.72	31.98	43.58	32.99
10	27.16	29.70	46.42	44.86	30.34	44.86	30.68	26.63	34.10	27.35
7	21.06	23.43	25.51	27.31	24.05	27.31	23.16	21.15	26.01	21.62
5	16.18	18.17	18.89	20.64	18.76	20.64	16.45	15.71	18.98	16.19
3	9.78	11.21	14.51	15.87	11.94	15.87	10.62	10.74	12.49	11.01
2	6.11	7.08	10.30	11.15	7.58	11.15	6.93	7.22	8.58	7.66
1.5	4.18	4.87	7.49	7.85	5.21	7.85	4.50	4.75	5.67	5.10
1	2.19	2.58	4.68	4.49	2.75	4.49	2.39	2.57	3.12	2.84
0.75	1.14	1.37	2.83	2.23	1.45	2.23	0.93	1.02	1.10	1.01

Figure 9-5 PSD for 150 um at 60 wt% solids in feed

150 microns aperture 50wt% feed solids PSD Data						
Size	25 tph	25 tph O/S	19 tph U/S	19 tph O/S	13 tph	13 tph O/S
850	100.00	100.00	100.00	99.90	100.00	100.00
600	100.00	100.00	100.00	99.59	100.00	100.00
425	100.00	99.49	100.00	99.06	100.00	99.89
300	99.99	96.98	100.00	96.74	100.00	99.00
212	99.92	93.53	99.94	81.17	99.95	94.18
150	98.32	70.68	98.68	65.30	99.01	74.35
106	96.94	64.79	95.01	54.39	95.73	61.41
75	91.66	54.74	89.23	47.29	90.31	52.61
53	83.13	47.09	81.37	42.02	82.75	46.08
38	72.46	41.56	71.61	33.72	73.02	41.51
25	50.84	32.73	50.93	31.40	50.75	32.08
20	44.66	30.11	45.46	28.57	45.07	29.51
15	37.80	26.94	39.45	25.14	38.80	26.40
10	30.37	23.07	32.96	22.23	32.05	22.69
7	24.79	19.84	27.96	18.99	26.91	19.60
5	19.52	16.49	22.96	14.97	21.86	16.34
3	13.41	12.11	17.28	10.91	16.02	12.37
2	8.62	8.39	12.05	7.88	11.04	8.80
1.5	5.81	6.01	8.42	4.98	7.71	6.30
1	3.22	3.52	5.18	2.40	4.67	3.93
0.75	1.63	1.85	2.40	0.00	2.20	1.91

Figure 9-6 PSD for 150 um at 50 wt% solids in feed

150 microns aperture 40 and 30wt% feed solids PSD Data						
	40 wt%				30 wt%	
Size	19 tph U/S	13 tph U/S	19 tph O/S	13 tph O/S	25 U/S	25O/S
8000	100.00	100.00	100.00	100.00	100.00	100.00
5600	100.00	100.00	100.00	100.00	100.00	100.00
4000	100.00	100.00	100.00	100.00	100.00	100.00
2800	100.00	100.00	100.00	100.00	100.00	100.00
2000	100.00	100.00	100.00	100.00	100.00	100.00
1400	100.00	100.00	100.00	100.00	100.00	100.00
1000	100.00	100.00	100.00	100.00	100.00	100.00
850	100.00	100.00	100.00	99.89	99.98	100.00
600	100.00	100.00	99.72	99.74	96.68	100.00
425	100.00	100.00	99.37	99.38	84.14	100.00
300	100.00	100.00	94.44	93.06	61.84	99.94
212	99.73	99.75	72.03	65.37	37.32	99.16
150	97.76	97.77	50.36	36.95	19.51	96.63
106	93.21	93.22	38.26	23.37	11.23	91.57
75	85.72	85.74	31.32	18.21	9.19	83.82
53	76.12	76.13	28.03	16.47	8.85	73.66
38	64.23	64.24	24.62	14.81	8.23	62.40
25	49.16	49.17	20.09	12.72	7.15	48.22
20	42.02	42.03	17.93	11.57	6.68	41.57
15	34.56	34.57	15.51	10.21	6.17	34.32
10	27.17	27.18	12.93	8.61	5.43	26.36
7	20.92	20.92	10.55	7.02	4.63	20.74
5	16.41	16.41	8.73	5.78	3.79	16.17
3	10.11	10.11	5.89	3.90	2.57	10.45
2	6.45	6.45	4.07	2.66	1.75	7.01
1.5	4.46	4.46	2.99	1.94	1.25	5.16
1	2.38	2.38	1.70	1.12	0.70	3.24
0.75	1.27	1.27	0.95	0.64	0.39	2.20

Figure 9-7 150 microns aperture 40 and 30wt% feed solids PSD data

PSD 106 Micron - 60% wt% solids								
size	35 tph u/s	35 tph o/s	30 tph u/s	30 tph o/s	19 tph u/s	19 tph o/s	13 tph u/s	13 tph o/s
8000	100.00	100.00	100.00	100.00	100.00	100.00	100.00	100.00
5600	100.00	100.00	100.00	100.00	100.00	100.00	100.00	100.00
4000	100.00	100.00	100.00	100.00	100.00	100.00	100.00	100.00
2800	100.00	100.00	100.00	100.00	100.00	100.00	100.00	100.00
2000	100.00	100.00	100.00	100.00	100.00	100.00	100.00	100.00
1400	100.00	100.00	100.00	100.00	100.00	100.00	100.00	100.00
1000	100.00	99.96	100.00	99.98	100.00	100.00	100.00	100.00
850	100.00	99.89	100.00	99.83	100.00	100.00	100.00	100.00
600	100.00	99.54	100.00	98.79	100.00	99.89	100.00	99.79
425	100.00	98.29	100.00	96.44	100.00	99.73	100.00	99.33
300	99.92	93.95	99.97	93.14	100.00	99.51	99.66	96.96
212	99.26	62.39	99.54	75.81	99.96	97.96	97.79	85.40
150	95.75	50.89	97.49	69.11	99.87	94.62	93.71	66.46
106	89.52	44.22	91.95	61.98	99.03	83.42	87.12	46.63
75	81.18	39.44	83.83	55.51	91.68	67.13	78.62	35.90
53	71.72	35.88	74.29	49.97	80.89	56.01	69.12	31.85
38	62.40	32.44	64.80	44.96	68.31	47.99	59.81	28.45
25	51.15	27.95	53.48	38.49	49.91	37.80	48.44	24.11
20	45.63	25.39	47.78	34.73	44.33	34.58	42.78	21.96
15	39.15	22.10	41.09	30.12	37.45	30.27	36.10	19.20
10	31.22	17.83	33.03	24.02	28.34	24.09	27.98	15.40
7	25.22	14.32	26.95	19.10	21.91	19.23	21.93	12.39
5	20.15	11.12	21.84	14.89	16.62	14.93	16.97	9.73
3	13.52	6.70	15.17	9.28	10.06	9.31	10.76	6.19
2	9.33	3.73	10.97	5.65	6.27	5.90	7.05	3.93
1.5	7.01	2.09	8.64	3.65	4.27	4.02	5.09	2.69
1	4.61	0.37	6.23	1.57	2.24	2.11	3.11	1.42
0.75	2.45	0.14	3.48	0.81	1.18	1.10	2.07	0.74

Figure 9-8 PSD 106 Micron - 60% wt% solids

PSD 106 Micron - 50% wt% solids							
Seive	Feed	25 tph u/s	25 tph o/s	19 tph u/s	13 tph u/s	13 tph o/s	9 tph u/s
8000	100.0	100.0	100.0	100.0	100.0	100.0	100.0
5600	100.0	100.0	100.0	100.0	100.0	100.0	100.0
4000	100.0	100.0	100.0	100.0	100.0	100.0	100.0
2800	100.0	100.0	100.0	100.0	100.0	100.0	100.0
2000	100.0	100.0	100.0	100.0	100.0	100.0	100.0
1400	100.0	100.0	100.0	100.0	100.0	100.0	100.0
1000	100.0	100.0	100.0	100.0	100.0	100.0	100.0
850	100.0	100.0	100.0	100.0	100.0	100.0	100.0
600	99.9	100.0	100.0	100.0	100.0	100.0	100.0
425	99.4	100.0	99.8	100.0	100.0	99.8	100.0
300	98.9	100.0	98.9	100.0	100.0	98.9	100.0
212	93.6	100.0	97.6	99.3	100.0	97.6	100.0
150	84.3	100.0	68.8	97.3	99.3	73.5	99.1
106	74.6	96.7	56.1	92.7	94.9	55.0	94.0
75	65.5	89.5	46.4	85.3	87.6	43.9	85.6
53	57.1	80.5	40.4	75.4	76.3	37.1	75.3
38	49.0	68.7	35.6	64.5	66.1	32.7	64.3
25	39.2	56.5	31.2	50.7	53.0	27.7	50.7
20	34.5	49.4	28.7	43.9	46.6	25.3	44.1
15	29.1	41.3	25.5	36.4	39.1	22.3	36.8
10	22.7	32.4	21.6	27.8	30.6	18.7	28.3
7	18.0	25.5	18.3	21.7	24.2	15.7	22.2
5	14.1	19.6	15.1	16.8	18.8	12.9	17.1
3	9.0	13.1	10.8	10.7	11.6	8.7	10.7
2	5.8	8.4	7.4	7.0	7.3	5.8	6.7
1.5	4.0	5.7	5.2	5.1	4.9	4.1	4.6
1	2.2	3.0	2.9	3.2	2.6	2.2	2.4
0.75	1.2	1.5	1.5	2.1	1.3	1.2	1.3
0.5	0.0	0.0	0.0	1.0	0.0	0.0	0.0

Figure 9-9 PSD 106 Micron - 50% wt% solids

PSD 106 Micron - 40 and 30wt% solids											
	40 wt%							30 wt%			
Size	19 tph	19 tph o/s	16 tph u/s	13 tph u/s	13 tpho/s	9 tph u/s	9 tpho/s	9 tph u/s	13 tph u/s	9 tph o/s	13 tph o/s
8000	100.00	100.00	100.00	100.00	100.00	100.00	100.00	100.00	100.00	100.00	100.00
5600	100.00	100.00	100.00	100.00	100.00	100.00	100.00	100.00	100.00	100.00	100.00
4000	100.00	100.00	100.00	100.00	100.00	100.00	100.00	100.00	100.00	100.00	100.00
2800	100.00	100.00	100.00	100.00	100.00	100.00	100.00	100.00	100.00	100.00	100.00
2000	100.00	100.00	100.00	100.00	100.00	100.00	100.00	100.00	100.00	100.00	100.00
1400	100.00	100.00	100.00	100.00	100.00	100.00	100.00	100.00	100.00	100.00	100.00
1000	100.00	99.79	100.00	100.00	100.00	100.00	100.00	100.00	100.00	100.00	100.00
850	100.00	98.17	100.00	100.00	100.00	100.00	99.74	100.00	100.00	99.84	99.99
600	100.00	97.57	100.00	100.00	98.57	100.00	93.60	100.00	100.00	94.96	97.38
425	100.00	91.60	100.00	100.00	91.60	100.00	76.68	100.00	100.00	80.27	87.83
300	100.00	76.93	99.87	100.00	76.93	100.00	51.46	100.00	100.00	56.55	71.58
212	100.00	56.64	98.73	100.00	57.48	99.61	28.11	100.00	100.00	32.18	54.28
150	99.27	39.03	95.30	96.22	27.48	96.96	13.41	100.00	100.00	15.59	41.75
106	92.52	27.37	88.61	89.45	18.04	91.22	7.64	97.71	90.71	8.42	35.07
75	83.07	21.75	79.27	80.25	13.66	83.03	5.75	94.17	79.74	6.80	31.62
53	72.55	19.16	68.99	70.43	12.21	74.56	5.26	86.00	71.38	6.42	28.77
38	62.97	17.20	59.64	61.07	11.08	61.71	4.74	73.82	64.10	5.72	25.85
25	50.07	14.55	49.09	50.14	9.62	47.15	3.99	60.06	54.94	4.70	22.24
20	43.78	13.15	43.90	44.52	8.81	41.88	3.69	55.41	49.89	4.29	20.43
15	36.84	11.49	37.56	37.78	7.77	35.74	3.30	49.31	43.62	3.87	18.16
10	28.46	9.35	29.32	30.02	6.43	27.53	2.74	40.16	35.67	3.31	14.96
7	21.95	7.55	22.89	23.79	5.25	21.04	2.24	32.01	28.58	2.74	12.14
5	16.61	5.93	17.60	18.58	4.23	15.79	1.78	24.55	22.10	2.19	9.60
3	10.05	3.79	11.11	11.72	2.81	9.32	1.17	15.06	14.16	1.42	6.24
2	6.19	2.44	7.27	7.51	1.88	5.39	0.75	9.15	8.93	0.93	4.14
1.5	4.15	1.68	5.23	5.10	1.31	3.26	0.50	5.53	5.81	0.63	2.98
1	2.08	0.86	3.17	2.68	0.70	1.11	0.20	2.33	3.10	0.27	1.76
0.75	1.02	0.43	2.10	1.40	0.37	0.00	0.03	0.60	1.58	0.06	1.12

Figure 9-10 PSD 106 Micron - 40 and 30wt% solids

75 micron PSD at 60 wt% solids										
size	35 tph u/s	35 tph o/s	30 tph u/s	30 tph o/s	25 tph u/s	Feed	19 tph u/s	19 tph o/s	13 tph u/s	13 tph o/s
8000	100.00	100.00	100.00	100.00	100.00	100.00	100.00	100.00	100.00	100.00
5600	100.00	100.00	100.00	100.00	100.00	100.00	100.00	100.00	100.00	100.00
4000	100.00	100.00	100.00	100.00	100.00	100.00	100.00	100.00	100.00	100.00
2800	100.00	100.00	100.00	100.00	100.00	100.00	100.00	100.00	100.00	100.00
2000	100.00	100.00	100.00	100.00	100.00	100.00	100.00	100.00	100.00	100.00
1400	100.00	100.00	100.00	100.00	100.00	100.00	100.00	100.00	100.00	100.00
1000	100.00	100.00	100.00	100.00	100.00	100.00	100.00	100.00	100.00	100.00
850	100.00	99.99	100.00	100.00	100.00	100.00	100.00	100.00	100.00	100.00
600	100.00	99.82	100.00	100.00	100.00	99.98	100.00	100.00	100.00	100.00
425	100.00	98.91	100.00	100.00	100.00	99.83	100.00	99.90	100.00	100.00
300	100.00	97.24	100.00	100.00	100.00	99.25	100.00	99.00	100.00	100.00
212	100.00	94.92	100.00	100.00	100.00	96.91	100.00	97.20	100.00	99.95
150	100.00	92.97	99.92	97.12	100.00	85.77	100.00	94.70	99.95	97.55
106	99.89	90.31	99.61	89.95	100.00	71.35	98.39	72.06	98.59	77.23
75	99.14	82.24	97.41	69.52	98.89	67.26	91.59	42.20	91.85	48.70
53	95.68	66.89	87.60	44.44	94.22	60.19	80.62	31.26	81.07	37.07
38	85.22	54.69	75.67	36.06	83.75	52.46	69.49	26.48	70.27	31.88
25	62.30	42.37	59.91	29.85	68.24	43.51	55.67	22.16	57.29	26.87
20	55.36	38.86	53.01	27.22	60.22	38.98	49.26	20.18	51.36	24.58
15	46.64	34.44	44.54	23.99	50.63	33.56	41.57	17.78	44.26	21.84
10	34.93	27.86	33.67	19.36	39.17	26.71	31.96	14.43	35.31	18.28
7	26.94	22.37	25.84	15.45	30.54	21.26	24.86	11.71	28.59	15.38
5	20.62	17.60	19.63	12.06	23.50	16.60	19.08	9.25	23.03	12.75
3	12.54	11.03	11.81	7.45	15.08	10.85	11.74	5.92	15.79	9.05
2	7.85	7.05	7.31	4.70	9.79	7.14	7.34	3.80	11.31	6.58
1.5	5.35	4.85	4.95	3.21	6.84	5.04	4.98	2.62	8.85	5.19
1	2.78	2.57	2.56	1.69	3.89	2.90	2.58	1.37	6.30	3.73
0.75	1.46	1.35	1.34	0.89	2.32	1.75	1.34	0.71	4.97	2.95

Figure 9-11 75 micron PSD at 60 wt% solids

75 micron PSD at 50 wt% solids								
Size	25 tph	25tph o/s	19 tph	19 tph o/s	13 tph	13 tpho/s	9 tph	9 tpho/s
1400	100.00	100.00	100.00	99.96	100.00	100.00	100.00	100.00
1000	100.00	100.00	100.00	99.90	100.00	100.00	100.00	100.00
850	100.00	100.00	100.00	99.88	100.00	100.00	100.00	100.00
600	100.00	100.00	100.00	99.79	100.00	100.00	100.00	100.00
425	100.00	99.61	100.00	99.19	100.00	99.86	100.00	98.44
300	100.00	97.31	100.00	96.44	100.00	97.76	100.00	93.41
212	100.00	92.00	100.00	88.08	100.00	88.51	100.00	84.18
150	100.00	83.90	100.00	71.33	100.00	66.71	100.00	38.64
106	100.00	73.27	99.93	67.38	99.80	61.99	100.00	27.49
75	98.92	64.64	98.65	59.46	98.46	55.11	98.79	24.00
53	94.69	57.22	93.04	52.34	92.93	48.73	92.58	20.58
38	85.31	51.04	82.77	46.62	82.98	43.73	83.42	18.56
25	70.50	43.96	68.46	40.40	69.55	38.44	72.28	16.72
20	62.64	40.35	60.66	37.00	61.34	35.28	64.51	15.48
15	53.10	35.83	51.54	32.90	51.80	31.48	55.91	14.00
10	40.94	29.59	40.55	27.53	41.15	26.33	46.09	12.11
7	31.25	24.10	31.75	22.77	32.71	21.58	37.43	10.26
5	23.34	19.02	24.38	18.26	25.46	17.16	29.72	8.36
3	14.08	12.12	15.50	12.04	16.66	11.47	20.89	6.00
2	8.62	7.71	9.70	7.82	10.81	7.55	14.28	4.18
1.5	5.72	5.27	6.49	5.39	7.43	5.22	9.93	2.94
1	2.89	2.75	3.32	2.84	3.98	2.80	5.47	1.66
0.75	1.48	1.43	1.69	1.47	2.08	1.46	2.79	0.86

Figure 9-12 75 micron PSD at 50 wt% solids

75 micron PSD at 30 and 40 wt% solids												
	40 wt%								30wt%			
Size	19 tph u/s	19 tph o/s	16 tph u/s	16 tpho/s	13 tph u/s	13 tpho/s	9 tph u/s	9 tpho/s	9 tph u/s	9 tph o/s	13 tph u/s	13 tph o/s
850	100.00	100.00	100.00	99.91	100.00	100.00	100.00	99.97	100.00	100.00	100.00	100.00
600	100.00	100.00	100.00	98.89	99.95	100.00	100.00	99.63	100.00	99.39	100.00	99.94
425	100.00	99.22	100.00	96.75	99.95	99.71	100.00	98.56	100.00	95.96	100.00	98.70
300	100.00	95.46	100.00	90.13	99.95	95.98	100.00	93.85	100.00	87.96	100.00	93.60
212	100.00	87.22	100.00	77.77	99.95	84.47	100.00	83.16	100.00	75.73	100.00	82.72
150	100.00	75.48	99.89	62.88	99.95	64.79	99.96	67.72	100.00	39.77	100.00	37.28
106	100.00	63.44	99.66	56.55	99.43	52.81	99.71	45.26	100.00	27.30	100.00	22.16
75	97.61	54.21	96.53	46.48	96.14	42.97	96.78	35.52	96.97	21.42	96.19	17.02
53	91.48	48.14	90.08	40.32	90.27	37.39	90.63	30.97	91.23	17.89	89.65	14.14
38	82.90	43.81	81.11	36.25	82.94	34.18	82.33	27.97	84.17	16.04	83.09	12.91
25	69.63	38.55	65.84	31.22	71.38	30.80	68.97	24.70	74.22	14.65	74.48	12.04
20	62.03	35.67	58.79	29.07	63.95	28.78	61.60	23.04	67.08	13.80	67.97	11.45
15	52.81	31.97	50.30	26.32	54.93	26.22	52.69	21.03	58.74	12.77	60.36	10.72
10	42.32	26.81	40.12	21.97	45.19	22.53	42.56	18.29	48.72	11.41	51.43	9.70
7	33.60	22.24	32.23	18.33	36.82	19.08	34.23	15.32	39.98	9.92	43.18	8.64
5	26.16	17.94	25.43	14.83	29.36	15.62	27.00	12.41	31.98	8.33	35.34	7.44
3	16.65	11.93	16.35	9.73	19.60	10.61	17.55	8.20	22.39	6.21	25.87	5.80
2	10.71	8.05	10.51	6.28	13.00	7.06	11.42	5.34	15.32	4.57	18.44	4.42
1.5	7.40	5.88	7.24	4.33	9.11	4.95	7.93	3.71	10.73	3.47	13.20	3.44
1	3.94	3.60	3.82	2.27	4.94	2.67	4.25	1.97	6.00	2.31	7.67	2.39
0.75	2.07	2.37	2.00	1.18	2.59	1.39	2.24		3.12	1.58	3.97	1.70

Figure 9-13 75 micron PSD at 30 and 40 wt% solids

9.2 Matlab function used to model

```
%% 'Fine wet screen Model'.
function screensimu(data_filename, conds_filename)
close all
input=data_filename;% make sure input is equal to loaded file name
col=hsv(7);
q=input(1,8);
Q=input(1,7);
% Initialize arrays to store fits and goodness-of-fit.
fitresult = cell( q, 1 );
gof = struct( 'sse', cell( q, 1 ), ...
    'rsquare', [], 'dfe', [], 'adjrsquare', [], 'rmse', [] );
for jx=2:q;
    %subplot(2,2,jx)
[xData1, yData1] = prepareCurveData(input(7:Q,1),input(7:Q,jx));
% Set up fittype and options.
ft = fittype( '100*exp(-A*a/(F*s*(x/p)^b))+F*c/((1-s))*(exp(-x/p))^b','problem',{'A','F','s','p'}, 'independent', 'x', 'dependent', 'y' );
Area=input(1,4)*input(1,5)*input(1,6);
FeedRate=input(2,jx);
Solids=input(3,jx);
Aperture=input(1,1);
opts = fitoptions( ft );
opts.Display = 'Off';
opts.Lower = [1 1 .01];
opts.StartPoint = [1 1 1];
opts.Upper = [Inf Inf Inf];
```

```
% Fit model to data.
[fitresult{jx}, gof(jx)] = fit( xData1, yData1, ft, opts,'problem',{Area,FeedRate,Solids,Aperture});
fitcoeff(:,jx)=coeffvalues(fitresult{jx}); % Creat a matix of fitted parameters
end
%% 'Delta regression Model'.
sd=input(3,2:q);% wt% solids
fd=input(2,2:q);% feed rate
delta=fitcoeff(3,2:q);% fitted delta coefficients
ap=input(6,2:q);% input aperture
X=[ones(size(sd')), sd', fd', ap'];% Matrix of input values
Y1=delta'; % Y axis data
dt = regress(Y1,X);% Produce regressed data for a regression equation
%Regression equation is y=a + bx1 + cx2 + dx3
l=1;
for jx=2:q;
delt(l)=dt(1)+dt(2)*sd(jx-1)+dt(3)*fd(jx-1)+dt(4)*ap(jx-1); % generate a matrix of delta values from the regression equation
l=l+1;
end
[xData, yData] = prepareCurveData( delt, delta );
% Fit calculated data to Fitted data
ft = fittype( 'poly1' ); opts = fitoptions( ft ); opts.Lower = [-Inf -Inf];
opts.Upper = [Inf Inf];
[Deltfit, Deltgof] = fit( xData, yData, ft, opts ); %Fit results and produce a goodness of fit mitrix
h = plot( Deltfit, xData, yData );
```

```
legend( h, 'delta data', 'delta fit', 'Location', 'NorthEast' );
% Label axes
Deltgof% Goodness of delta fit
xlabel( 'Fitted \delta' );
ylabel( 'Calculated \delta' );
%% 'Linear fit k values'
K=fitcoeff(1,2:q);
Y2=K';
af = regress(Y2,X);
j=1;
for jx=2:q;
kay(j)=af(1)+af(2)*sd(jx-1)+af(3)*fd(jx-1)+af(4)*ap(jx-1);
j=j+1;
end
% Fit: 'K correlation'.
[xData, yData] = prepareCurveData( K, kay );
% Set up fittype and options.
ft = fittype( 'poly1' );
opts = fitoptions( ft );
opts.Lower = [-Inf -Inf];
opts.Upper = [Inf Inf];
% Fit model to data.
[Kftrst, Kgof] = fit( xData, yData, ft, opts );
% Plot fit with data.
figure( 'Name', 'K correlation' );
h = plot( Kftrst, xData, yData );
```

```
legend( h, 'K data', 'K correlation line', 'Location', 'NorthEast' );
% Label axes
Kgof %goodness of K fit
title('Calculated vs Fitted K values')
ylabel( 'Calculated K values' );
xlabel( 'Fitted K values' );
%% 'Alpha Model'
w=1;
for x=2:q;
    %q=34;
    Mf=input(1,2)*input(2,x); %mass of undersize in feed
    mu=input(4,x)/1000; %viscosity
    rho=input(1,3); %ore density
    F=input(2,x);% Feed rate
    a=input(1,1);% aperture size
    s=input(3,x); % solids concentration
    rhos=(F*(1-s)/s+F)/(F*(1-s)/s+F/rho);% slurry pulp density
    alp=fitcoeff(2,x);% alpha
    A=input(1,4)*input(1,5)*input(1,6);%Area
    D50=input(5,x);
    X3(w)=(A^3*rhos^2/(Mf^2)); X4(w)=F/(mu*A^.5); %d50 model
    X5(w)=D50/a; X6(w)=X3(w)*X4(w);
    X1(w)=A^3*rhos^2*F/(Mf^2*mu*A^.5);  X2(w)=alp*(a*10^-6)^2/A;  % alpha
model
    [P,z]=polyfit(X1,X2,1);%generate coefficients gamma and delta for Alpha
Model
```

```
[D,y]=polyfit(X6,X5,1);%generate coefficients gamma and delta for D50 Model

t(w)= P(1)*(A^3.5*rhos^2*F/(Mf^2*mu*(a*10^-6)^2))+ P(2)*(A/(a*10^-6)^2); %Predicted Alpha Value

j(w)=D(1)*a*X6(w)+D(2)*a; %Predicted d50 value

w=w+1;

end

%=========================================

%% 'Plotting Alpha correlation'

[xData, yData] = prepareCurveData( fitcoeff(2,2:q),t );

% Set up fittype and options.

ft = fittype( 'poly1' );

opts = fitoptions( ft );

% Fit model to data.

[alphftrslt, alphgof] = fit( xData, yData, ft, opts );

% Create a figure for the plots.

figure;

h = plot( alphftrslt, xData, yData );

legend( h, 'Data', 'Correlation line', 'Location', 'NE' );

% Label axes

title('Fitted \alpha vs predicted \alpha');

xlabel( 'Predicted \alpha' );

ylabel( 'fitted \alpha' );

% Plot alpha residuals.

figure;

h = plot( alphftrslt, xData, yData, 'residuals' );

legend( h, 'd50 - residuals', 'Zero Line', 'Location', 'NE' );
```

```
% Label axes
title('\alpha Residual plot')
%axis([0 120 -20 20])
alphgof %Goodness of Alpha fit
xlabel( 'Observed \alpha' );
ylabel( 'Residual' );
%==========================================
%% 'plotting D_5_0 correlation'
[xData, yData] = prepareCurveData( input(5,2:q),j);
% Set up fittype and options.
ft = fittype( 'poly1' );
opts = fitoptions( ft );
% Fit model to data.
[D50ftrst, D50gof] = fit( xData, yData, ft, opts );

% Create a figure for the plots.
% Plot fit with data.
figure;
h = plot( D50ftrst, xData, yData );
legend( h, 'Data', 'Correlation line', 'Location', 'NE' );
% Label axes
D50gof %Goodness of D50 fit
title('Observed d50 vs predicted d50');
xlabel( 'Predicted d50 um' );
ylabel( 'Observed d50 um' );
```

```
%% 'Plotting partition curve using correlation function'
ptclsz=input(7:Q,1);
e=Q-6;
for xj=q-5;
   for i=1:e;
   eff(i)=100*exp(-A*kay(xj-1)/(input(2,xj)*input(3,xj)*(ptclsz(i)/input(1,1))^t(xj-
1)))...
       +input(2,xj)/(delt(xj-1)*(1-input(3,xj)))*(exp(-ptclsz(i)/input(1,1)))^t(xj-1);
   end
end
effd=(input(7:Q,xj) );
semilogx(ptclsz,effd,'*' )
hold on; plot(ptclsz,eff,'r','LineWidth',1.5)
axis([0 10000 0 100])
legend('Data','Model')
title('Prediction using correlation function')
ylabel ('Partition %')
xlabel('Particle size um')
%% 'Parity and Residual plot using correlation functions'.
[xData, yData] = prepareCurveData( effd, eff );
% Set up fittype and options.
ft = fittype( 'poly1' ); opts = fitoptions( ft ); opts.Lower = [-Inf -Inf];
opts.Upper = [Inf Inf];
% Fit model to data.
[fitresult, Corgof] = fit( xData, yData, ft, opts );
% Plot fit with data.
```

```
figure( 'Name', 'untitled fit 1' );
h = plot( fitresult, xData, yData );
legend( h, 'Measured vs predicted', 'Correlation line', 'Location', 'NW' );
% Label axes
title('Measured versus predicted partition using correlation functions')
xlabel( 'Predicted partition values' );
ylabel( 'Measured partition values' );
%text(20,80,'R^2: 0.9912');
%text(20,75,'SSE: 317.3')
axis([0 100 0 100])
Corgof %Goodness of Model fit with correlations
figure
h = plot( fitresult, xData, yData, 'residuals' );
legend( h, 'Residuals', 'Zero Line', 'Location', 'NorthEast' );
% Label axes
title('Residual plot for Model with correlation function')
xlabel( 'Measured Partition values %' );
ylabel( 'Residuals %' );
axis([0 100 -10 20])
zb=[0,0];
za=[0,100];
hold on
plot(za,zb,'r')
%% 'Simulate new conditions'
%=========================================================
================
```

```
 simulate=conds_filename; %make sure input is equal to loaded file name
%=========================================================
================
y=simulate(1,8);
col=hsv(y);
v=1;
figure
for c=2:y;
    F=simulate(2,c);% Feed rate
    Mf=simulate(1,2)*F; %mass of undersize in feed
    mu=simulate(4,c)/1000; %viscosity
        a=simulate(1,1);% aperture size
    s=simulate(3,c); % solids concentration
    rho=simulate(1,3);% Ore density
    A=simulate(1,4)*simulate(1,5)*simulate(1,6);%Area
    rhos=(F*(1-s)/s+F)/(F*(1-s)/s+F/rho);% slurry pulp density
    ts    =    P(1)*(A^3.5*rhos^2*F/(Mf^2*mu*(a*10^-6)^2))+    P(2)*(A/(a*10^-
6)^2); %Predicted Alpha Value
    kays =af(1)+af(2)*sd(jx-1)+af(3)*fd(jx-1)+af(4)*ap(jx-1);%Predicted K Value
    delts   =dt(1)+dt(2)*sd(jx-1)+dt(3)*fd(jx-1)+dt(4)*ap(jx-1);%Predicted   delta
Value
    for i=1:e;
    effs(i)=100*exp(-A*kays/(F*s*(ptclsz(i)/a)^ts))...
        +F/(delts*(1-s))*(exp(-ptclsz(i)/a))^ts;    %Calculate partition values
    end
    labls2{v} = [" num2str(F),'tph ',num2str(s*100),'%  \alpha = ',num2str(ts),' -
',num2str(a),'\mum' "];
```

```
    v = v + 1;
        semilogx(ptclsz,effs,'color',col(c,:),'LineWidth',2.5)    %    Plot    partition
values
        legend(labls2,'Location','NE');
    hold on
end
    title('Simulated partition values')
ylabel ('Partition %')
xlabel('Particle size \mum')
```